AN INFORMATION THEORETIC STUDY OF MODELING AND CONTROL OF DYNAMICAL SYSTEMS

BY

YU SUN

DISSERTATION

Submitted in partial fulfillment of the requirements
for the degree of Doctor of Philosophy in Mechanical Engineering
in the Graduate College of the
University of Illinois at Urbana-Champaign, 2011

Urbana, Illinois

Doctoral Committee:

Assistant Professor Prashant G.Mehta, Chair and Director of Research
Professor Tamer Başar
Assistant Professor Todd P. Coleman
Professor Geir Dullerud

Abstract

This dissertation concerns fundamental performance limitation in control of nonlinear systems. It consists of three coherent, closely related studies where the unifying theme is the use of information theoretic tools to investigate modeling and control issues in dynamical systems.

The first study focuses on entropy based fundamental limitation results for the nonlinear disturbance rejection problem. The starting point of our analysis is the so-called Kolmogorov-Bode formula for linear dynamics, which relates the fundamental limitation to certain entropy rates of the input/output signals. We propose a hidden Markov model (HMM) framework for the closed-loop system, under which the entropy rate calculations become straight forward. Explicit entropy bounds are thus obtained for both the classical Bode problem (with linear dynamics) as well as certain cases of nonlinear dynamics. An important implication of this study is that the limitations arise due to fundamental issues pertaining to estimation *as opposed to* the stabilization control problem.

The second study is concerned with information theoretic "pseudo-metrics" for comparing two dynamical systems. It can be regarded as extending the Kolmogorov-Bode formula for model comparison and robustness analysis. Central to the considerations here is the notion of *uncertainty in the model*: the comparisons are made in terms of additional uncertainty that results for the prediction problem with an incorrect choice of the model. A Kullback-Leibler (K-L) rate pseudo-metric is adopted to quantify this additional uncertainty. The utility of the K-L pseudo-metric to a range of model reduction and model selection problems are demonstrated by examples. It is shown that model reduction of nonlinear system using this pseudo-metric leads to the so-called optimal prediction model. For the particular case of linear systems, an algorithm is provided to obtain optimal prediction auto regressive (AR) models.

The third study concerns discrete time nonlinear systems, where the fundamental limitations are expressed in terms of the average cost of an infinite horizon optimal control problem. Unlike usual optimal control problem, the control cost here is defined by a certain K-L divergence metric. Under this cost structure, the limitations can be obtained via analysis of a linear eigenvalue problem defined only by the open loop dynamics. The fundamental limitations are

investigated for both linear time invariant (LTI) system and nonlinear systems. It is shown that for LTI systems the limitation depend upon the unstable eigenvalues, as in the classical Bode formula. For more general class of nonlinear systems the limitation arise only if the open-loop dynamics are non-ergodic.

Taken together, these studies represent some preliminary effort towards an information theoretical paradigm for studying control of dynamical systems. The essential interest is to understand the interaction between uncertainties and dynamics, and its implication in closed-loop control systems.

This thesis also contain my work on two relevant applications, one is about sensor placement design for distributed estimation and the other is about convergence analysis of a distributed optimization algorithm.

To Mother and Father

Acknowledgement

This work would not have been possible without the support of many people.

I would like to convey my sincere respect and many thanks to my advisor, Professor Prashant G. Mehta, for his invaluable guidance and endless support. It has been a pleasure working with him during the past five years. He is truly my mentor and friend.

I would also like to thank my other committee members, Professor Tamer Basar, Professor Todd Coleman and Professor Geir Dullerud, for their insightful comments and suggestions, which helped me make this work stronger.

I would next like to thank all my collaborators and co-workers, especially Professor Prabir Barooah, Dr. Alberto Speranzon, Dr. Xiaofeng Wang, Yanen Li, Kun Deng, Tao Yang and Huibing Yin. Their passion, patience and diligence always influences me from the past to the future.

My special thanks go to my friends in Urbana-Champaign, for making my everyday life colorful. Without them I could not have made it through these years.

Finally, I send my largest thank you to my mother Dong Guiying and my father Sun Guozhong. Although you have not been here physically throughout my years at University of Illinois, I always feel your support and love.

Table of Contents

List of Tables

List of Figures

Chapter 1

Introduction

1.1 Motivation and Objectives

Spurred by advances in communication networks, several recent studies have considered information theoretic aspects of feedback and networked control systems. As an example, the classical Bode and Kolomogorov formulae provide the first glimpse of connection between information theory and control theory. For a discrete-time linear time invariant (LTI) SISO feedback system, the Bode formula is given by the first equality below

$$\frac{1}{2\pi}\int_{-\pi}^{\pi} \ln|S(e^{i\omega})|d\omega = \sum_k \ln|p_k| = \mathscr{H}(\mathbf{y}) - \mathscr{H}(\mathbf{d}), \tag{1.1}$$

where $S(e^{i\omega})$ is the sensitivity transfer function from the disturbance $\mathbf{d}$ to the output $\mathbf{y}$, and p_k are the unstable eigenvalues of the open-loop dynamics [1, 2].

The sum $\sum_k \ln|p_k|$ reflects the performance penalty that arises due to unstable aspects of the dynamics. The information-theoretic extension hinges on the Kolmogorov formula, which is the second equality in (2.2), where $\mathscr{H}(\mathbf{y})$ and $\mathscr{H}(\mathbf{d})$ denote the entropy rate of the stochastic processes $\mathbf{y}$ and $\mathbf{d}$ respectively [3]. These extensions have been particularly relevant to control problems over networks and research at the interstices of communication with control [4, 5]. For example, the performance penalty term $\sum_k \ln|p_k|$ also reflects the minimal data rate required to stabilize an unstable LTI system over a feedback channel [6, 7].

Bode formula suggests that information flow is central to the fundamental limitations analysis of dynamical systems. Although networks have provided a renewed impetus, information flow in nonlinear dynamical systems is an important topic of recent and historical interest. We mention a few examples:

1. Feedback loops are central to information processing by neural circuits in brain [8, 9]. The issue is that neurons "compute" by firing a train of action potentials – limit cycle oscillations that arise as a result of the equilibrium solution (resting potential) becoming unstable [10]. Whether there are some fundamental advantages of this to information flow remains a subject of intense speculation and debate [11, 12, 13].

2. A study of fundamental limitation is central to combustion and flow control [14]. In these settings, the nonlinear

dynamics and noise can interact in subtle and counter-intuitive ways to affect performance. For example, it is conjectured in [15] that when there is large enough noise in a physical system with saturation nonlinearities (e.g. burning rate nonlinearity in combustor), unstable eigenvalues no longer limit performance. An explanation based on analysis of information flow appears in [16], where we showed that $\mathscr{H}(\mathbf{y}) \downarrow \mathscr{H}(\mathbf{d})$ as the noise size goes to infinity for a simple example with saturation.

3. In distributed control, the famous Witsenhausen counter-example shows that an LQG problem with non-classical information structure can lead to nonlinear optimal decision rules [17].

The main objectives of this work are categorized into the following overlapping areas:

- Fundamental limitations analysis of nonlinear feedback systems
- Metrics for model comparison and robustness analysis

The common theme is *information theory in control*. On the topic of fundamental performance limitations, there are two separate areas of investigation:

- Bode-like performance limitations in control of nonlinear systems. This research is summarized in Section 1.3.1 with details in Chapter 2.
- Fundamental performance limitations based on optimal control of nonlinear systems. The preliminary research on this topic is described in Section 1.3.3 with details in Chapter 4.

The research on the topic of model comparison is reported in Chapter 3 and summarized in Section 1.3.2.

1.2 Literature Survey

The idea of an information theoretic framework for feedback systems has a rich history going back to Wiener [18] and Witsenhausen [19]. The problem of control over communication channels (see [5, 4]) has led to a number of recent studies on the topics of control in the presence of communication constraints [6, 7, 20], control viewpoint of communication schemes [21, 22], stabilization with quantization [23, 24, 25], distributed control [26, 27, 28, 29, 30] and extensions of Bode formula summarized next.

1.2.1 Bode-like Fundamental Performance Limitations

The last three decades has witnessed a number of seminal contributions on Bode formula including the publications of Freudenberg and Looze [31, 32, 33], Boyd and Desoer [34], Sung and Hara [1], Chen and co-workers [35, 36], Seron *et. al.* [37, 38].

In recent years, Martins and Dahleh [39, 40] present several information theoretic extensions of the Bode formula for LTI plants and a general class of control. A detailed comparison to these papers appears in Section IV.D of Chapter 2 .

Fundamental limitations in control of nonlinear systems is another problem of longstanding theoretical and practical interest; cf., [41] for an early reference. Several recent papers on flow and combustion control (see Banaszuk *et. al.* [15] and Rowley et. al. [42]) have highlighted their relevance in nonlinear and distributed settings. An information theoretic approach for nonlinear extension is pioneered in the work of Iglesias and co-workers [43, 44, 3]. Recent results on these extensions for nonlinear systems appear in Sun and Mehta [16, 45, 46]. For additional details on comparison to Iglesias's work, see Section III.A in [46].

Entropy is also relevant to the study of deterministic and stochastic nonlinear dynamical systems via methods of Ergodic theory; cf., [47]. One important notion is topological entropy, that is used to estimate the growth rate of the number of distinguishable orbits on taking finer and finer partitions of the phase space. In [48], Nair *et. al.* extend this to define topological feedback entropy (TFE) and express fundamental limitation results in nonlinear stabilization as bounds on TFE. Certain measure theoretic characterizations of entropy rates for this problem appear in Mehta et. al. [49].

Apart from Bode formula and its information theoretic extensions, fundamental performance limits have also been considered in terms of performance bounds with optimal control. One avenue of research has been the so-called *cheap control* framework pioneered by Kokotovic and co-workers [38, 37]. In [38], it is shown that fundamental limitation for the cheap control problem arise due to unstable zero dynamics. In linear settings, this limitation is related to a Bode-type integral formula for complementary sensitivity function. A dual result in terms of the Bode formula (2.2) for the sensitivity function is given in [37]. Additional details on the cheap control problem appears in Section 4.1 of Chapter 4.

1.2.2 Model Comparison

Metrics for comparing dynamic models are central to robustness analysis. For example, the H^∞ system norm is used in robust control [50]. Our focus is to study the robustness questions in terms of information theoretic metrics. The core idea comes from the recent work of T. Georgiou on the information geometry of spectral densities [51, 52, 53, 54].

Information based criterion for model comparison/reduction has a rich history in both statistics and control community. Akaike introduced the celebrated Akaike information criterion (AIC) for the purposes of statistical model identification [55]. In [56], a normalized maximum log likelihood function, referred to by the authors as the ambiguity function, is introduced for approximation of a time-varying linear system by an linear time-invariant (LTI) system. An algorithm is described to obtain the approximation by solving a min-max problem for the ambiguity function.

The Kullback-Leibler (K-L) distance is commonly used for comparing probability densities. Suppose one considers system identification of model parameters by using the method of maximum likelihood. It turns out that the maximum likelihood or maximum a posteriori probability estimation minimizes asymptotically the K-L distance from the empirical distribution of the time-series data produced by the true model [57]. The K-L rate and the related maximum log likelihood criterion appears in hypothesis testing [58, 59], statistical inference [60], model identification [61], and nonlinear filtering [57]. A variant of the classical K-L rate is considered in [62] for model reduction of open- and closed-loop LTI distributed-parameter systems. An extension to continuous time systems is given in [63]. A related approach based on matching the Markov parameters of the full order and reduced order system, the so called q-cover technique, appears in [64]. A metric based on difference of conditional entropies is introduced and used for model reduction in [65].

The use of K-L divergence rate as a metric for model comparison recently appears in Deng et. al. [66] and in Vidyasagar et. al. [67], as well as in the extension of Sanov's theorem to Markov chains [68, 69]. The focus of [66] is on aggregation-based methods for model reduction of Markov chain models. In [67], the K-L divergence rate metric is used to quantify the disparity between multi-step Markov models of coding regions in genomes.

1.2.3 Fundamental Performance Limitation with Kullback-Leibler Control Cost

The study of fundamental performance limitation based on optimal control formulation appears in Seron *et. al.* [70, 37]. Using the so-called *cheap control* formulation, it is shown that fundamental limitations arise due to the unstable zero dynamics. For the LTI case, a connection is made to the Bode integral formula for the complementary sensitivity function (see [70] and also Qiu-Davison [71]). Other works along this line includes the work of R. H. Middleton and J. H. Braslavsky [72], where the link between logarithmic sensitivity integrals and limiting optimal control problems are studied. In the work of Graham C. Goodwin *et. al.* [73], the authors investigated optimal performance limitations for linear feedback control systems, as specified by the $\mathscr{L}_2$ norm of the output, in the presence of stochastic plant uncertainty.

The use of Kullback-Leibler metric is motivated by the recent work of Todorov [74, 75], and by the recent papers on information theoretic extensions of the Bode formula [39, 3, 46]. Kullback-Leibler control cost is seen to be a generalization to the work of H.J.Kappen, where a class of nonlinear control problems are formulated as a path integral and computed by Monte Carlo integration or Laplace approximation.

Under the K-L cost structure, the HJB equation reduces to linear eigenvalue problem [75]. This eigenvalue problem is related to the eigenvalue problem that arises in the risk sensitive optimal control problem [76]. In Fleming and McEneaney [77] and Fleming and Sheu [78], asymptotic formulae for the principle eigenvalue of a certain linear operator are considered in the small-noise limit. The linear operator is obtained from consideration of a risk sensitive

optimal control problem and the value of the principal eigenvalue is related to the optimal cost. Using the so-called logarithmic transformation, the eigenvalue is also seen as an optimal cost for an average cost optimal control problem; cf., Chapter VI in [79].

1.3 Overview of Contributions

In this section, we summarize contributions of our work on fundamental limitation analysis (Section 1.3.1, and 1.3.3) and model comparison (Section 1.3.2).

1.3.1 Bode-like Fundamental Performance Limitations

In our paper [46], we proposed a hidden Markov model (HMM) framework for establishing Bode-like fundamental limitations for the disturbance rejection problem in nonlinear dynamical systems. In particular, we show that analysis of the asymptotic dynamics of the belief process can be used for evaluating these limitations (right-hand side of the Bode formula for the LTI system) as entropy rate of the output process.

The closed-loop system is defined for a signal $\mathbf{s}_t \doteq (\mathbf{x}_t, \mathbf{y}_t)$ comprising of the (hidden) state $\mathbf{x}_t \in X \subset \mathbb{R}^m$ and the output $\mathbf{y}_t \in Y \subset \mathbb{R}^1$, where t is the discrete time. By assuming an i.i.d model of disturbance, the signal process $\{\mathbf{s}_t\}$ is a Feller-Markov process that is additionally assumed to be ergodic. To compute the entropy rate of interest (in (2.2)), the key idea is to consider the so-called belief process – conditional pdf of $\mathbf{s}_t$ given the history of past observations due to output. The belief process is constructed using the recursive Bayesian estimation (nonlinear filter) for the signal process $\{\mathbf{s}_t\}$. Formally, the entropy rate expresses average uncertainty in the belief. Under suitable technical conditions (pertaining to ergodicity of the filter [80, 81, 82, 83]), this is made precise by using the Blackwell's integral entropy formula [84].

With the aid of this framework, we obtain several novel extensions and interpretations of the Bode formula:

1. Bode formula is intrinsically related to uncertainty associated with estimation (filtering problem) and *not* the stabilization of an equilibrium (control problem). For example, Bode-like performance limitations (in terms of extra entropy) arise even if the equilibrium is not stable but the state of the closed-loop system remains bounded.

2. There are no limitations due to dynamics if the plant (nonlinear dynamical system) is contractive. The Bode formula for open-loop stable dynamics is a special case of this general result. Here, a Lyapunov function can be used to define a contractive norm.

3. The performance limitations for LTI plants with Gaussian disturbance is easily understood using equations of Kalman filtering. For the general LTV case, a counterpart of Bode formula arises with positive Lyapunov

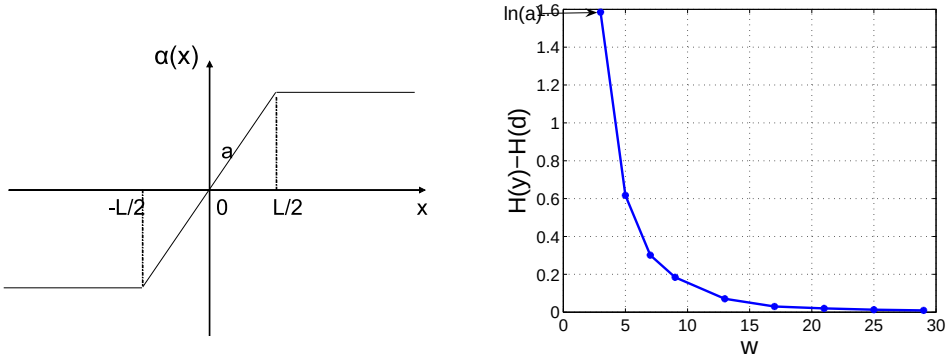

(a) (b)

Figure 1.1: (a) Non-uniform dynamics $\alpha(x)$ and (b) Plot of numerically computed entropy rate.

exponents. There are no additional limitations due to dynamics for the LTV case with negative Lyapunov exponents.

4. For the case of non-uniform expansion, we gave some asymptotic results for a special choice of dynamics (expansion+saturation). It is shown that the performance limitations arise only due to disturbance in the limit of very large disturbance. A simple example is described in the following to illustrate this result.

Consider a scalar nonlinear system $\mathbf{x}_{t+1} = \alpha(\mathbf{x}_t) + u_t$, where x is the state and u is the control input. $\alpha(x)$ is a continuous function that is linear for small values of x, saturates for large values of x, and has $\alpha(0) = 0$ and $a \doteq |\alpha'(0)| > 1$ (see Fig. A.2(a)). So control is necessary to stabilize the equilibrium at 0. The control input is determined by causal measurements of the output $\mathbf{y}_t = \mathbf{x}_t + \mathbf{d}_t$ where $\mathbf{d}_t$ is i.i.d. noise (disturbance) and takes values from a uniform distribution in the interval $[-w, w]$. For a given control law $u_t = k(\mathbf{y}_t)$, these equations describe a nonlinear feedback system.

For this example, there are two sources of uncertainty that fundamentally affect the performance of the feedback system: *uncertainty due to disturbance* ($\mathscr{H}(\mathbf{d})$) that scales according to the size of the disturbance (w), and *uncertainty due to dynamics* (see the Bode formula 2.2). For a linear system, the fundamental limitation is expressed in terms of the entropy rate $\mathscr{H}(\mathbf{y}) = \mathscr{H}(\mathbf{d}) + \ln(a)$, where $\ln(a)$ is the uncertainty due to dynamics. This formula also holds for the example considered here *provided* the disturbance is sufficiently small – so a stabilizing control keeps the dynamics in a linear regime. With large disturbance, however, the uncertainty due to dynamics decreases due to the interplay between nonlinearity (saturation) and disturbance. In particular as $w \to \infty$, the performance limitation was proved to arise *only* due to the disturbance, i.e., $\mathscr{H}(\mathbf{y}) \downarrow \mathscr{H}(\mathbf{d})$. Figure A.2(b) gives a plot of numerically computed entropy rate for the example.

1.3.2 Model Comparison

Our work on model comparison is motivated by Tryphon Georgiou's recent paper [53] where he considers the problem of comparing power spectral densities. Georgiou bases his considerations on a prediction (filtering) based approach. The main idea is to measure distance between spectral densities in terms of prediction error. With the correct spectral density $S_1(e^{j\omega})$ of a random process, the optimal prediction error is given by the celebrated Kolmogorov-Szego formula:

$$\varepsilon = \exp\left(\frac{1}{2\pi}\int_{-\pi}^{\pi} \ln S_1(e^{j\omega})d\omega\right) \tag{1.2}$$

where ε denotes the variance of the prediction error. To measure distance between spectral densities, Georgiou proposes a pseudo-metric as $\ln(\rho)$. The quantity ρ denotes the ratio of the prediction error obtained with an assumed (incorrect) spectral density S_2 to the one obtained with the correct spectral density S_1. The spectral densities here are used to construct an optimal filter for a random process that is generated according to the correct spectral density. The metric proposed by Georgiou serves to quantify the degradation of prediction error due to an (incorrect) assumption on the spectral density. Certain frequency domain formulae are given that lead to a straightforward method for evaluation of the metric for any two densities S_1 and S_2.

The key idea in Georgiou's work is to compare systems via a prediction based approach. If one agrees that a model is a representation of reality (some causal input-output relationship) then it is meaningful to quantify the goodness of the model in terms of the fidelity of its prediction. The degradation of prediction error results from the incorrect assumption on the model, and is therefore used to characterize the deviation of the assumed model to the true model. This is closely related to the robust estimation literature[85, 86, 87].

In our paper [88], we follow the idea in Georgiou's work. Since we are concerned with dynamic processes here, a filtering based approach is used to take into account all the available data – in this case, the time history of the past observations. The timely significance of ideas in [53] and here is due to the strong information theoretic flavor of the proposed metrics. Georgiou uses the metric $\ln(\rho)$ to describe the information geometry of the space of spectral densities [53]. We show that $\ln(\rho)$ is in fact closely related to the information theoretic metric of Kullback-Leibler (K-L) rate that is used to compare stochastic processes. The overall theme fits in nicely with recent attempts to build bridges between information and control theory; cf. [4] and references therein.

Central to the considerations of our work is the notion of *uncertainty*. In particular, we compare systems in terms of additional uncertainty that results for the prediction problem with an incorrect choice of the model. While [53] used variance of the prediction error, we quantify the additional uncertainty in terms of the K-L rate. From an information theory perspective, this makes sense because the K-L rate after all is a measure of uncertainty due to incorrect choice of model; cf., [89]. From a control theory perspective, the starting point for us is the Kolmogorov-Bode formula (2.2).

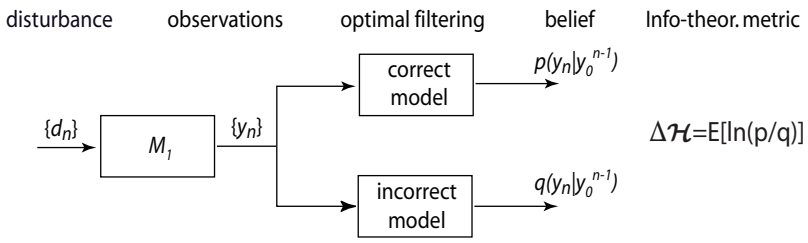

Figure 1.2: Prediction-based comparison of dynamical systems: $\{\mathbf{y}_t\}$ is an output process for dynamical system M_1. $p(\mathbf{y}_t|\mathbf{y}_0^{t-1})$ is the belief (conditional pdf) with correct model M_1; $q(\mathbf{y}_t|\mathbf{y}_0^{t-1})$ is the belief with (incorrect) model M_2. Entropy $\mathscr{H} = -\mathsf{E}[\ln(p)]$ is the average uncertainty in predicting $\mathbf{y}_t$ if the model (M_1) is known; K-L rate $\Delta\mathscr{H} = \mathsf{E}[\ln(\frac{p}{q})]$ is the additional uncertainty that results with an incorrect model (M_2).

The prediction-based methodology outlined in this paper extends the Kolmogorov-Bode formula for model comparison and robustness analysis. Figure 3.1 presents the methodology. The prediction problem is considered with the aid of the so-called belief process $p(\mathbf{y}_t|\mathbf{y}_0^{t-1})$, the conditional probability distribution function (pdf). In the Bode formula (2.2), the entropy rate $\mathscr{H}(\mathbf{y}) = \mathsf{E}[-\ln(p(\mathbf{y}_t|\mathbf{y}_0^{t-1}))]$ is a measure of the nominal uncertainty in the belief with an exact knowledge of the dynamic model [16]. With an assumed (possibly incorrect) belief, $q(\mathbf{y}_t|\mathbf{y}_0^{t-1})$, the entropy rate equals $\mathsf{E}[-\ln(q(\mathbf{y}_t|\mathbf{y}_0^{t-1}))]$. The Kullback-Leibler (K-L) rate is defined as the difference between the two rates,

$$\Delta\mathscr{H}(\mathbf{y}) = -\mathsf{E}[\ln(q)] + \mathsf{E}[\ln(p)].$$

The K-L rate captures the additional uncertainty that results due to an incorrect choice of the dynamic model. It thus provides a measure of degradation of prediction performance due to modeling error.

Since the belief process is well defined for nonlinear systems, we can utilize the K-L rate to consider model reduction issues in such systems. Model reduction in terms of belief process directly is shown to lead to the so-called *optimal prediction model* that appear in the recent work of Chorin [90] and Meyn [91]. For the particular case of linear systems, these considerations can be applied to obtain a solution of the model reduction problem for auto regressive (AR) models. We also used the K-L rate to obtain formula for stochastic linearization of a nonlinear dynamical system. Additional details appear in our paper [88].

1.3.3 Fundamental Performance Limitation with Kullback-Leibler Control Cost

The work in Chapter 4 is partly motivated by the optimal control analogue of the Bode sensitivity integral in a technical report by Seron [37]. For a single-input feedback system, the optimal control problem is to find a state-feedback control u which minimizes the functional:

$$J_\varepsilon = \frac{1}{2}\int_0^\infty (\varepsilon x(t)^T x(t) + u(t)^2)dt, \tag{1.3}$$

where $\varepsilon > 0$ is small. As $\varepsilon \to 0$, the limiting optimal cost J_0^* is used to express the fundamental limitation: it reflects the minimum control effort needed to drive the system state $x(0)$ to the origin. This problem and the cheap control problem are seen to be dual to each other [37].

We consider fundamental limitation in control of discrete time nonlinear systems by posing an average cost optimal control problem. The control objective is to minimize

$$J_\varepsilon = \lim_{N\to\infty} \frac{1}{N} \mathsf{E}[\sum_{t=0}^{N-1} \{\varepsilon c(\mathbf{x}_t) + \mathrm{KL}(q(\mathbf{x}_{t+1}|\mathbf{x}_t) \| p(\mathbf{x}_{t+1}|\mathbf{x}_t))\}],$$

where $c(x) \geq 0$, and $\varepsilon > 0$ is small. The usual quadratic control cost metric (the term u^2) is replaced by an information theoretic Kullback-Leibler (K-L) divergence metric.

$$\mathrm{KL}(q\|p) = \mathsf{E}[\ln(\frac{q}{p})],$$

where $q = q(x'|x)$ is the transition kernel (conditional probability density function (pdf)) for the closed-loop dynamics, and $p = p(x'|x)$ is the transition kernel for the open-loop dynamics.

The minimal average cost is denoted as J_ε^* and J_0^* denotes the limit as $\varepsilon \to 0$. As in [37], the fundamental limitation is expressed in terms of the value of J_0^*. A contribution of this work is to show that the fundamental limitation (value of J_0^*) can be obtained via analysis of the following linear eigenvalue problem (see also [74, 92])

$$\lambda_0 Z_0(x) = \mathsf{E}_{p(x'|x)}[Z_0(x')],$$

which depends only upon the open-loop dynamics $p(x'|x)$. Here $Z_0(x)$ is an auxiliary function defined in Chapter 4.

For a LTI system, the limitation is shown to be given by $J_0^* = \sum_k \ln|p_k|$, where p_k are the unstable poles. And $J_0^* = 0$ as the open-loop system is asymptotically stable. This is consistent with the Bode formula. However, it is shown that for the general nonlinear systems, $J_0^* = 0$ if the open-loop dynamics are ergodic. *The limitations thus arise only if the open-loop dynamics are non-ergodic*.

The fact that there are no fundamental limitations in control of ergodic open-loop dynamics is consistent with the *control of chaos* papers in the Dynamical Systems literature. There have been several studies such as the Ott-Grebogi-Yorke (OGY) method of controlling chaos which seek to exploit nonlinear dynamics for the purpose of stabilization: "*Assuming the motion of the free-running (uncontrolled) chaotic orbit to be ergodic, eventually the chaotic wandering of an orbit trajectory will bring it close to the chosen unstable periodic orbit or steady state. When this occurs, we can apply small controlling perturbations to direct the orbit to the desired periodic motion or steady state [93].*"

1.3.4 Optimal Sensor Location Design for Tracking Agents with Uncertain Dynamics

In Chapter 5 we consider in-building monitoring systems with spatially distributed sensors. The goal is to estimate the location of the agents in a building utilizing knowledge about their dynamics and the information collected from various types of sensors, including video cameras, CO_2 sensors and motion sensors. A particular application is the estimation of location of people during emergency evacuation (egress) [94].

In such applications complexity is a common difficulty, arising from both the uncertain dynamic nature of agent movement, and the large number of sensors [95, 96]. This makes the task of finding an "optimal" locations of the sensors a challenging problem. In recent years, this problem is of interest to the wireless sensor networks community [97, 98, 99]. In [98], the authors propose an approach to optimize sensor locations for localization of a target at a fixed location. In [97], certain heuristics are proposed for choosing sensor location that leads to maximum entropy reduction of the posterior target location distribution. In [100, 99], combinatorial optimization based approaches are considered for choosing sensor locations in order to maximize mutual information while maintaining constraints on communication quality among sensors.

Our work is focused on addressing the challenges posed by non-linear and uncertain dynamics in solving the sensor location design problem. To this end, we consider models of dynamics as a Markov chain on a finite graph. Apart from models of agent movement [101, 94], such Markov models have been used for simulating traffic in buildings, planes, and outdoor walkways [101, 102, 103, 104, 105]. Markov chains on finite graphs are also obtained after discretizing a nonlinear dynamical system over a bounded domain [106], and as such represent a useful paradigm for modeling nonlinear dynamics.

We measure the quality of an estimate at a certain time in terms of uncertainty – conditional entropy of the state given the history of past observations. To evaluate the performance of a given choice of sensor locations, we propose the time-cumulative uncertainty in the state estimates. One important feature of this metric is that it is algorithm-independent: it provides a lower bound on uncertainty for any algorithmic implementation of the estimator. Computation cost of this metric, however, is in general high since it involves entropy rates of Hidden Markov Model (HMM)s, which are costly to compute [107]. To address this issue, we derive certain upper bounds that are much easier to compute. These bounds are tight under certain conditions on the dynamics that are relevant to the building evacuation problem. Numerical investigations show that even when the bounds are not tight, they are close to the true metric, so that optimal sensor locations can be designed by optimizing over the bound. Computation of the bound takes a fraction of the time needed to estimate the true metric using Monte Carlo simulations.

1.3.5 Convergence Rate For Distributed Optimization Methods

In Chapter 6 we consider the convergence rate of consensus subgradient methods [108, 109, 110, 111] over large networks. The consensus subgradient methods is suitable for solving the following convex optimization problem defined on a network of n agents:

$$\min_{x \in C} \frac{1}{n} \sum_{i=1}^{n} f_i(x), \tag{1.4}$$

where $x \in \mathbb{R}^m$ is the decision variable, C is a convex constraint set, and each convex function $f_i : \mathbb{R}^m \to \mathbb{R}$ is associated to a particular agent i in the network. The network topology is specified by an undirected graph $G = (V, E)$. Such networked optimization problem arises in a broad range of applications, e.g., in distributed estimation [112, 113, 114], resource allocation in communication networks [115, 116, 117, 118], distributed Model Predictive Control [119], etc.

In consensus subgradient method, each agent maintains an estimate of the solution and updates it iteratively by exchanging messages with neighbors. Our goal is to understand the impact of graph topology on the convergence rate of consensus subgradient algorithm. In a recent work on distributed dual averaging algorithm [120], Duchi *et. al.* obtained a bound for the convergence rate explicitly in terms of the spectral gap of the network. In this chapter we establish similar results for unconstrained consensus subgradient algorithm, where the step size is constant. A tighter bound on the second term is provided using the spectral gap of the graph, which compares favorably to previous results [108, 109]. For large networks with poor connectivity, based on the observation that the Markov chains for such networks usually mix faster for small t, we proposed a much improved bound in which the dependence on size of graph n is also eliminated.

We also discussed the distributed computation of this bound, which requires estimation of the spectral gap of the graph in a distributed fashion. We describe a novel distributed algorithm based on the simulation of the wave equation on a graph. This algorithm is in general much faster than consensus based algorithms, and provides provably correct estimates of the spectrum of a graph [121, 122].

Chapter 2

Bode-like Performance Limitation for Feedback Control of Nonlinear Systems

2.1 Introduction

The fundamental limitations in the classical control settings address closed-loop system trade-offs and best possible performance with causal stabilizing feedback. One important result is the Bode integral formula

$$\frac{1}{2\pi}\int_{-\pi}^{\pi}\ln|S(e^{i\omega})|d\omega=\sum_{k}\ln|p_k|, \tag{2.1}$$

where $S=\frac{1}{1+PC}$ is the sensitivity transfer function of the closed-loop (see Fig. 2.1) from the disturbance $\mathbf{d}$ to the output $\mathbf{y}$. Here, it is assumed that S is stable and that there are no unstable pole-zero cancelations in the loop PC. In the right-hand side, p_k are unstable poles (i.e., $|p_k|>1$) of the open-loop (both plant and control); see Sung and Hara [1] for an early reference on the Bode formula (2.1) for discrete-time LTI systems. Entropy rate of the signals in the feedback loop help provide another interpretation of the Bode integral formula:

$$\mathscr{H}(\mathbf{y})-\mathscr{H}(\mathbf{d})=\frac{1}{2\pi}\int_{-\pi}^{\pi}\ln|S(e^{i\omega})|d\omega, \tag{2.2}$$

where S now is any stable transfer function between the input $\mathbf{d}$ and the output $\mathbf{y}$. Here, $\mathscr{H}(\mathbf{y})$ and $\mathscr{H}(\mathbf{d})$ denote the entropy rates (see [123, 89]) of the random processes associated with the output $\mathbf{y}$ and disturbance $\mathbf{d}$ respectively. Combining (2.1) with (2.2), the open-loop unstable poles are seen to lead to a positive entropy rate. Iglesias [43] was one of the first to point out the connection between (2.1) with (2.2) as a way to investigate fundamental limitations in general settings. As noted in [43] and in Zang and Iglesias [3], the entropy rates are well-defined even in time-domain and provide for a framework for studying fundamental limitations in nonlinear systems.

In recent years, several studies have considered information theoretic extensions and interpretations of the Bode formula. Martins and Dahleh [39, 40] present several extensions of the Bode formula for linear time-invariant (LTI) plants and a general class of control. These information-theoretic extensions have been particularly relevant to control problems over networks. One closely related result is the so-called data rate theorem: the rate of instability of the open-loop plant must be compensated by the information transmission rate over the communication channel in any

stabilizing feedback [6]. In particular, the right-hand side of (2.1), $\sum_k \ln|p_k|$, reflects the minimal data rate required to stabilize an unstable LTI system over a feedback channel [6, 40]. Related results on performance limitations with communication constraints due to limited channel capacity appear in [21, 7, 28].

Generalization of Bode formula to express fundamental limitations in control of nonlinear systems is another problem of longstanding theoretical and practical interest; cf., [41] for an early reference. Several recent papers on flow and combustion control (see [124, 125] and references therein) have highlighted not only the universality of Bode-like limitations but also the need to study these questions in general nonlinear and distributed settings. An information theoretic approach for nonlinear extension is pioneered in the work of Iglesias and co-workers; cf., [43, 44, 3]. The paper [44] treats the linear time-varying (LTV) case while in [3], the authors derive certain entropy estimates for globally exponentially stable closed-loop system that additionally has certain minimum phase and fading memory properties.

Entropy is also relevant to the study of deterministic and stochastic nonlinear dynamical systems via methods of ergodic theory; cf., [47]. One important notion is topological entropy, that is used to estimate the growth rate of the number of distinguishable orbits on taking finer and finer partitions of the phase space. In [48], Nair *et. al.* extend this to define topological feedback entropy (TFE) and express fundamental limitation results in nonlinear stabilization as bounds on TFE. Certain measure theoretic characterizations of entropy rates for this problem also appear in our own earlier paper [49].

In this chapter, we propose a hidden Markov model (HMM) framework for characterizing fundamental limitations in the SISO nonlinear disturbance rejection problem. The closed-loop system is defined for a signal $\mathbf{s}_n \doteq (\mathbf{x}_n, \mathbf{y}_n)$ comprising of the (hidden) state $\mathbf{x}_n \in X \subset \mathbb{R}^m$ and the output $\mathbf{y}_n \in Y \subset \mathbb{R}^1$. By assuming an i.i.d model of disturbance, the signal process $\{\mathbf{s}_n\}$ is a Feller-Markov process that is additionally assumed to be ergodic. To compute the entropy rate of interest (in (2.2)), the key idea is to consider the so-called belief process – conditional pdf of $\mathbf{s}_n$ given the history of past observations due to output. The belief process is constructed using the recursive Bayesian estimation (nonlinear filter) for the signal process $\{\mathbf{s}_n\}$. Formally, the entropy rate expresses average uncertainty in the belief. Under suitable technical conditions (pertaining to ergodicity of the filter [80, 81, 82, 83]), this is made precise by using the Blackwell's integral entropy formula [84].

With the aid of this framework, we obtain several novel extensions and interpretations of the Bode formula. For nonlinear contractive dynamics (dynamical systems with Lipschitz constant less than 1), we show that there are no limitations due to dynamics, i.e., the right-hand side of (2.1) is zero (Theorem 2.3.4 and the Corollary 2.3.8). For linear time invariant (LTI) dynamics, we obtain the Bode formula for general class of control (as in [40]) and furthermore relate the formula to Kalman filtering (Theorem 2.4.2). For linear time varying (LTV) dynamics, we provide an extension of the Bode formula for two cases: one where the Lyapunov exponents are all negative (Theorem 2.4.4), and

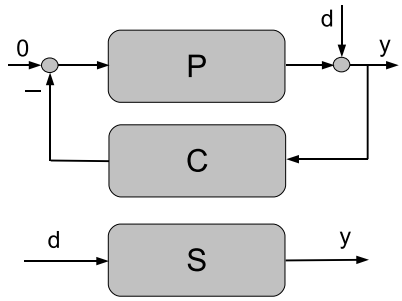

Figure 2.1: Feedback loop and the sensitivity transfer function

the other where they are all positive (Theorem 2.4.5). The proof of Theorem 2.4.5 is based on a direct information-theoretic argument. The problem of disturbance rejection with a general (non-contractive) nonlinear plant is discussed with the aid of an example. Certain fundamental estimates of the entropy rate are given for the large disturbance case (Theorem 2.5.1). Some numerical examples where entropy rates are computed using stochastic simulations are used to illustrate the various results and conclusions.

The outline of the remainder of this chapter is as follows. In Section 2.2, we cast the closed-loop dynamical system as a hidden Markov model (HMM) and connect the Bode formula to belief propagation. In Section 2.3 and 2.4, we present extensions of Bode formula for nonlinear contractive and linear dynamics respectively. In Sections 2.5, we present certain limiting entropy estimates for a specific non-contractive nonlinear example. A summary of main conclusions appear in Section 5.4. The numerical examples appear in Appendix A.1.

2.2 Control Problem Formulation

In this chapter, we consider the disturbance rejection problem for the following single-input-single-output (SISO) feedback system:

$$\text{state}: \quad \mathbf{x}_{n+1} = \alpha(\mathbf{x}_n) + \beta(\mathbf{u}_n) \doteq T(\mathbf{x}_n, \mathbf{u}_n), \tag{2.3}$$

$$\text{output}: \quad \mathbf{y}_n = c(\mathbf{x}_n) + \mathbf{d}_n, \tag{2.4}$$

$$\text{control}: \quad \mathbf{u}_n = k(\mathbf{y}_n) \tag{2.5}$$

where n is the discrete time step, $\mathbf{x}_n \in X \subset \mathbb{R}^m$ is the state, $\mathbf{y}_n \in Y \subset \mathbb{R}^1$ is the output, $\mathbf{d}_n \in \mathbb{R}^1$ is i.i.d. disturbance, and $\mathbf{u}_n \in U \subset \mathbb{R}^1$ represents the control input. The structure is general: state equations are assumed to include dynamics due to both plant and control, and $T : X \times U \to X$, $\beta : U \to \mathbb{R}^m$, $c : X \to \mathbb{R}^1$ and $k : Y \to U$ are discrete-time maps. Additional technical assumptions pertaining to stability, controllability, and observability will be made as needed in

the following sections. For now, the main assumptions are: 1) α is C^1 and invertible, 2) $\mathbf{u}_n$ and $\mathbf{y}_n$ are scalar discrete-time signals, 3) control enters in an additive fashion to the state equation, and 4) the disturbance enters in an additive fashion to the output equation. The assumed structure is motivated by applications in flow and combustion control (see Appendix A.1 and also [124]).

The closed-loop system (2.3)-(2.5) is expressed as a composition of deterministic and stochastic maps:

$$\begin{array}{c} X \times Y \xrightarrow{K} X \times U \xrightarrow{T} X \xrightarrow{D} X \times Y \\ (\mathbf{x}_n, \mathbf{y}_n) \longrightarrow (\mathbf{x}_n, k(\mathbf{x}_n)) \longrightarrow \mathbf{x}_{n+1} \longrightarrow (\mathbf{x}_{n+1}, \mathbf{y}_{n+1}) \end{array} \tag{2.6}$$

$K(\mathbf{x}_n, \mathbf{y}_n) \doteq (\mathbf{x}_n, k(\mathbf{y}_n))$ is the control map, $T(\mathbf{x}_n, \mathbf{u}_n) \doteq \alpha(\mathbf{x}_n) + \beta(\mathbf{u}_n)$ represents the effect of dynamics, and $D(\mathbf{x}_n) \doteq (\mathbf{x}_n, c(\mathbf{x}_n) + \mathbf{d}_n)$ is the random dynamical system due to the i.i.d disturbance. We denote $\mathbf{s}_n \doteq (\mathbf{x}_n, \mathbf{y}_n)$ to be an element of the joint state space $S \doteq X \times Y$. For $\mathbf{s}_n \in S$, $T_c \doteq D \circ T \circ K$ defines the closed-loop system:

$$\mathbf{s}_{n+1} = T_c(\mathbf{s}_n). \tag{2.7}$$

For a general nonlinear closed-loop system (2.3)-(2.5), we assume that the disturbance $\{\mathbf{d}_n\}$ has bounded support, and X and Y are compact sets. The initial condition $\mathbf{x}_0 \in X$ but may be unknown. For linear systems, we will relax the assumption on compactness of these sets but assume a certain weak notion of stability termed as entropic stability (see Definition 2.2.2). If X is compact, entropic stability automatically holds.

This formalism is useful because on the joint space S, the *signal* $\{\mathbf{s}_n\}$ is a Markov process:

$$\text{Prob}(\mathbf{s}_n | \mathbf{s}_0^{n-1}) = \text{Prob}(\mathbf{s}_n | \mathbf{s}_{n-1}),$$

where $\mathbf{s}_0^{n-1} \doteq \{\mathbf{s}_0, \mathbf{s}_1, \ldots, \mathbf{s}_{n-1}\}$. We analyze the dynamics of the closed-loop system by considering the evolution of probability density function (pdf) $l_n(x,y)$ on S. The space of pdfs on S, endowed with a weak convergence topology, is denoted as ∇_S ($\pi_n \xrightarrow{*} \pi$ if $< \phi, \pi_n > \rightarrow < \phi, \pi >$ for all $\phi \in C(S)$, where $< \phi, \pi > \doteq \int_S \phi(x,y)\pi(x,y)dxdy$ and $C(S)$ is the space of continuous functions on S). $\mathbb{P}_c$ is used to denote the Markov transition operator for the signal process (closed-loop map T_c in (2.7)).

In the remainder of this chapter, we assume a unique (physical) invariant measure μ^* for $\mathbb{P}_c$ (i.e., the signal process of the closed-loop system is assumed to be ergodic).

For numerical computation of entropy rates, we consider also the discrete state-space counterpart of (2.6). The underline notation (e.g., $\underline{\mathbf{x}} \in \underline{X}$) is used to denote discrete variables. Analogous to the continuous state space case, $\underline{\mathbf{x}}$ and $\underline{\mathbf{y}}$ denote the state and the output, respectively. Their state spaces $\underline{X}$ and $\underline{Y}$ are finite-dimensional and obtained by discretizing (quantizing) the continuous state spaces X and Y. Additional details on the discretization appear in the

Appendix A.1.

2.2.1 Belief Propagation in Closed-loop System

The objective of this chapter is to obtain formula for the entropy rate

$$\mathscr{H}(\mathbf{y}) = \lim_{N\to\infty} \frac{1}{N} \sum_{n=0}^{N-1} H(\mathbf{y}_n|\mathbf{y}_{n-1},\ldots,\mathbf{y}_0), \tag{2.8}$$

of the output process $\{\mathbf{y}_n\}$, where $H(\mathbf{y}_n|\mathbf{y}_{n-1},\ldots,\mathbf{y}_0)$ denotes the differential entropy (see [123]). An estimate of entropy rate will be obtained by constructing the so-called belief process $\pi_n(x,y) \in \nabla_S$. It is the conditional pdf of the joint process $\{\mathbf{s}_n\}$, where the conditioning is due to the history of observations $\mathbf{y}_0^{n-1} \doteq \{\mathbf{y}_{n-1},\ldots,\mathbf{y}_0\}$. Let $f_n(x) = \int_Y \pi_n(x,y)dy$ denote the marginal on the state space X. Since disturbance is taken to be i.i.d. with pdf $q(\cdot)$, the conditional pdf of the output $p(y|x) = q(y-c(x))$; the symbol $p(\cdot)$ is reserved to denote a pdf. As a result, we have a representation

$$\pi_n(x,y) = f_n(x)\cdot q(y-c(x)). \tag{2.9}$$

From $n \to n+1$, the belief evolves in two steps:

$$\text{conditioning:} \quad \hat{f}_n(x) = \frac{f_n(x)\cdot q(\mathbf{y}_n - c(x))}{\int_X f_n(x)\cdot q(\mathbf{y}_n - c(x))dx} \tag{2.10}$$

$$\begin{aligned}\text{dynamics:} \quad f_{n+1}(x) &= \frac{1}{|J(x)|}\hat{f}_n(\alpha^{-1}(x-\beta(\mathbf{u}_n))) \\ &\doteq \quad \mathbb{P}^{u_n}\hat{f}_n(x),\end{aligned} \tag{2.11}$$

where $\mathbf{y}_n$ is the current output, $\mathbf{u}_n = k(\mathbf{y}_n)$ is the control, $J(x) = \frac{d\alpha}{dx}(x)$ is the Jacobian matrix and $|\cdot|$ denotes the determinant. The operator $\mathbb{P}^{u_n}$ is the stochastic counterpart of the dynamical system T in (2.3). In deterministic settings, it is referred to as the Perron-Frobenius (P-F) operator (see [126]).

These equations represent the recursive Bayesian estimation (nonlinear filter) for the HMM corresponding to the closed-loop system (2.3)-(2.5). Using representation (2.9),

$$\pi_{n+1}(x,y) = f_{n+1}(x)\cdot q(y-c(x)). \tag{2.12}$$

Equations (2.9)-(2.12) describe the evolution of the belief process from $n \to n+1$. It is a random dynamical system (RDS) because the evolution depends upon the value of $\mathbf{y}_n$ that is random. We initialize the RDS with some distribution $f_0(x)$ with support on X.

To obtain the entropy rate in (3.10), the approach here is based on the method of Markov processes pioneered by Kunita [80]. In [80], it is shown that if $\{\mathbf{s}_n\}$ is a Feller-Markov process on a compact state space S then the belief process $\{\pi_n\}$ is a Feller-Markov process on the state space ∇_S. The operator Π is used to denote the Markov transition operator for the belief process (RDS (2.9)-(2.12)). The entropy rate can be expressed in terms of the invariant measure μ of Π, where μ exists because $\{\pi_n\}$ is Feller-Markov (see Theorem 3.1 in [80]).

Explicitly, the entropy rate

$$\begin{aligned}\mathscr{H}(\mathbf{y}) &= \lim_{N\to\infty}\frac{1}{N}\sum_{n=0}^{N-1} H(\mathbf{y}_n|\mathbf{y}_0^{n-1}) \\ &= \lim_{N\to\infty}\frac{1}{N}\sum_{n=0}^{N-1} \mathsf{E}[h_y(\pi_n)] \end{aligned} \tag{2.13}$$

where $\pi_n \in \nabla_S$ is the belief process at time n and $h_y(\pi) \doteq -\int g(y)\ln g(y)dy$ is the entropy function, where $g(y) = \int_X \pi(x,y)dx$ is the marginal on the output space Y. Note that $H(\mathbf{y}_n|\mathbf{y}_0^{n-1})$ is the expected value of a function of the belief process $h_y(\pi_n)$ and the entropy rate arises as a time-average. In [80], it is shown that if the invariant measure μ for Π is unique, then the time-average (2.13) can be obtained as

$$\begin{aligned}\lim_{N\to\infty}\frac{1}{N}\sum_{n=0}^{N-1}\mathsf{E}[h_y(\pi_n)] &= \int_{\nabla_s} h_y(\pi)\mu(d\pi), \\ \therefore,\ \mathscr{H}(\mathbf{y}) &= \int_{\nabla_s} h_y(\pi)\mu(d\pi). \end{aligned} \tag{2.14}$$

Although, the results of [80] are stated in continuous-time settings, we refer the reader to Budhiraja and Kushner (see Theorems 5.1, 5.2 in [82]) and Budhiraja [81] for discrete-time counterparts used here. The formula (2.14) is referred to as the integral formulation of the entropy rate. It is originally due to Blackwell for a Markov chain on a finite state-space [84].

The crucial assumption in using (2.14) thus is *the uniqueness of the invariant measure of* Π. For ergodic signals $\{s_n\}$, conditions for the same appear in [80, 127, 82, 81, 83]. One such condition is based on the following definition:

Definition 2.2.1 (see Def. 5.1 in [82])**.** *A filter* forgets its initial conditions *if for all* $f_0, f_0' \in \nabla_S$ *and for all* $\phi \in C(S)$*:*

$$\lim_{n\to\infty} |<\pi_n,\phi> - <\pi_n',\phi>| = 0,$$

where π_n, π_n' *denote the belief with initial condition* f_0, f_0' *respectively.*

In [82] (Theorem 5.1), it is shown that if the filter forgets its initial condition then Π has a unique invariant measure. So, formula (2.14) holds.

In this chapter, the entropy rate (3.10) is obtained using the formula (2.14). Apart from the technical conditions

of ergodicity for both signal and the belief process (existence and uniqueness of invariant measures μ^* and μ, respectively), we will require only a very weak form of stability for the closed-loop system:

Definition 2.2.2 (Entropic stability)**.** *Consider the closed-loop system (2.3)-(2.5). The closed-loop system is said to be entropic stable if:*

$$\sup_{\pi \in \mathscr{A}} h_x(\pi) < \infty,$$

where $h_x(\pi) = -\int_X f(x)\ln f(x)dx$ is the entropy function for the marginal $f(x) = \int_Y \pi(x,y)dy$ and $\mathscr{A}$ is the ω-limit set of the belief process ($\pi \in \mathscr{A}$ is any limiting conditional distribution $\lim_{n\to\infty} p(\boldsymbol{x}_n|\boldsymbol{y}_0^{n-1})$).

The assumption amounts to *choosing a control* such that asymptotic uncertainty in the state (after conditioning with respect to history of observations) remains bounded.

Example 2.2.3. *In general, the entropic stability of the closed-loop will depend upon the choice of the control and observability properties. In this example, we outline a few special case where it can be apriori established. In all instance, we assume that the uncertainty due to the i.i.d disturbance $\mathscr{H}(\boldsymbol{d})$ is bounded.*

1. *If one apriori knows that the state $\{\boldsymbol{x}_n\}$ remains bounded for all time then the entropic stability condition is trivially satisfied:*

   $$|\boldsymbol{x}_n| < M \Longrightarrow h_x(\pi) < \ln(M).$$

   As a result, the important case to consider is where the compactness assumption does not hold (as with Gaussian disturbance).

2. *Consider an LTI system with general i.i.d disturbance. Then observability of (A,C) implies entropic stability. The details of the straightforward calculation appear in the Appendix A.2.*

3. *Consider the LTI Gaussian case where (A,C) is observable. In this case, the marginal $f(x)$ is Gaussian with covariance matrix P that is obtained as a solution of the DARE (see Sec. 2.4.1). So, $h_x(\pi) = \frac{1}{2}\ln((2\pi e)^m|P|)$.*

4. *Consider the general LTV Gaussian case. Here, solution of the Kalman filtering equations need not converge to a single point (in the space of beliefs). Nevertheless, if (A_n,C) is stochastically observable (see pp. 106 in [128]) then the variances of the asymptotic estimates are known to be bounded. As a result, uncertainty $h_x(\pi)$ is bounded.*

To make these ideas precise, we consider belief propagation in the following simple scalar example:

$$\text{Linear state}: \quad \mathbf{x}_{n+1} = a\,\mathbf{x}_n + \mathbf{u}_n, \tag{2.15}$$

$$\text{Linear output}: \quad \mathbf{y}_n = \mathbf{x}_n + \mathbf{d}_n, \tag{2.16}$$

$$\text{Control}: \quad \mathbf{u}_n = k(\mathbf{y}_n), \tag{2.17}$$

where $k(\cdot)$ is an arbitrary deterministic map, and $\mathbf{d}_n$ is an i.i.d disturbance taken from a uniform distribution $q(\cdot) = \frac{1}{d}\chi_d(\cdot)$ – an indicator function of width d centered at 0. The Bode formula for this case is presented with the aid of the following theorem:

Theorem 2.2.4. *Consider the closed-loop system (2.15)-(2.17). The disturbance $\{\boldsymbol{d}_n\}$ is i.i.d with pdf $q(\cdot) = \frac{1}{d}\chi_d(\cdot)$ and initial condition $\boldsymbol{x}_0$ is uncertain with pdf $f_0(x) = \frac{1}{r_0}\chi_{r_0}(x-\hat{x}_0)$. The control law $k(\cdot)$ is an arbitrary deterministic map chosen so that $\boldsymbol{x}_n$ lies in a bounded set $X \subset \mathbb{R}^1$. Then*

$$\mathscr{H}(\boldsymbol{y}) = \mathscr{H}(\boldsymbol{d}) + \max\{\ln(|a|), 0\}.$$

Proof. With linear dynamics and uniform disturbance, $f_n(x) = \frac{1}{r_n}\chi_{r_n}(x-\hat{x}_n)$ where $\hat{x}_n$ is the estimate of the state $\mathbf{x}_n$. Using (2.9),

$$\pi_n(x,y) = \frac{1}{r_n}\chi_{r_n}(x-\hat{x}_n)\cdot\frac{1}{d}\chi_d(y-x). \tag{2.18}$$

Note $r_n \in [0, ad]$ for $n \geq 1$ because $q(\cdot)$ has width d.

We consider the $|a| > 1$ case first. The entropy rate is obtained by considering the Markov operator Π for the belief process:

$$\rho_{n+1}(\hat{r}) = \int_0^{ad} p(\hat{r}|r)\rho_n(r)dr, \tag{2.19}$$

where $p(\hat{r}|r)$ is the conditional pdf for the RDS $\mathbf{r}_n \to \mathbf{r}_{n+1}$, and ρ_n and ρ_{n+1} are densities for the widths $\mathbf{r}_n$ and $\mathbf{r}_{n+1}$ defined on $[0, ad]$; the details of this and the subsequent calculations appear in Appendix A.3. The invariant density (corresponding to μ) is obtained as the fixed-point of this equation and takes the form:

$$\rho(r) = \sum_{n=1}^{\infty} b_n r^n + b_0\delta(r-ad), \tag{2.20}$$

where $\delta(\cdot)$ denotes the Dirac delta function. Denoting $g(y) = \int_X \pi(x,y)dx$ to be the marginal of $\pi(x,y)$ in (2.18), the

entropy function

$$\begin{aligned} h_y(\pi) &= -\int_Y g(y)\ln g(y)dy \\ &= \begin{cases} -2\int_0^r \frac{x}{rd}\ln\frac{x}{rd}dx - \int_r^d \frac{1}{d}\ln\frac{1}{d}dx & d \geq r \\ -2\int_0^d \frac{x}{rd}\ln\frac{x}{rd}dx - \int_d^r \frac{1}{r}\ln\frac{1}{r}dx & r \geq d \end{cases} \\ &= \begin{cases} \ln(d) + \frac{r}{2d} & d \geq r \\ \ln(r) + \frac{d}{2r} & r \geq d. \end{cases} \end{aligned} \tag{2.21}$$

We use $h(r,d)$ to denote the formula for $h_y(\pi)$ (right-hand side of (2.21)) and express entropy as:

$$\mathscr{H}(\mathbf{y}) = \int_{\nabla_S} h_y(\pi)d\mu(\pi) = \int_0^{ad} h(r,d)\rho(r)dr, \tag{2.22}$$

where $\rho(r)$ is the invariant density (2.20). Using (2.20) in (2.22) and after some calculations, one obtains the Bode formula

$$\mathscr{H}(\mathbf{y}) = \ln(|a|) + \ln(d). \tag{2.23}$$

The details of the calculations including formulas for $p(\hat{r}|r)$ and b_n appear in the Appendix A.3. The uniqueness of (2.20) is shown by explicitly constructing a Lyapunov function for Π.

For $|a| < 1$, the dynamics are contractive and $\mathscr{H}(\mathbf{y}) = \mathscr{H}(\mathbf{d})$. This result is proved for the general contractive case in Sec. 2.3. Since the argument is the same, we omit the discussion of this case. □

Besides analysis, considerations of this section are also useful for numerical evaluation (via discrete approximation of Markov operator) of the entropy rate in examples. A discrete counterpart of the Theorem 2.2.4 appears in the Appendix A.6.

2.3 Results For Contractive Dynamics

Definition 2.3.1. *A dynamical system (2.3) is contractive if there exists a Lipschitz constant $a \in [0,1)$ and a norm $\|\cdot\|$ in $\mathbb{R}^m$ such that*

$$\|\alpha(x_1) - \alpha(x_2)\| < a\|x_1 - x_2\|,; \quad for\ all\ x_1, x_2 \in X.$$

The scalar linear dynamics (2.15) in Theorem 2.2.4 is contractive if $|a| < 1$. Contractive maps are special because asymptotic dynamics of belief propagation can be easily characterized in this case. The key is the result given in the following Lemma. Before stating the result, we define first the concept of the diameter of a pdf.

Definition 2.3.2. *Let $f \in \nabla_X$ be a pdf on X with a bounded support, denoted as $supp(f)$. Then*

$$diam(f) = \sup_{x_1,x_2 \in supp(f)} \|x_1 - x_2\|,$$

for some given norm $\|\cdot\|$.

Lemma 2.3.3. *Consider a dynamical system (2.3) with the associated PF operator $\mathbb{P}^u$ for $u_n = u$. Suppose α is a contractive map with a Lipschitz constant $a \in [0,1)$ in a norm $\|\cdot\|$ in $\mathbb{R}^m$. Then*

$$diam(\mathbb{P}^u f) \leq a \cdot diam(f).$$

Proof. Suppose $y_1, y_2 \in \text{supp}(\mathbb{P}^u f)$. Let $x_1, x_2 \in X$ be their pre-images, i.e., $y_1 = \alpha(x_1) + u$ and $y_2 = \alpha(x_2) + u$, then $x_1, x_2 \in \text{supp}(f)$. Using the Lipschitz condition,

$$||y_1 - y_2|| < a \cdot \|x_1 - x_2\| \leq a \cdot \text{diam}(f).$$

Since y_1, y_2 are arbitrary, we have

$$\text{diam}(\mathbb{P}^u f) \leq a \cdot \text{diam}(f).$$

□

Theorem 2.3.4. *Consider the closed-loop system (2.3)-(2.5) where the map $\alpha(\cdot)$ is assumed to be contractive with a Lipschitz constant $a \in [0,1)$ in a norm $\|\cdot\|$, X is compact and the pdf $f_0(x)$ (representing uncertainty of initial condition $\mathbf{x}_0$) is supported on X. The disturbance process $\{\boldsymbol{d}_n\}$ is i.i.d with pdf $q(\cdot)$ and entropy $\mathscr{H}(\boldsymbol{d})$. The control $k(\cdot)$ is assumed to be a deterministic but otherwise an arbitrary map. Then*

$$\mathscr{H}(\boldsymbol{y}) = \mathscr{H}(\boldsymbol{d}). \tag{2.24}$$

Proof. We consider the evolution of belief process $\pi_n(x,y)$ and its marginal $f_n(x)$ according to (2.9)-(2.12) as described in Sec. 2.2.1. $\hat{f}_n(x)$ is used to denote the distribution after the conditioning step (see (2.10)). To obtain (2.24), it is sufficient to characterize the asymptotic dynamics for the diameter

$$\mathbf{r}_n \doteq \text{diam}(f_n(x))$$

The belief propagation induces a random dynamical system:

$$\mathbf{r}_n \overset{\text{conditioning}}{\longrightarrow} \hat{\mathbf{r}}_n \overset{\text{dynamics}}{\longrightarrow} \mathbf{r}_{n+1},$$

where $\hat{\mathbf{r}}_n = \text{diam}(\hat{f}_n(x))$. These dynamics arise as

$$\begin{aligned} \text{conditioning}: \quad \hat{\mathbf{r}}_n &= m_c(\mathbf{r}_n; \mathbf{y}_n, f_n) \\ \text{dynamics}: \quad \mathbf{r}_{n+1} &= m_d(\hat{\mathbf{r}}_n; \mathbf{u}_n, \hat{f}_n). \end{aligned} \tag{2.25}$$

The conditioning map m_c is time-dependent and random due to its dependence upon the random output $\mathbf{y}_n$. m_d is the map induced by the PF operator $\mathbb{P}^{u_n}$ (see (2.11)) where we recall that the control merely serves to shift the pdf $f_n(x)$. The semicolon notation is being used to draw attention to the fact that the maps also depend upon the pdfs.

Two crucial observations are:

1. Conditioning does not increase the diameter of the pdf, i.e., $\hat{\mathbf{r}}_n \leq \mathbf{r}_n$, and
2. $\mathbf{r}_{n+1} \leq a\hat{\mathbf{r}}_n$ because of the contraction assumption (see Lemma 2.3.3).

These two observations imply that

$$\mathbf{r}_{n+1} \leq a\mathbf{r}_n$$

and $\mathbf{r}_n \to 0$ as $n \to \infty$. As a consequence, the marginal $f_n(x)$ for the belief process asymptotes to a Dirac delta $\delta(x - \hat{\mathbf{x}}_n)$ as $n \to \infty$. So, asymptotic beliefs are of the form

$$\pi_n(x,y) = \delta(x - \hat{\mathbf{x}}_n) \cdot q(y - c(x)), \tag{2.26}$$

and the estimate $\hat{\mathbf{x}}_n = \mathbf{x}_n$, the state process.

The representation (2.26) of the asymptotic belief process also means that the filter forgets the initial condition $f_0(x)$. In particular for any $\phi \in C(S)$, asymptotically

$$< \pi_n, \phi >= \int_Y \phi(\mathbf{x}_n, y) q(y - c(\mathbf{x}_n)) dy$$

is independent of the initial distribution $f_0(x)$ (see Definition 2.2.1). Using Theorem 5.1 in [82], it follows that the limiting measure μ for the belief process is unique. Moreover, it is supported entirely on a set of measures π of the

form given in (2.26). It is then easy to verify that

$$h_y(\pi) = \int_Y q(y - c(\hat{\mathbf{x}}_n)) \ln(q(y - c(\hat{\mathbf{x}}_n)))dy = \mathscr{H}(\mathbf{d})$$

on each such π. Finally,

$$\mathscr{H}(\mathbf{y}) = \int_{\nabla_S} \mathscr{H}(\mathbf{d})d\mu = \mathscr{H}(\mathbf{d}).$$

□

For contractive dynamics, the attractor set $\mathscr{A}$ for the belief process lies in a subset $\mathscr{D} \subset \nabla_S$ whose arbitrary element $\pi = \delta(x - \hat{x}) \cdot q(y - c(x))$ for some $\hat{x} \in X$. We denote elements of $\mathscr{D}$ as $\pi_{\hat{x}}$ and consider the bijection $\theta : \mathscr{D} \to X$ where $\theta(\pi_{\hat{x}}) = \hat{x}$ and $\theta^{-1}(\hat{x}) = \delta(x - \hat{x})q(y - c(x))$. With these definitions, one can give an explicit characterization of the invariant measure μ of the belief process in terms of the invariant measure μ^* of $\{\mathbf{x}_n\}$. This is done with the aid of the following Lemma.

Lemma 2.3.5. *Assume the notation of the Theorem 2.3.4 where $\alpha(\cdot)$ is assumed to be contractive. Let μ denote the invariant measure for the belief process and μ^* the (physical) invariant measure (on X) for the closed-loop system (2.3)-(2.5). Then*

$$\mu(B) = \mu(B \cap \mathscr{D}) = \mu^*(\theta(B \cap \mathscr{D})) \tag{2.27}$$

for $B \in \mathscr{B}(\nabla_S)$.

Proof. We claim that if $\tilde{B} \in \mathscr{B}(X)$ then $\mu^*(\tilde{B}) = \mu(\theta^{-1}(\tilde{B}))$. The result then follows because μ is supported on $\mathscr{D}$ and $\theta : \mathscr{D} \to X$ is a bijection.

The claim is proved by using the *barycenter formula* for invariant measures originally due to Kunita (see Theorem 3.1 in [80], Proposition 4.5 in [81]):

$$\mu^*(\tilde{B}) = \int_{\nabla_S} < \chi_{\tilde{B}}(x), \pi(x,y) > d\mu(\pi),$$

where $\chi_{\tilde{B}}(x)$ denotes the indicator function with support on $\tilde{B} \in \mathscr{B}(X)$. Now, μ is supported on $\mathscr{D} \subset \nabla_S$ and we write

$$\mu^*(\tilde{B}) = \int_{\mathscr{D}} < \chi_{\tilde{B}}, \pi_{\hat{x}} > d\mu(\pi_{\hat{x}}), \tag{2.28}$$

where $\pi_{\hat{x}} = \delta(x - \hat{x}) \cdot q(y - c(x))$ denotes an arbitrary element of $\mathscr{D}$. It is straightforward to verify that

$$< \chi_{\tilde{B}}(x), \pi_{\hat{x}} >= \chi_{\tilde{B}}(\hat{x}) = \chi_{\theta^{-1}\tilde{B}}(\pi_{\hat{x}}).$$

Using this in (2.28), we have

$$\mu^*(\tilde{B}) = \int_{\mathscr{D}} \chi_{\theta^{-1}\tilde{B}}(\pi_{\hat{x}}) d\mu(\pi_{\hat{x}}) = \mu(\theta^{-1}\tilde{B}),$$

where we note that $\theta^{-1}\tilde{B} \subset \mathscr{D}$. The claim and the result follows. □

In the derivation of the entropy estimate, we did not make any assumption concerning observability of the pair $(\alpha(\cdot), c(\cdot))$. The primary reason for this is the bounded support assumption for the pdf $f_0(x)$. Such an assumption makes sense in part because the state space X is assumed to be bounded. If one relaxes the assumption of bounded initial support then one would require some form of observability condition for the dynamics. Some of these issues are discussed for the LTI systems in the following corollary and again in Sec. 2.4.

Corollary 2.3.6. *Consider a closed-loop system (2.3)-(2.5) with assumptions as in Theorem 2.3.4 where now the map $\alpha(x) = Ax$ is assumed to be linear. Suppose A is Picard (has eigenvalues strictly inside the unit circle) then*

$$\mathscr{H}(\boldsymbol{y}) = \mathscr{H}(\boldsymbol{d}),$$

where the control $k(\cdot)$ is assumed to be a deterministic but otherwise arbitrary map.

Proof. The key is to construct a contractive norm on $\mathbb{R}^m$. If A is Picard then there exists a constant $a \in [0,1)$ and a positive definite symmetric matrix $P \succ 0$ such that

$$A'PA - a^2 P \prec 0.$$

The function $V(x) = x'Px$ is a Lyapunov function for the open-loop system (with $u_n = 0$). We propose to use

$$\|x-y\| \doteq \sqrt{(x-y)'P(x-y)} \quad \text{for} \quad x,y \in X$$

as the norm. Indeed, $\|x-y\|$ is a norm because $P \succ 0$ and

$$\begin{aligned} \|Ax-Ay\| &= \sqrt{(x-y)'A'PA(x-y)} \\ &< a\sqrt{(x-y)'P(x-y)} \\ &= a\|x-y\|. \end{aligned}$$

The Bode formula then follows from using the result in Theorem 2.3.4. □

Remark 2.3.7. *There are two remarks to be made concerning the role of control $\boldsymbol{u}_n$ and observation $\boldsymbol{y}_n$. An additive*

deterministic control serves to merely shift the pdf. As a result of the identity

$$\|Ax+u-(Ay+u)\| = \|Ax-Ay\|,$$

one asymptotically obtains perfect belief in the state irrespective of the control $\{\boldsymbol{u}_n\}$. *We note that the state* $\{\boldsymbol{x}_n\}$ *depends upon the control law, but uncertainty regarding the value of state does not.*

The second remark concerns the role of observation in a feedback system whose open-loop dynamics are linear and stable. If we relax the assumption that $f_0(x)$ *has bounded support then one would require observability of the pair* (A,C) *in the linear case. With bounded disturbance,* $f_n(x)$ *then has bounded support for a finite n (see Appendix A.2).*

For the Bode formula, the contractive assumption is the nonlinear counterpart of the open-loop stability in linear system. In these cases, even with weak assumptions on control and the closed-loop stability, asymptotic dynamics of belief propagation are readily understood by above considerations. Moreover, Lemma 2.3.5 gives the formula for the invariant measure μ in terms of the physical measure μ^* on X. One can thus consider many generalizations of the Bode formula. One particular case of special interest is where the disturbance process $\{\mathbf{d}_n\}$ is state-dependent in the following sense: the current value of the disturbance $\mathbf{d}_n$ is conditionally independent of the past values, i.e., $\text{Prob}(\mathbf{d}_n|\mathbf{d}_0^{n-1}) = \text{Prob}(\mathbf{d}_n)$, but it is allowed to depend upon the current value of the state $\mathbf{x}_n$. This is modeled via a state-dependent pdf $q_x(\cdot)$ defined for each $x \in X$. We refer to the process $\{\mathbf{d}_n\}$ as a state-dependent disturbance with pdf $q_x(\cdot)$.

Corollary 2.3.8. *Consider a closed-loop system (2.3)-(2.5) as in Theorem 2.3.4 where now* $\{\boldsymbol{d}_n\}$ *is a state-dependent disturbance with pdf* $q_x(\cdot)$. *Let* μ^* *denote the physical invariant measure of the closed-loop system then*

$$\mathscr{H}(\mathbf{y}) = \int_X \mathscr{H}(d(x))d\mu^*(x), \tag{2.29}$$

where $\mathscr{H}(d(x)) \doteq -\int q_x(d)\ln(q_x(d))\mathrm{d}d$.

Proof. The proof is similar to the proof of Theorem 2.3.4. The important point here is that even with a state-dependent disturbance, $\text{Prob}(\mathbf{s}_n|\mathbf{s}_0^{n-1}) = \text{Prob}(\mathbf{s}_n|\mathbf{s}_{n-1})$, i.e., the signal process is Markov on S. As a result, the belief process $\{\pi_n\}$ is Markov on ∇_S. The main difference now is that the conditioning step in (2.10) is given by

$$\text{conditioning:} \quad \hat{f}_n(x) = \frac{f_n(x)\cdot q_x(\mathbf{y}_n - c(x))}{\int_X f_n(x)\cdot q_x(\mathbf{y}_n - c(x))dx}.$$

With a unique invariant measure μ^* of the state process $\{\mathbf{x}_n\}$, the problem reduces to (i) establishing that the invariant measure μ of the belief process is unique, and (ii) using the integral formula (2.14) to deduce the entropy rate.

As in the proof of Theorem 2.3.4, let $\mathbf{r}_n \doteq \text{diam}(f_n(x))$ and $\hat{\mathbf{r}}_n \doteq \text{diam}(\hat{f}_n(x))$. The evolution $\pi_n \to \pi_{n+1}$ induces a dynamical system $\mathbf{r}_n \to \mathbf{r}_{n+1}$ as in (2.25). Noting $\hat{f}_n(x) \propto f_n(x) \cdot q_x(\mathbf{y}_n - c(x))$, we have $\text{supp}(\hat{f}_n(x)) \subset \text{supp}(f_n(x))$ irrespective of $q_x(\cdot)$. So, $\hat{\mathbf{r}}_n \leq \mathbf{r}_n$. As before, this together with the contractive nature of the dynamics implies $\mathbf{r}_{n+1} \leq |a|\mathbf{r}_n$, and asymptotic dynamics of the belief process arise as:

$$\pi_n(x,y) = f_n(x)q_x(y-c(x)) = \delta(x-\mathbf{x}_n) \cdot q_x(y-c(x)).$$

This also implies that the filter forgets the initial condition asymptotically (for any $\phi \in C(S)$, $< \pi_n, \phi > = \int_Y \phi(\mathbf{x}_n, y) q_{x_n}(y - c(\mathbf{x}_n))dy$ is independent of the initial distribution $f_0(x)$). So, the invariant measure μ of the belief process is unique. As shown in Lemma 2.3.5, the invariant measure μ^* of the state $\{\mathbf{x}_n\}$ is obtained as a barycenter of μ. Using the integral formula (2.14) formula (2.14) for the entropy rate together with (2.27), one obtains the result. □

2.3.1 Comparison to Earlier Work

The results of this section, Theorem 2.3.4 and Corollaries 2.3.6-2.3.8, are closely related to the Theorem 6 in Zang and Iglesias [3], where the equality $\mathscr{H}(\mathbf{y}) = \mathscr{H}(\mathbf{d})$ was first derived for a nonlinear feedback control system. These results can be viewed as the nonlinear generalization of the classical Bode formula for the open-loop stable LTI system. The equality is important because it means that there are no additional limitations (in terms of extra entropy) due to dynamics.

In deriving the results, certain assumptions need to be made for the open and closed-loop dynamics that are outlined next for both our paper and [3]:

1. *Open-loop stability.* We require the open-loop dynamics, that includes dynamics of both the plant and controller, to be contractive with respect to some norm. For an open-loop stable LTI system, a Lyapunov function can be used to define a contractive norm (see Corollary 2.3.6).

   The considerations of [3] are based on the closed-loop sensitivity transfer operator, denoted as Σ_S, from disturbance to the output. The form of open-loop stability assumed is in terms of a minimum phase requirement on Σ_S. Σ_S is defined to be minimum phase if the inverse system, denoted as $\Sigma_{S^{-1}}$, is globally exponentially stable (GES). Note that the sensitivity transfer function for an open-loop stable LTI system is minimum phase.

2. *Closed-loop stability.* We require the closed-loop dynamics for the nonlinear system to be bounded. In [3], the closed-loop system is assumed to be GES.

3. *Ergodicity.* The contractive assumption on open-loop dynamics allows us to conclude that the filter forgets its initial condition (see Definition 2.2.1). In [3], Σ_S and $\Sigma_{S^{-1}}$ are both assumed to have a fading memory property,

whereby the infinite-dimensional input-output operator can be approximated to any desired accuracy by a finite-dimensional polynomial approximation (see Theorem 3 in [3]). This ensures that the effect of past values of the input diminishes to zero over time.

We remark that while the contractive assumption on dynamics is stronger than GES, the form of closed-loop stability assumed is weaker. A detailed investigation of the trade-off between the two will be a subject of future investigation. However, Appendix A.7 presents an example of control Markov chain *on finite state space*, where $\mathscr{H}(\underline{\mathbf{y}}) > \mathscr{H}(\underline{\mathbf{d}})$, even though both the open-loop and closed-loop Markov chains are GES stable.

2.4 Results for Linear Dynamics

In this section, we consider the closed-loop system (2.3)-(2.5) where the maps $\alpha(\cdot)$, $\beta(\cdot)$ and $c(\cdot)$ are additionally assumed to be linear:

$$\mathbf{x}_{n+1} = A_n\mathbf{x}_n + B\mathbf{u}_n, \tag{2.30}$$

$$\mathbf{y}_n = C\mathbf{x}_n + \mathbf{d}_n, \tag{2.31}$$

$$\mathbf{u}_n = k(\mathbf{y}_n). \tag{2.32}$$

The focus here will be on characterizing limitations due to the unstable aspects of dynamics.

For the time-dependent case, we assume that $\ln\|A_n\| < \infty$. We set $A^{(N)} \doteq \Pi_{k=0}^{N-1} A_k$ and assume that the following limit exists:

$$\lim_{N\to\infty} \left(A^{(N)'}A^{(N)}\right)^{\frac{1}{2N}} = \Lambda. \tag{2.33}$$

The logarithms of the eigenvalues of Λ are called the Lyapunov exponents, denoted as $\lambda_1 \geq \lambda_2 \geq \ldots \geq \lambda_m$. The limit in (2.33) is known to exist for several important cases of interest such as where A_n is obtained by linearization, about a bounded trajectory, of an autonomous nonlinear system (see [129]). For the time-invariant case, $A_n = A$.

Example 2.4.1. *For the linear time-invariant case, the Lyapunov exponents are* $\ln|p_k|$*, where* p_k *are the eigenvalues of the matrix A. This is because the eigenvalues of* $A^{(N)'}A^{(N)}$ *are* $|p_k|^{2N}$.

In the following subsections, we present the Bode formula for the LTI Gaussian, and for the two LTV cases: one where the Lyapunov exponents are all negative, and the other where they are all positive.

2.4.1 Linear Time-Invariant Gaussian Case

We first consider A to be time-invariant, the disturbance $\{\mathbf{d}_n\} \sim N(0,r)$ to be i.i.d. and Gaussian and the pdf for the initial condition $f_0 = N(\hat{x}_0, P_0)$. This case is particularly interesting because equations for evolution of the belief process ($\pi_n \to \pi_{n+1}$) reduce to the Kalman filtering equations. The simplification arises because π_n and f_n are all Gaussian in this case. Denoting $f_n = N(\hat{\mathbf{x}}_n, P_n)$, the update equations for mean and covariance matrices are:

$$\text{Conditioning:} \quad \begin{cases} \hat{\mathbf{x}}_n^+ &= \hat{\mathbf{x}}_n + K_n(\mathbf{y}_n - C\hat{\mathbf{x}}_n) \\ P_n^+ &= (I - K_n C)P_n \end{cases} \tag{2.34}$$

$$\text{Dynamics:} \quad \begin{cases} \hat{\mathbf{x}}_{n+1} &= A\hat{\mathbf{x}}_n^+ + B\mathbf{u}_n \\ P_n &= AP_n^+A' \end{cases} \tag{2.35}$$

where $K_n = P_nC'(CP_nC' + rI)^{-1}$ is the Kalman gain. For a Gaussian random variable, entropy depends only upon its variance and one is thus interested in asymptotic values of $\{P_n\}$. If (A,C) is observable, P_n converges to the unique positive semi-definite solution of the Discrete Algebraic Riccati Equation (DARE):

$$P = A(P - PC'(CPC' + rI)^{-1}CP)A' \tag{2.36}$$

This renders the entropy calculations straightforward. We present the Bode formula in the following Theorem:

Theorem 2.4.2. *Consider the closed-loop system (2.30)-(2.32) with linear time-invariant dynamics. The pair (A,C) is assumed to be observable, the disturbance $\{\boldsymbol{d}_n\}$ is i.i.d with pdf $q = N(0,r)$, and initial condition $\boldsymbol{x}_0$ is uncertain with pdf $f_0 = N(\hat{x}_0, P_0)$. The control $k(\cdot)$ is chosen to ensure that $\{\hat{x}_n\}$ has a bounded ω-limit set (see Remark 2.4.3 below). Then*

$$\mathscr{H}(\boldsymbol{y}) = \mathscr{H}(\boldsymbol{d}) + \sum_k \ln|p_k|,$$

where $|p_k| > 1$ are the unstable eigenvalues of A.

Proof. The entropy is obtained with respect to the asymptotic dynamics of (2.34)-(2.35), solution of DARE (2.36) in this case. The proof is carried out in three steps:

1. Consider a decomposition of $\mathbb{R}^m = \mathbb{R}^{m_s} \oplus \mathbb{R}^{m_u}$ into stable and unstable eigenspaces and write $A = \begin{pmatrix} A_s & 0 \\ 0 & A_u \end{pmatrix}$, $C = (C_s \;\; C_u)$. For such a decomposition, $P = \begin{pmatrix} O & O \\ O & P_u \end{pmatrix}$, where the covariance matrix $P_u \succ 0$ and is a solution

to the DARE written now in the unstable eigenspace:

$$P_u = A_u(P_u - P_uC_u'(C_uP_uC_u' + rI)^{-1}C_uP_u)A_u'. \tag{2.37}$$

The details of the calculations appear in the Appendix A.4.

2. Using the Woodbury matrix identity, (2.37) leads to a Lyapunov equation

$$A_u'P_u^{-1}A_u = P_u^{-1} + C_u'r^{-1}C_u.$$

Taking determinant $|\cdot|$ on both sides, one obtains

$$|A_u|^2 r^{m_u} = |rI + C_u'C_uP_u|. \tag{2.38}$$

Now, $C_u'C_uP_u$ is a rank 1 matrix so

$$|rI + C_u'C_uP_u| = r^{m_u} + \text{trace}(C_u'C_uP_u)r^{m_u-1}.$$

Using (2.38),

$$\begin{aligned} (|A_u|^2 - 1)r^{m_u} &= \text{trace}(C_u'C_uP_u)r^{m_u-1} \\ \therefore, \quad (|A_u|^2 - 1)r &= \text{trace}(C_u'C_uP_u) = C_uP_uC_u'. \end{aligned}$$

3. Finally the entropy is computed for the limiting Gaussian pdf. Using the decomposition,

$$CPC' = C_uP_uC_u' = (|A_u|^2 - 1)r,$$

and the asymptotic variance for the conditional pdf of the output $\mathbf{y}_n$ is given by

$$\sigma_y^2 = CPC' + r = r|A_u|^2.$$

Hence,

$$\begin{aligned}\lim_{n\to\infty} h_y(\pi_n) &= \frac{1}{2}\ln(2\pi e\sigma_y^2)\\ &= \ln(2\pi er)+\ln|A_u|\\ &= \mathscr{H}(\mathbf{d})+\ln|A_u|\end{aligned}$$

The result follows.

□

Remark 2.4.3. *For an observable LTI Gaussian case, the uncertainty (described here by covariance matrix P_n) is independent of observations and converges to a unique equilibrium value P. For P to characterize asymptotic uncertainty, $f_n = N(\hat{\mathbf{x}}_n, P_n)$ must be well-defined in an asymptotic sense, i.e., the random sequence $\{\hat{\mathbf{x}}_n\}$ must have a bounded ω-limit set. This then provides the condition for the entropic stability of the closed-loop (2.30)-(2.32). One can also verify that a necessary condition for this is that (A,B) be controllable. The observability of the (A,C) ensures that the DARE (2.36) admits a unique positive-definite solution P irrespective of the initial condition f_0. So, the integral formula applies.*

2.4.2 Linear Time-Varying Case: Negative Lyapunov Exponents

In the following, we consider the LTV case where the Lyapunov exponents exist and are *all* negative. As a result of this assumption, the open-loop dynamics are contractive only in an asymptotic sense. In particular, negative Lyapunov exponents imply that the equilibrium at 0 is asymptotically stable *without control* [129]. Denoting $\mathbf{x}_N$ as the N^{th}-iterate, we have

$$\lim_{N\to\infty}\|\mathbf{x}_N\| = \lim_{N\to\infty}\|A^{(N)}\mathbf{x}_0\| = 0,$$

where recall $A^{(N)} \doteq \Pi_{k=0}^{N-1} A_k$. Now, with a non-zero control law $\mathbf{u}_n = k(\mathbf{y}_n)$ this may no longer be true. However, the distance $\mathbf{r}_n$ between trajectories starting from two initial conditions $x_0, z_0 \in X$ asymptotically converges to 0 irrespective of the choice of control law. This is seen by explicitly writing the solution

$$\begin{aligned}\mathbf{x}_N &= A^{(N)}x_0 + \mathbb{B}(\mathbf{u}_0^{N-1}),\\ \mathbf{z}_N &= A^{(N)}z_0 + \mathbb{B}(\mathbf{u}_0^{N-1}),\end{aligned}$$

where $\mathbb{B}(\mathbf{u}_0^{N-1}) = \beta(\mathbf{u}_{N-1}) + \sum_{j=0}^{N-2}\left[\Pi_{k=j+1}^{N-1} A_k\right]\beta(\mathbf{u}_j)$, which depends only upon the control input. It follows that

$$\lim_{N\to\infty} \|\mathbf{x}_N - \mathbf{z}_N\| = \lim_{N\to\infty} \|A^{(N)}(x_0 - z_0)\| = 0. \tag{2.39}$$

Even though the width $\mathbf{r}_n$ of the belief f_n may not monotonically decrease (as in the contractive case), it still goes to zero as $n \to \infty$. In particular, we have the following counterpart of the Bode formula:

Theorem 2.4.4. *Consider the closed-loop system (2.30)-(2.32) with linear time-varying dynamics on a bounded set X. The disturbance process $\{\boldsymbol{d}_n\}$ is i.i.d with pdf $q(\cdot)$ and entropy $\mathscr{H}(\boldsymbol{d})$, and the initial condition $x_0 \sim f_0(x)$ has support on X. Suppose the Lyapunov exponents of $\{A_n\}$ exist and all negative then*

$$\mathscr{H}(\boldsymbol{y}) = \mathscr{H}(\boldsymbol{d}).$$

where the control $k(\cdot)$ is assumed to be a deterministic but an otherwise arbitrary map.

Proof. As in the proof of Theorem 2.3.4, we consider the evolution of belief process $\pi_n(x,y)$ and its marginal $f_n(x)$. Denoting $\mathbf{r}_n \doteq \mathrm{diam}(f_n(x))$, the formula (2.39) implies that

$$\lim_{n\to\infty} \mathbf{r}_n = 0.$$

The remainder of the proof, including the argument for the uniqueness of invariant measure μ, is the same as in the proof of Theorem 2.3.4, yielding

$$\mathscr{H}(\mathbf{y}) = \int_{\nabla_S} \mathscr{H}(\mathbf{d}) d\mu = \mathscr{H}(\mathbf{d}).$$

□

2.4.3 Linear Time-varying Case: Positive Lyapunov Exponents

In the following, we consider the LTV case where the Lyapunov exponents exist and are all positive. The crucial property regarding Lyapunov exponents that we will utilize in this section is that:

$$\lim_{N\to\infty} \frac{1}{N} \ln |A^{(N)}| = \sum_{k=1}^{m} \lambda_k. \tag{2.40}$$

For the LTI system, this simply says $\ln|A| = \sum_{k=1}^{m} \lambda_k$.

Theorem 2.4.5. *Consider the closed-loop system (2.30)-(2.32) with linear time-varying dynamics $\{A_n\}$ with all Lyapunov exponents $\{\lambda_k\}_{k=1}^m$ assumed to be positive. The disturbance $\{\boldsymbol{d}_n\}$ is i.i.d with the pdf $q(\cdot)$ and entropy $\mathscr{H}(\boldsymbol{d})$.*

Assume entropic stability of the closed-loop system (see Definition 2.2.2). Then

$$\mathscr{H}(\boldsymbol{y}) \geq \mathscr{H}(\boldsymbol{d}) + \sum_k \lambda_k.$$

Proof. Conditioned on the observations till time N, the uncertainty in the value of state $\mathbf{x}_N$ is

$$H(\mathbf{x}_N|\mathbf{y}_0^N) = H(\mathbf{x}_0|\mathbf{y}_0) + \underbrace{\sum_{n=1}^{N} \left[H(\mathbf{x}_n|\mathbf{y}_0^{n-1}) - H(\mathbf{x}_{n-1}|\mathbf{y}_0^{n-1})\right]}_{\text{term (i)}} + \underbrace{\sum_{n=2}^{N} \left[H(\mathbf{x}_n|\mathbf{y}_0^{n}) - H(\mathbf{x}_n|\mathbf{y}_0^{n-1})\right]}_{\text{term (ii)}}. \tag{2.41}$$

The term (i) measures the uncertainty only due to the dynamics

$$\begin{aligned} H(\mathbf{x}_n|\mathbf{y}^{n-1}) - H(\mathbf{x}_{n-1}|\mathbf{y}^{n-1}) &= \ln|A_n|, \\ \therefore, \sum_{n=1}^{N} \left[H(\mathbf{x}_n|\mathbf{y}_0^{n-1}) - H(\mathbf{x}_{n-1}|\mathbf{y}_0^{n-1})\right] &= \sum_{n=1}^{N} \ln|A_n|, \end{aligned} \tag{2.42}$$

where the first equality holds for any deterministic choice of control law ($u_n = k(\mathbf{y}_n)$ is known). The term (ii) may be simplified using the chain rule for entropy

$$\begin{aligned} H(\mathbf{y}_n|\mathbf{y}_0^{n-1}) + H(\mathbf{x}_n|\mathbf{y}_0^{n-1}, \mathbf{y}_n) &= H(\mathbf{x}_n|\mathbf{y}_0^{n-1}) + H(\mathbf{y}_n|\mathbf{x}_n, \mathbf{y}_0^{n-1}) \\ &= H(\mathbf{x}_n|\mathbf{y}_0^{n-1}) + \mathscr{H}(\mathbf{d}). \end{aligned}$$

As a result,

$$H(\mathbf{x}_n|\mathbf{y}_0^{n}) - H(\mathbf{x}_n|\mathbf{y}_0^{n-1}) = -H(\mathbf{y}_n|\mathbf{y}_0^{n-1}) + \mathscr{H}(\mathbf{d}).$$

On taking a summation,

$$\sum_{n=2}^{N} \left[H(\mathbf{x}_n|\mathbf{y}_0^{n}) - H(\mathbf{x}_n|\mathbf{y}_0^{n-1})\right] = -\sum_{n=2}^{N} \left[H(\mathbf{y}_n|\mathbf{y}_0^{n-1}) - \mathscr{H}(\mathbf{d})\right]. \tag{2.43}$$

Substituting (2.42)-(2.43) in (2.41), one obtains

$$H(\mathbf{x}_N|\mathbf{y}_0^N) = H(\mathbf{x}_0|\mathbf{y}_0) + \sum_{n=1}^{N} \ln|A_n| - \sum_{n=2}^{N} \left[H(\mathbf{y}_n|\mathbf{y}_0^{n-1}) - \mathscr{H}(\mathbf{d})\right]. \tag{2.44}$$

Now, the entropic stability assumption implies

$$H(\mathbf{x}_N|\mathbf{y}_0^N) < M \quad \text{for some finite } M,$$

for all sufficiently large N. This is the crucial requirement.

Using the apriori bound in (2.44), we have for sufficiently large N:

$$\frac{1}{N}\sum_{n=2}^{N} H(\mathbf{y}_n|\mathbf{y}_0^{n-1}) \geq \frac{1}{N}\sum_{n=1}^{N} \ln|A_n| + \frac{1}{N}\sum_{n=2}^{N} \mathscr{H}(\mathbf{d}) - \frac{M}{N}.$$

Letting $N \to \infty$, one obtains

$$\mathscr{H}(\mathbf{y}) \;\geq\; \lim_{n\to\infty} \frac{1}{N}\sum_{n=1}^{N} \ln|A_n| + \mathscr{H}(\mathbf{d}) = \sum_k \lambda_k + \mathscr{H}(\mathbf{d}), \tag{2.45}$$

where we have used (2.40) for the final equality. □

2.4.4 Comparison to Earlier Work

With the additive structure of disturbance input, it is well-known that $\mathscr{H}(\mathbf{y}) \geq \mathscr{H}(\mathbf{d})$ on account of causality; cf., [89, 123, 43]. For LTI systems, the Bode formula provides a strict equality for the gap between the two entropy rates (see also Sec. 15.3 in [123]). The results of this section are closely related to the recent work of Martins and Dahleh [39, 40]. In [39] (Theorem 4.1), the authors derive an inequality for LTI plants and a general class of control. They also consider the effect of preview via a limited-bandwidth channel. Theorems 2.4.2 and 2.4.5 in this chapter are natural extensions of these results for LTI and LTV plants respectively. For LTI plants with static but arbitrary control, Theorem 2.4.2 gives an equality for the gap in terms of unstable eigenvalues of the plant. For LTV plants, the inequality in Theorem 2.4.5 is similar to equation (27) in [39]. The differences arise because we consider here LTV dynamics and derive the bound for a very weak condition (entropic stability) on closed-loop stability. Unlike [39], we do not consider preview. Theorem 2.4.4 gives an equality for LTV systems with negative Lyapunov exponents. To the best of our knowledge, there is no counterpart of such a result in literature.

Let $F_{yy}(e^{i\omega})$ denote the spectral density of the output process $\{\mathbf{y}_n\}$. Lemma 4.3 in [39] shows that

$$\frac{1}{4\pi}\int_{-\pi}^{\pi} \ln(2\pi e F_{yy}(e^{i\omega}))d\omega \geq \mathscr{H}(\mathbf{y}) \tag{2.46}$$

with an equality if $\{\mathbf{y}_n\}$ is a Gaussian process (see also Theorem 11.6 in [89]). As done in Sec. IV.C in [39], one can use (2.46) together with results of this chapter to obtain frequency domain inequalities in terms of spectral density. For Gaussian disturbance with a spectral density $F_{dd}(e^{i\omega})$, one can also obtain a counterpart of (2.1) – with an inequality – where the sensitivity function in the general case is defined by $S(e^{i\omega}) \doteq \frac{F_{yy}(e^{i\omega})}{F_{dd}(e^{i\omega})}$.

2.5 Results For Nonlinear Expanding Dynamics

The general nonlinear case is significantly more difficult than the special cases considered thusfar. For non-contractive nonlinear dynamics, different parts of the phase space can account for different uncertainty rates. In general, one can not expect to obtain fundamental (control-independent) entropy estimates as in the preceding sections. The role of disturbance is important here. For infinitesimally small levels of disturbance, one can show that the entropy is a function of local linearization; for example, see [48, 49] for results on nonlinear stabilization. For very large disturbance, results from certain combustion control experiments [124] also suggest that one recovers effective linearization for certain classes of nonlinearities. This application provides a motivation for the following example.

2.5.1 Example

In this section, we consider a limiting case where dynamics are assumed to be

$$\alpha(x) = \begin{cases} ax & \text{for } |x| < \frac{L}{2a}, \\ \text{sgn}(x)\frac{L}{2} & \text{otherwise,} \end{cases} \tag{2.47}$$

where $a > 1$ and $X \doteq [-\frac{L}{2}, \frac{L}{2}]$. This is an example with non-uniform expansion where different regions in the phase space X experience different rates of expansion; see Fig. A.2 (a). For small enough levels of disturbance and a stabilizing control action, one would expect the asymptotic dynamics to be *not* influenced by saturation. For such a case, the results of the preceding section would hold. Here, we are concerned with the entropy rate in the limit of large disturbance for which we have the following result:

Theorem 2.5.1. *Consider the closed-loop system (2.3)-(2.5) with $\alpha(x)$ given by (2.47). We assume a control law $u = k(y)$ such that the signal process and the belief process are both ergodic (with invariant measures μ^* and μ respectively). In the limit of large disturbance (as $d \to \infty$), the conditional entropy of the output process is given by the asymptotic formula:*

$$\mathscr{H}(\mathbf{y}) \sim \ln(d) + O(\frac{\ln(d)}{d}).$$

Proof. As $n \to \infty$, the marginal $f_n(x)$ arises from a general distribution of the form:

$$f(x) = p_1\delta(x - z_1) + \frac{p_3}{r}\chi_r(x - z_2) + p_2\delta(x - z_3), \tag{2.48}$$

where $r \in [0, L]$, $p_3 = 1 - p_1 - p_2$, and $z_i \in X$ are arbitrary points such that $z_2 = \frac{z_1+z_3}{2}$. For such distributions, $h_y(\pi)$ has the following general form

$$h_y(\pi) = -\frac{C_1}{d} + C_2\frac{\ln(d)}{d} + \ln(d), \tag{2.49}$$

where C_1, C_2 are finite constants. The details of the calculation appears in Appendix A.5. Using (2.49), one uses a uniform boundedness argument to write an asymptotic formula

$$\int_{\nabla_s} h_y(\pi) d\mu(\pi) \sim \ln(d) + O(\frac{\ln(d)}{d})$$

in the limit as $d \to \infty$. □

Numerical illustration of the asymptotic result appears in the Appendix A.8.

2.6 Conclusion

In this chapter, we proposed a hidden Markov model (HMM) framework for establishing Bode-like fundamental limitations for the disturbance rejection problem in nonlinear dynamical systems. In particular, we show that analysis of the asymptotic dynamics of the belief process can be used for evaluating these limitations (right-hand side of the Bode formula for the LTI system) as entropy rate of the output process. The main conclusions of this chapter are:

1. Bode formula is intrinsically related to uncertainty associated with estimation (filtering problem) and *not* the stabilization of an equilibrium (control problem). For example, Bode-like performance limitations (in terms of extra entropy) arise even if the equilibrium is not stable but the state of the closed-loop system remains bounded.

2. There are no limitations due to dynamics if the plant (nonlinear dynamical system) is contractive. The Bode formula for open-loop stable dynamics is a special case of this general result. Here, a Lyapunov function can be used to define a contractive norm.

3. The performance limitations for LTI plants with Gaussian disturbance is easily understood using equations of Kalman filtering. For the general LTV case, a counterpart of Bode formula arises with positive Lyapunov exponents. There are no additional limitations due to dynamics for the LTV case with negative Lyapunov exponents.

4. For the case of non-uniform expansion, we gave some asymptotic results for a special choice of dynamics (expansion+saturation). It is shown that the performance limitations arise only due to disturbance in the limit of very large disturbance. This is consistent with the experimental results of [124].

Chapter 3

Kullback-Leibler Divergence Rate Metric for Comparing Dynamic Systems

3.1 Introduction

In a recent important work, Tryphon Georgiou considers the problem of comparing power spectral densities [130]. Georgiou bases his considerations on a prediction (filtering) based approach. The main idea is to measure distance between spectral densities in terms of prediction error. With the correct spectral density $S_1(e^{j\omega})$ of a discrete-time random process, the optimal prediction error is given by the celebrated Kolmogorov-Szego formula:

$$\varepsilon = \exp\left(\frac{1}{2\pi}\int_{-\pi}^{\pi} \ln S_1(e^{j\omega}) d\omega\right) \tag{3.1}$$

where ε denotes the variance of the prediction error. To measure distance between spectral densities, Georgiou proposes a pseudo-metric as $\ln(\rho)$. The quantity ρ denotes the ratio of the variance of prediction error obtained with an assumed (incorrect) spectral density S_2 to the one obtained with the correct spectral density S_1. The spectral densities here are used to construct an optimal filter for a random process that is generated according to the correct spectral density. The metric proposed by Georgiou serves to quantify the degradation of prediction error due to an (incorrect) assumption on the spectral density. Certain frequency domain formulae are given that lead to a straightforward method for evaluation of the metric for any two densities S_1 and S_2.

In this chapter we follow the key idea appearing in Georgiou's work: that of comparing systems based upon a prediction based approach. If one agrees that a model is a representation of reality (some causal input-output relationship) then it is meaningful to quantify the goodness of the model in terms of the fidelity of its prediction. Since we are concerned with dynamic processes here, a filtering based approach is used to take into account all the available data – in this case, the time history of the past observations. The timely significance of ideas in [130] and here is due to the strong information theoretic flavor of the proposed metrics. Georgiou uses the metric $\ln(\rho)$ to describe the information geometry of the space of spectral densities [130, 53]. We show that $\ln(\rho)$ is in fact closely related to the classical Kullback-Leibler (K-L) rate pseudo-metric that is used to compare stochastic processes. The overall theme fits in nicely with recent attempts to build bridges between information and control theory; cf. [131] and references

therein.

The main goal of this chapter is to outline a prediction based framework for comparing linear and nonlinear input-output systems (see Figure 3.1). Central to the considerations of this chapter is the notion of *uncertainty*. In particular, we compare systems in terms of additional uncertainty that results for the prediction problem with an incorrect choice of the model. While [130] used variance of the prediction error, we quantify the additional uncertainty in terms of the K-L rate. From an information theory perspective, this makes sense because the K-L rate after all is a measure of uncertainty due to an incorrect choice of model; cf., [89]. From a control theory perspective, the starting point for us is the Kolmogorov-Bode formula:

$$\mathscr{H}(\mathbf{y}) - \mathscr{H}(\mathbf{d}) = \frac{1}{2\pi}\int_{-\pi}^{\pi} \ln|L_1(e^{j\omega})|d\omega \tag{3.2}$$

where L_1 is the transfer function of a discrete-time linear time-invariant system from input $\mathbf{d}$ to the output $\mathbf{y}$, and $\mathscr{H}(\mathbf{d})$ and $\mathscr{H}(\mathbf{y})$ denote their respective entropy rates; cf., [123, 89]. In recent years, several authors including Elia [21], Iglesias [3, 44], Martins and Dahleh [132, 40], Nair, Evans and Mareels [48], and Sun and Mehta [16, 49] have considered information-theoretic extensions of the Bode formula. As noted by Iglesias in [3], the entropy rates are well-defined even in time-domain and provide for a framework for performance analysis of nonlinear systems. Using the entropy rate, performance bounds for nonlinear systems have appeared in Chapter 2.

The prediction-based methodology outlined in this chapter extends these bounds now for model comparison and robustness analysis. Figure 3.1 presents the methodology. The prediction problem is considered with the aid of the conditional probability distribution function (pdf) $p(y_n|y_0^{n-1})$. In the Bode formula (3.2), the entropy rate $\mathscr{H}(\mathbf{y}) = \mathsf{E}[-\ln(p(\mathbf{y}_n|\mathbf{y}_0^{n-1}))]$ is a measure of the nominal uncertainty regarding one-step prediction with an exact knowledge of the dynamic model [16]. With an assumed (possibly incorrect) conditional pdf, $q(y_n|y_0^{n-1})$, the entropy rate equals $\mathsf{E}[-\ln(q(\mathbf{y}_n|\mathbf{y}_0^{n-1}))]$. The Kullback-Leibler (K-L) rate is defined as the difference between the two rates,

$$\Delta\mathscr{H}(\mathbf{y}) = -\mathsf{E}[\ln(q)] + \mathsf{E}[\ln(p)].$$

The K-L rate captures the additional uncertainty that results due to an incorrect choice of the dynamic model. It thus provides a measure of degradation of prediction performance due to modeling error. In the remainder of this chapter, we refer to the conditional pdfs $p(y_n|y_0^{n-1})$ and $q(y_n|y_0^{n-1})$ as the "belief-process" with the true model and the assumed model, respectively.

The primary difference between our work and [130] is in the choice of quantity used to measure the additional uncertainty – K-L rate here and variance of the prediction error in [130]. In the prediction-based setting of Fig. 3.1, the use of K-L rate can be justified as an extension of the large deviation theorem of Sanov [133] (see also Theorem 12.4.1

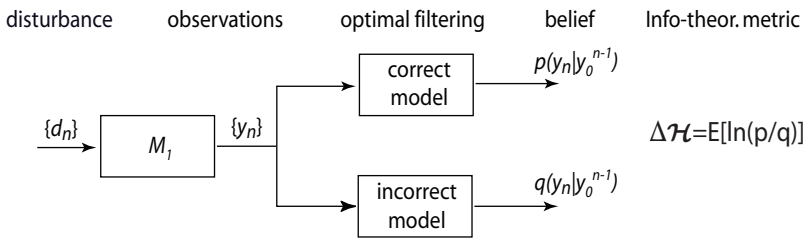

Figure 3.1: Prediction-based comparison of dynamical systems: $\{\mathbf{y}_n\}$ is an output process for dynamical system M_1. $p(y_n|y_0^{n-1})$ is the belief (conditional pdf) with true model M_1; $q(y_n|y_0^{n-1})$ is the belief with the assumed model M_2. Entropy rate $\mathscr{H} = -\mathsf{E}[\ln(p)]$ is the average uncertainty in predicting $\mathbf{y}_n$ if the model (M_1) is known; K-L rate $\Delta\mathscr{H} = \mathsf{E}[\ln(\frac{p}{q})]$ is the additional uncertainty that results with the assumed possibly incorrect model (M_2).

in [89]). Suppose one considers system identification of model parameters by using the method of maximum likelihood. It turns out that the maximum likelihood or maximum a posteriori probability estimation minimizes asymptotically the K-L distance from the empirical distribution of the time-series data produced by the true model [57]. So, the K-L rate is a natural candidate for comparing dynamic models. The use of K-L rate and the related maximum log likelihood criterion appears in hypothesis testing [58, 59], statistical inference [60], model identification [61], and nonlinear filtering [57].

In systems theory, Akaike introduced the celebrated Akaike information criterion (AIC) for the purposes of statistical model identification [55]. In [56], a normalized maximum log likelihood function, referred to by the authors as the ambiguity function, is introduced for approximation of a time-varying linear system by an linear time-invariant (LTI) system. An algorithm is described to obtain the approximation by solving a min-max problem for the ambiguity function. A variant of the classical K-L rate is considered in [62] for model reduction of open- and closed-loop LTI distributed-parameter systems. An extension to continuous time systems is given in [63]. A related approach based on matching the Markov parameters of the full order and reduced order system, the so called q-cover technique, appears in [64]. A metric based on difference of conditional entropies is introduced and used for model reduction in [65].

Relative to literature, the contributions of this chapter are as follows. One, we clarify the relationship between the K-L rate and the metric proposed in [130, 53]. This relationship helps explain some aspects of the information geometry described in their paper [53]. Two, we provide detailed frequency domain formulae for the K-L rate in the linear Gaussian case. These formulae establish the relationship of the K-L rate to the Bode formula whose information theoretic interpretation has been a topic of intense investigation in recent years (see [21, 3, 132, 40, 48, 16, 49]). To the best of our knowledge, such frequency domain formulae do not appear in the literature. Three, we consider nonlinear extensions in terms of the optimal prediction model and the stochastic linearization. In addition to constructive model reduction algorithms given here, such extensions can aid in further development of information-theoretic approaches for robustness analysis in control of nonlinear systems.

The chapter is organized in two parts. In the first part, we consider the prediction-based methodology of Fig. 3.1

for linear models and the Gaussian noise. The goal of the first part is to interpret and extend the results of [130, 53] in terms of K-L rate. Using a formula for pair of Gaussian processes [57], we show that for a single-input-single-output (SISO) system,

$$\Delta\mathscr{H}(L_1,L_2) = \underbrace{\frac{1}{2r}\{\rho-1\}}_{\text{term (i)}} + \underbrace{\frac{1}{2}\left\{\ln(r)+\frac{1}{r}-1\right\}}_{\text{term (ii)}}, \quad \text{(Corollary 3.3.3)} \tag{3.3}$$

where ρ is the ratio of the variance of the prediction error with L_2 (assumed model) to the variance of the prediction error with L_1 (true model), and r is the ratio of variance of the belief process with L_2 to the variance of the belief process with L_1. The significance of the two terms is discussed in detail. In particular, the term (ii) is closely related to the standard K-L distance between two pdfs for i.i.d processes. In dynamic settings, it captures the effect of scaling (multiplying one of the models by a constant) and non-minimum phase zeros. The term (i) is related to Georgiou's metric $\ln(\rho)$. Just as $\ln(\rho)$, it is a measure of the extra prediction error resulting due to modeling error. Frequency-domain interpretations of the K-L rate (formula (3.3)) are also discussed.

One of the differences between the K-L rate and a metric (such as $\ln(\rho)$) based solely on the quantity ρ is that the latter is independent of simply scaling one model with respect to the other. The K-L rate however is sensitive to scaling because multiplying one of the models by a constant factor affects the value of r. For given SISO transfer function models L_1 (true model) and L_2 (assumed model), one may ask what is the optimal scaling constant k that minimizes the K-L rate between L_1 and kL_2. In this chapter, we show that the minimal value

$$\Delta\mathscr{H}^* = \min_{k\in\mathbb{R}} \Delta\mathscr{H}(L_1,kL_2) = \frac{1}{2}\ln(\rho) \qquad \text{(Theorem 3.3.7)} \tag{3.4}$$

actually gives the metric proposed in [130]. In words, $\frac{1}{2}\ln(\rho)$ is the K-L rate provided one chooses the scaling constant k optimally. It is additionally shown that $\rho = r$ in this case. This property has some interesting implications in model reduction applications that are discussed.

While the use of entropy (as opposed to variance) is different and perhaps even mildly interesting, one may ask the reason for pursuing this thread given the same justification and the basic overall methodology as in [130]. This is addressed in the second part of this chapter that is concerned with application to nonlinear dynamical systems.

One difference between this work and [130] is in the nature of modeling: [130] uses power spectral density as a means to represent the model while the considerations of this chapter are based upon the belief process (conditional pdf) $p(y_n|y_0^{n-1})$. The belief process is well defined for nonlinear systems and we utilize the K-L rate to consider model reduction issues in such systems. Model reduction in terms of the belief process directly is shown to lead to the so-called *optimal prediction model* that appear in the recent work of Chorin [90] and Meyn [91]. For the particular case of linear systems, these considerations are applied to obtain a solution of the model reduction problem for auto

regressive (AR) models. Finally, we also use the K-L rate to obtain a formula for stochastic linearization of a nonlinear dynamical system. These three examples serve to illustrate the utility of the proposed metric to a range of modeling issues.

The outline of this chapter is as follows. In Section 3.2, we introduce the problem and express the K-L rate in terms of the belief process. In Section 3.3, we present time-domain and frequency domain formulae for the linear (model) and Gaussian (noise) case. We discuss the effect of scaling and non-minimum phase zeros, and relate the K-L rate to the metric proposed in Georgiou's work [130]. In Section 3.4, we present three examples where the metric is used for model reduction purposes. Finally, conclusions and some directions for future research are discussed in Section 3.5.

3.2 Problem Setup

In this chapter we consider nonlinear discrete-time dynamical system:

$$\begin{aligned} \mathbf{x}_{n+1} &= T(\mathbf{x}_n, \mathbf{d}_n) \\ \mathbf{y}_n &= C(\mathbf{x}_n, \mathbf{d}_n), \end{aligned} \tag{3.5}$$

where n is the discrete time-step, $\mathbf{x}_n \in X \subset \mathbb{R}^m$ is the state, $\mathbf{y}_n \in Y \subset \mathbb{R}^{m_o}$ is the *output*, $\mathbf{d}_n \in D \subset \mathbb{R}^{m_i}$ is an i.i.d. noise *input* with a known distribution, and the noise $\mathbf{d}_n$ is also assumed to be independent of current and past values of state $\mathbf{x}_0^n$. At this stage, the structure is fairly general: $T : X \times D \to X$ and $C : X \times D \to Y$ are assumed to be discrete-time maps. The initial condition $\mathbf{x}_0 \in X$ is assumed unknown. For well-posedness purposes, we assume maps T and C to be continuous and X to be compact in the general nonlinear case. For linear models, X need not be compact but we require dynamics to be stable and observable. In expressing frequency domain formulae for linear models, we will restrict to the single-input-single-output (SISO) case.

To help with the analysis, we employ a stochastic formalism to represent the dynamical system (3.5). In particular,

$$\text{Prob}(\mathbf{x}_n | \mathbf{x}_0^{n-1}) = \text{Prob}(\mathbf{x}_n | \mathbf{x}_{n-1}).$$

So, the dynamical system T defines a Markov chain on X. Taking the output $\mathbf{y}_n$ to be the observation and $\mathbf{x}_n$ to be the underlying state, we have a hidden Markov model (HMM). We analyze the dynamics of (3.5) by considering the evolution of pdf $p_{\mathbf{x}_n}(x)$ on X and $p_{\mathbf{y}_n}(y)$ on Y. The Markov formalism is utilized for propagation of these density

functions; cf., [126, 134]. In particular (3.5) is written as:

$$\begin{aligned} p_{\mathbf{x}_{n+1}}(x) &= \int_X t(x|\tilde{x}) p_{\mathbf{x}_n}(\tilde{x}) d\tilde{x} \\ p_{\mathbf{y}_n}(y) &= \int_X c(y|\tilde{x}) p_{\mathbf{x}_n}(\tilde{x}) d\tilde{x}, \end{aligned} \tag{3.6}$$

where $t(x|\tilde{x})$ and $c(y|\tilde{x})$ are the so-called stochastic kernels for T and C respectively (see Ch., 7 in [126]).

3.2.1 Belief Propagation and Entropy Rate

To assess uncertainty associated with the prediction problem, the starting point is the conditional entropy

$$\mathscr{H}(\mathbf{y}) = \lim_{n\to\infty} H(\mathbf{y}_n|\mathbf{y}_{n-1},\ldots,\mathbf{y}_0), \tag{3.7}$$

of the output process $\{\mathbf{y}_n\}$, provided the limit exists. The conditional entropy is a measure of uncertainty regarding the next observation conditioned on the entire history of past observations. It is obtained by considering the asymptotic dynamics of the belief process about state x_n, denoted as $\pi_n(x) \doteq p_{\mathbf{x}_n|\mathbf{y}_0^{n-1}}(x|y_0^{n-1})$; cf., [107]. The conditional pdf represents ones belief in the current state given all the past observations.

From $n \to n+1$, the belief process is obtained by considering the filtering problem. It evolves in two steps: first conditioning based on the current observation $\mathbf{y}_n = y_n$, followed by an update step to account for the effect of dynamics:

$$\begin{aligned} \text{conditioning:} \quad \pi_n^+(x) &= \frac{\pi_n(x)\cdot c(y_n|x)}{\int_X \pi_n(s)\cdot c(y_n|s)ds} \\ \text{dynamics:} \quad \pi_{n+1}(x) &= \int_X t(x|s)\pi_n^+(s)ds, \end{aligned} \tag{3.8}$$

Given $\pi_n(x)$, the conditional pdf for the output process is given by

$$p_n(y|y_0^{n-1}) \doteq p_{\mathbf{y}_n|\mathbf{y}_0^{n-1}}(y|y_0^{n-1}) = \int_X c(y|x)\pi_n(x)dx. \tag{3.9}$$

In terms of the conditional pdf, the conditional entropy of interest is an expectation of $\left[-\ln p(\mathbf{y}_n|\mathbf{y}_0^{n-1})\right]$:

$$\mathscr{H}(y) = \lim_{n\to\infty} \mathsf{E}_{p(y_0^n)}\left[-\ln p(\mathbf{y}_n|\mathbf{y}_0^{n-1})\right], \tag{3.10}$$

provided the limit exists. Note $p(y_0^n)$ is the joint pdf of the output process $\{\mathbf{y}_n\}$ obtained using the true model. If $\{\mathbf{y}_n\}$ is an i.i.d process then (3.10) is the expected value of $-\ln[p(\mathbf{y}_n)]$ which gives the entropy of a random variable. With

a slight abuse of terminology, we will refer to the conditional pdf $p_{\mathbf{y}_n|\mathbf{y}_0^{n-1}}(y|y_0^{n-1})$ as the belief process with the true model.

Remark 3.2.1. *In the theorems and examples described in this chapter, the limit in both (3.7) and (3.10) can be shown to exist. If the limit does not exist then one may consider the entropy rate, provided it exists, instead of the conditional entropy. In the case where the conditional entropy exist, the two are equal [123].*

The conditional entropy is chosen as a metric because we are concerned here only with the uncertainty in the steady-state asymptotic regime. In obtaining bounds and model approximation results, we will thus frequently invoke stationarity of the output process $\{\boldsymbol{y}_n\}$*. Such a setting is consistent with the spectral density based approach of [130] and allows us to make comparisons with their results. In principle, however, it is possible to extend the prediction-based methodology of Fig. 3.1 to consider transient behavior. This may be done, for instance, by using entropy* $H(\{\boldsymbol{y}_0,\boldsymbol{y}_1,\ldots\})$ *instead of the entropy rate.*

3.2.2 Kullback-Leibler Rate Metric

The belief process $p(y_n|y_0^{n-1})$ depends upon the model (transition kernels t and c in (3.8)) that is used for the purposes of filtering. We reserve the notation $p(y_n|y_0^{n-1})$ to denote the belief process for the true model and the notation $q(y_n|y_0^{n-1})$ to denote it for the assumed (possibly incorrect) model. With the latter, the formula for the conditional entropy is given by

$$\hat{\mathscr{H}}(y) = \lim_{n\to\infty} \mathsf{E}_{p(y_0^n)}\left[-\ln q(\mathbf{y}_n|\mathbf{y}_0^{n-1})\right], \tag{3.11}$$

where the hat notation is used to draw attention to the fact that it is the entropy rate with the assumed model. Note that the observation process $\{\mathbf{y}_n\}$ is still obtained using the true model. Thus, the expectation operator in (3.11) is the same as in (3.10), i.e., $p(y_0^n)$ is the (true) joint pdf of the output. With an i.i.d assumption, this is just the expected value of $-\ln[q(\mathbf{y}_n)]$.

Now, the Kullback-Leibler (K-L) rate – measure of additional uncertainty between the true model (associated belief $p(y_n|y_0^{n-1})$) and the assumed model (associated belief $q(y_n|y_0^{n-1})$) – is defined to be the difference between the two rates (3.10) and (3.11):

$$\Delta\mathscr{H} = \hat{\mathscr{H}}(\mathbf{y}) - \mathscr{H}(\mathbf{y}).$$

In terms of the two belief processes,

$$\begin{aligned}\Delta\mathscr{H} &= \lim_{n\to\infty} \mathsf{E}_{p(y_0^n)} \ln\frac{p(\mathbf{y}_n|\mathbf{y}_0^{n-1})}{q(\mathbf{y}_n|\mathbf{y}_0^{n-1})} \\ &= \lim_{n\to\infty} \mathsf{E}_{p(y_0^{n-1})} D_{KL}(p_n(y|\mathbf{y}_0^{n-1})\|q_n(y|\mathbf{y}_0^{n-1})),\end{aligned} \tag{3.12}$$

where

$$D_{KL}(p_n(y|\mathbf{y}_0^{n-1})||q_n(y|\mathbf{y}_0^{n-1})) = \mathsf{E}_{p(y_n|y_0^{n-1})}\left[\ln\frac{p(\mathbf{y}_n|\mathbf{y}_0^{n-1})}{q(\mathbf{y}_n|\mathbf{y}_0^{n-1})}\right].$$

If the process $\{\mathbf{y}_n\}$ is N^{th} order Markov (i.e., if $p(y_n|y_0^{n-1}) = p(y_n|y_{n-N}^{n-1})$ and $q(y_n|y_0^{n-1}) = q(y_n|y_{n-N}^{n-1})$) then

$$\Delta\mathscr{H} = \lim_{n\to\infty}\mathsf{E}_{p(y_{n-N}^{n-1})}D_{KL}(p(y_n|\mathbf{y}_{n-N}^{n-1})||q(y_n|\mathbf{y}_{n-N}^{n-1})).$$

The K-L rate $\Delta\mathscr{H}$ is non-negative but not symmetric and does not satisfy the triangle inequality.

Example 3.2.2. *To clarify some of these concepts and notation, we consider a first-order auto regressive (AR) example with true model*

$$M_1: \quad \boldsymbol{y}_{n+1} = \alpha_1\boldsymbol{y}_n + \boldsymbol{d}_n, \tag{3.13}$$

and an assumed model

$$M_2: \quad \boldsymbol{y}_{n+1} = \alpha_2\boldsymbol{y}_n + \boldsymbol{d}_n, \tag{3.14}$$

where $\alpha_1, \alpha_2 \in (-1,1)$, and $\boldsymbol{d}_n \sim \mathbf{N}(0,\sigma^2)$ is an input process assumed here to be Gaussian and i.i.d (white noise). It is straightforward to verify that the output process $\{\boldsymbol{y}_n\}$, obtained using the true model M_1, is Gaussian with stationary density given by $\mathbf{N}(0,\frac{\sigma^2}{1-\alpha_1^2})$. We also recall that the entropy of the white noise input $\mathscr{H}(\boldsymbol{d}) = \frac{1}{2}\ln(2\pi e\sigma^2)$ (see pp. 560 in [123]).

The first-order AR model implies that the belief process is first-order Markov, i.e.,

$$p(y_n|y_0^{n-1}) = p(y_n|y_{n-1}), \qquad q(y_n|y_0^{n-1}) = q(y_n|y_{n-1}).$$

Assuming stationarity, we have

$$\begin{aligned} p(y_n|y_{n-1}) &= \mathbf{N}(\alpha_1 y_{n-1},\sigma^2), \\ q(y_n|y_{n-1}) &= \mathbf{N}(\alpha_2 y_{n-1},\sigma^2), \\ p(y_n,y_{n-1}) &= \mathbf{N}(0,\Sigma), \end{aligned} \tag{3.15}$$

where $\Sigma^{-1} = \frac{1}{\sigma^2}\begin{bmatrix} 1 & -\alpha_1 \\ -\alpha_1 & 1 \end{bmatrix}$. The baseline (true) conditional entropy is given by

$$\begin{aligned} \mathscr{H}(\boldsymbol{y}) &= \lim_{n\to\infty} H(\boldsymbol{y}_n|\boldsymbol{y}_{n-1}) \\ &= \lim_{n\to\infty}\mathsf{E}_{p(y_n,y_{n-1})}\ln[-p(\boldsymbol{y}_n|\boldsymbol{y}_{n-1})] = \mathscr{H}(\boldsymbol{d}). \end{aligned} \tag{3.16}$$

This means that the uncertainty in predicting $\boldsymbol{y}_n$ arises only due to the unknown noise. Clearly, given the past observations $\boldsymbol{y}_0^{n-1}$, the prediction of the current output, denoted by $\hat{\boldsymbol{y}}_n = \alpha_1 \boldsymbol{y}_{n-1}$. The variance of the prediction error

$$\begin{aligned} \varepsilon_1 &\doteq \lim_{n\to\infty} \mathsf{E}[(\boldsymbol{y}_n - \hat{\boldsymbol{y}}_n)^2] \\ &= \lim_{n\to\infty} \mathsf{E}[(\boldsymbol{y}_n - \alpha_1 \boldsymbol{y}_{n-1})^2] \\ &= \lim_{n\to\infty} \mathsf{E}[\boldsymbol{d}_n^2] = \sigma^2 \end{aligned} \tag{3.17}$$

is the variance of the noise. This is also consistent with the conclusion of (3.16).

With the assumed model M_2,

$$\begin{aligned} \hat{\mathscr{H}}(\boldsymbol{y}) &= H(\boldsymbol{d}) + \lim_{n\to\infty} \mathsf{E}_{p(y_n, y_{n-1})} \ln\left(\frac{p(\boldsymbol{y}_n|\boldsymbol{y}_{n-1})}{q(\boldsymbol{y}_n|\boldsymbol{y}_{n-1})}\right) \\ &= H(\boldsymbol{d}) + \Delta\mathscr{H}. \end{aligned}$$

Using (3.15), one obtains an explicit formula

$$\begin{aligned} \Delta\mathscr{H} &= \lim_{n\to\infty} \mathsf{E}_{p(y_n, y_{n-1})} \ln\left(\frac{p(\boldsymbol{y}_n|\boldsymbol{y}_{n-1})}{q(\boldsymbol{y}_n|\boldsymbol{y}_{n-1})}\right) \\ &= \frac{(\alpha_2 - \alpha_1)^2}{2(1-\alpha_1^2)}. \end{aligned} \tag{3.18}$$

This means that additional uncertainty results due to the modeling error. While (3.18) describes this additional uncertainty in terms of entropy, one can instead also consider variance of the prediction error. With the assumed model M_2, the prediction $\hat{\boldsymbol{y}}_n = \alpha_2 \boldsymbol{y}_{n-1}$. The variance of the prediction error

$$\begin{aligned} \varepsilon_2 &\doteq \lim_{n\to\infty} \mathsf{E}[(\boldsymbol{y}_n - \hat{\boldsymbol{y}}_n)^2] \\ &= \lim_{n\to\infty} \mathsf{E}[(\alpha_1 \boldsymbol{y}_{n-1} + \boldsymbol{d}_n - \alpha_2 \boldsymbol{y}_{n-1})^2] \\ &= \lim_{n\to\infty} (\alpha_2 - \alpha_1)^2 \mathsf{E}[\boldsymbol{y}_{n-1}^2] + \mathsf{E}[\boldsymbol{d}_n^2] \\ &= \frac{(\alpha_2 - \alpha_1)^2}{1-\alpha_1^2}\sigma^2 + \sigma^2. \end{aligned} \tag{3.19}$$

The first term is a measure of the additional uncertainty in terms of variance of the prediction error. In particular, using (3.17) and (3.19),

$$\rho = 1 + \frac{(\alpha_2 - \alpha_1)^2}{1-\alpha_1^2}, \tag{3.20}$$

where we recall that ρ denotes the ratio of the variance of the prediction error with the assumed model M_2 to the

variance of the prediction error with the true model M_1.

Before closing this section, we note connections to

1. **Bode formula:** *The conditional entropy for the true model ($\mathscr{H}(\mathbf{y})$ in (3.16)) is also obtained as consequence of Bode formula (3.2). The right hand side of (3.2) is zero in this case.*

2. **Georgiou's metric:** *Comparing (3.18) and (3.20), we have*

$$\Delta\mathscr{H} = \frac{1}{2}\{\rho - 1\}. \tag{3.21}$$

The quantity ρ was introduced to define a metric in [130] (see equation (8) in [130]). The relationship in (3.21) is no coincidence. A more general expression for this relationship appears in the following section.

In the remainder of this chapter, the K-L rate (3.12) is used to compare two dynamical systems. In theory, the Markovian representation (3.6) allows one the flexibility to compare a general class of nonlinear dynamical systems. In practice, entropy rates for a general HMM are difficult to compute for all but certain special cases. Nevertheless, one can use the framework to obtain meaningful bounds and algorithms for important class of problems.

3.3 Linear Gaussian Case

In this section, we consider a special case where the maps T and C in (3.5) are assumed be linear and time-invariant. As before, M_1 denotes the true model while M_2 is the assumed model. The state-space equations for the two systems are:

$$M_i: \quad \begin{aligned} \mathbf{x}_{n+1} &= A_i\mathbf{x}_n + B_i\mathbf{d}_n \\ \mathbf{y}_n &= C_i\mathbf{x}_n + D_i\mathbf{d}_n, \end{aligned} \tag{3.22}$$

where $\mathbf{x}_n \in \mathbb{R}^m$, $\mathbf{y}_n \in \mathbb{R}^{m_o}$, $\mathbf{d}_n \in \mathbb{R}^{m_d}$, with $m_o, m_d \geq 1$. A_i is assumed to have all its eigenvalues inside the unit circle, (A_i, C_i) is observable, and $\mathbf{d}_n \sim \mathbf{N}(0, R)$ is i.i.d and Gaussian. We denote $L_i(z) = C_i(zI - A_i)^{-1}B_i + D_i$ to be the input-output transfer function obtained after taking the z-transform of (3.22). In the following, these models are used for the purposes of prediction (filtering) only. $\{\mathbf{y}_n\}$ is used to denote the output process obtained from the true model M_1 (see Fig. 3.1).

3.3.1 Belief Propagation – Kalman Filtering

For the linear Gaussian problem, the evolution of the belief process ($\pi_n \to \pi_{n+1}$) reduces to the Kalman filtering equations. The simplification arises because, assuming stationarity, $\pi_{i,n}$ (denoting π_n for $i = 1, 2$), p_n and q_n are all

Gaussian in this case:

$$\begin{aligned}\pi_{i,n}(x) &= p_{\mathbf{y}_n|\mathbf{y}_0^{n-1}}(x|y_0^{n-1}) = \mathbf{N}(\hat{x}_{i,n}, P_{i,n}),\\ p_n(y) &= p_{\mathbf{y}_n|\mathbf{y}_0^{n-1}}(y|y_0^{n-1}) = \mathbf{N}(\hat{y}_{1,n}, \Sigma_{1,n}),\\ q_n(y) &= q_{\mathbf{y}_n|\mathbf{y}_0^{n-1}}(y|y_0^{n-1}) = \mathbf{N}(\hat{y}_{2,n}, \Sigma_{2,n}),\end{aligned} \tag{3.23}$$

where we recall that p_n and q_n denote belief processes with models M_1 and M_2, respectively. The Kalman filtering equations give the recursion formula, special case of (3.8), for $\hat{x}_{i,n}, P_{i,n}$, and $\Sigma_{i,n} = C_i P_{i,n} C_i' + D_i R D_i'$ (see Ch. 9 in [135]).

Since the entropy rate is a measure of the uncertainty in the steady-state (asymptotically as $n \to \infty$), it suffices to consider only the asymptotic dynamics of $P_{i,n}$. If (A_i, C_i) is observable, $P_{i,n}$ converges to a unique positive semi-definite solution P_i of the discrete algebraic Riccati equation (DARE):

$$P_i = A_i P_i A_i' + B_i R B_i' - (A_i P_i C_i' + B_i R D_i')(C_i P_i C_i' + R)^{-1}(A_i P_i C_i' + B_i R D_i')'. \tag{3.24}$$

We denote the steady-state covariance matrix of the belief process p_n as Σ_1 and the covariance matrix of the belief process q_n as Σ_2. These are given by

$$\Sigma_i = \lim_{n\to\infty} \Sigma_{i,n} = C_i P_i C_i' + D_i R D_i'. \tag{3.25}$$

With the true model M_1, the covariance of the prediction error is

$$\varepsilon_1 = \lim_{n\to\infty} \mathsf{E}\left[(\mathbf{y}_n - \hat{\mathbf{y}}_{1,n})(\mathbf{y}_n - \hat{\mathbf{y}}_{1,n})'\right] = \Sigma_1.$$

With the assumed model M_2, it is

$$\begin{aligned}\varepsilon_2 &= \lim_{n\to\infty} \mathsf{E}\left[(\mathbf{y}_n - \hat{\mathbf{y}}_{2,n})(\mathbf{y}_n - \hat{\mathbf{y}}_{2,n})'\right]\\ &= \varepsilon_1 + \lim_{n\to\infty} \mathsf{E}[(\hat{\mathbf{y}}_{1,n} - \hat{\mathbf{y}}_{2,n})'(\hat{\mathbf{y}}_{1,n} - \hat{\mathbf{y}}_{2,n})].\end{aligned} \tag{3.26}$$

3.3.2 Formula for $\Delta\mathscr{H}(M_1, M_2)$

We first state the following simple lemma for the K-L distance between a pair of Gaussian pdfs (see [57]):

Lemma 3.3.1. *Consider two m_o-dimensional normal random vectors $\boldsymbol{s}_1 \sim N(\mu_1, \Sigma_1)$ and $\boldsymbol{s}_2 \sim N(\mu_2, \Sigma_2)$, then the K-L distance between their pdfs is given by*

$$D_{KL}(\boldsymbol{s}_1||\boldsymbol{s}_2) = \frac{1}{2}\left(\ln(\frac{|\Sigma_2|}{|\Sigma_1|}) + \mathrm{tr}(\Sigma_2^{-1}\Sigma_1) - m_o\right) + \frac{1}{2}\mathrm{tr}(\Sigma_2^{-1}\{(\mu_2 - \mu_1)'(\mu_2 - \mu_1)\}), \tag{3.27}$$

Using this lemma, we have the following theorem for LTI systems with Gaussian noise as input:

Theorem 3.3.2. *Consider two stable MIMO linear systems M_1 and M_2 with a m_o-dimensional output space (see (3.22)). (A_i, C_i) is observable, and $\boldsymbol{d}_n \sim \mathbf{N}(0, R)$ is i.i.d. Let Σ_1 and Σ_2 denote the steady-state covariance matrices of the two belief processes with models M_1 and M_2 (see (3.25)), and ε_2 denotes the covariance matrix of the prediction error with model M_2 (see (3.26)). With this notation, the K-L rate is given by*

$$\Delta\mathscr{H}(M_1, M_2) = \frac{1}{2}\left(\mathrm{tr}(\Sigma_2^{-1}\varepsilon_2) + \ln\frac{|\Sigma_2|}{|\Sigma_1|} - m_o\right). \tag{3.28}$$

Proof. Using Lemma 3.3.1 together with notation of (3.23), we have

$$D_{KL}(p_n||q_n) = \frac{1}{2}\left(\ln(\frac{|\Sigma_{2,n}|}{|\Sigma_{1,n}|}) + \mathrm{tr}(\Sigma_{2,n}^{-1}\Sigma_{1,n}) - m_o\right) + \frac{1}{2}\mathrm{tr}(\Sigma_{2,n}^{-1}\{(\hat{\mathbf{y}}_{2,n} - \hat{\mathbf{y}}_{1,n})'(\hat{\mathbf{y}}_{2,n} - \hat{\mathbf{y}}_{1,n})\}).$$

From the K-L rate formula (3.12), $\Delta\mathscr{H}(M_1, M_2)$ takes the following form:

$$\begin{aligned}
&\lim_{n\to\infty} \mathsf{E}_{p(y_0^{n-1})} D_{KL}(p_n \| q_n) \\
=\ &\lim_{n\to\infty} \frac{1}{2}\left(\ln(\frac{|\Sigma_{2,n}|}{|\Sigma_{1,n}|}) + \mathrm{tr}(\Sigma_{2,n}^{-1}\Sigma_{1,n}) - m_o\right) \\
+\ &\frac{1}{2}\mathrm{tr}(\Sigma_{2,n}^{-1} \lim_{n\to\infty} \mathsf{E}_{p(y_0^{n-1})}\{(\hat{\mathbf{y}}_{2,n} - \hat{\mathbf{y}}_{1,n})'(\hat{\mathbf{y}}_{2,n} - \hat{\mathbf{y}}_{1,n})\}) \\
=\ &\frac{1}{2}\left\{\mathrm{tr}(\Sigma_2^{-1}\Sigma_1) + \ln\frac{|\Sigma_2|}{|\Sigma_1|} - m_o\right\} + \frac{1}{2}\mathrm{tr}(\Sigma_2^{-1}(\varepsilon_2 - \Sigma_1)),
\end{aligned} \tag{3.29}$$

where the final equality is obtained by taking the limit, which exists because (A_i, C_i) is observable. It is a straightforward calculation to see that the two terms are both non-negative. Let $Y \doteq \Sigma_2^{-1}\Sigma_1$ and $\lambda_1, \lambda_2, \ldots, \lambda_{m_o}$ be its eigenvalues. Using these eigenvalues, the first term equals

$$\frac{1}{2}\left\{\sum_{i=1}^{m_o}(\lambda_i - \ln\lambda_i - 1)\right\},$$

which is non-negative because $\lambda_i - \ln\lambda_i - 1 \geq 0$. The second term $\mathrm{tr}(\Sigma_2^{-1}(\varepsilon_2 - \Sigma_1)) \geq 0$ because the trace of the product of two positive semi-definite matrices Σ_2^{-1} and $\varepsilon_2 - \Sigma_1$ is non-negative. Note $\varepsilon_2 - \Sigma_1$ is positive semi-definite on account of (3.26). □

In the SISO case, the variances of the prediction error ε_1 and ε_2 are scalar with $\varepsilon_2 \geq \varepsilon_1$. After [130], we denote

$$\rho(M_1, M_2) \doteq \frac{\varepsilon_2}{\varepsilon_1} \tag{3.30}$$

to be their ratio. As originally noted in [130], ρ provides a measure of degradation in prediction performance because of assuming an incorrect model. In the SISO case, we take the variance of noise $R = \sigma^2$, and denote $\sigma_2^2 \doteq \Sigma_2$ and $\sigma_1^2 \doteq \Sigma_1$. Using these, we define a non-dimensional quantity:

$$r(M_1, M_2) \doteq \frac{\sigma_2^2}{\sigma_1^2}. \tag{3.31}$$

In words, r is the ratio of steady-state variance of the belief process with assumed model M_2 to variance of the belief process with the true model M_1.

For the SISO case, the K-L rate can be expressed in terms of ρ and r:

Corollary 3.3.3. *Consider two stable SISO linear systems M_1 and M_2 as in (3.22) where (A_i, C_i) is observable, and $d_n \sim N(0, \sigma^2)$ is i.i.d and Gaussian input with variance σ^2. The K-L rate*

$$\Delta\mathscr{H}(M_1, M_2) = \frac{1}{2r}\{\rho - 1\} + \frac{1}{2}\left\{\ln(r) + \frac{1}{r} - 1\right\}, \tag{3.32}$$

where ρ is given by (3.30) and r by (3.31).

Proof. The formula follows from direct substitution of (3.30) and (3.31) in (3.29). □

In many situations of interest, $r = 1$ and thus $\Delta\mathscr{H} = \frac{1}{2}(\rho - 1)$. In the following, we discuss one such example that is a generalization of the Example 3.2.2.

Example 3.3.4. *Let M_i be a stable AR(N) model:*

$$\boldsymbol{y}_{n+1} = a_{N-1}^i \boldsymbol{y}_n + a_{N-2}^i \boldsymbol{y}_{n-1} + \cdots + a_0^i \boldsymbol{y}_{n-N+1} + \boldsymbol{d}_n,$$

where $\{\boldsymbol{d}_n\} \sim \mathbf{N}(0, \sigma^2)$ is a white noise input. Consider a coordinate for the state

$$\boldsymbol{x}_n \doteq (\boldsymbol{y}_{n-N+1}, \cdots, \boldsymbol{y}_n)'_{1\times N}, \tag{3.33}$$

to write the state-space matrices (for representation (3.22)):

$$
\begin{aligned}
A_i &= \begin{pmatrix} 0 & 1 & 0 & 0 & \cdots & 0 \\ 0 & 0 & 1 & 0 & \cdots & 0 \\ 0 & 0 & 0 & 1 & \cdots & 0 \\ \vdots & & \vdots & & \vdots & \\ a_0^i & a_1^i & a_2^i & a_3^i & \cdots & a_{N-1}^i \end{pmatrix}_{N\times N} \\
B_i &= (0,0,\cdots,1)'_{1\times N} \doteq B \\
C_i &= (0,0,\cdots,1)_{1\times N} \doteq C.
\end{aligned}
$$

Using (3.33), the knowledge of past observations $\mathbf{y}_0^{n-1}$ is sufficient to determine the state $\mathbf{x}_{n-1}$ for values of $n > N$. In such a case, assuming stationarity, the two belief processes are given by

$$
\begin{aligned}
p_n(y) &= \frac{1}{\sqrt{2\pi(CB)^2\sigma^2}}\exp\{-\frac{(y-CA_1x_{n-1})^2}{2(CB)^2\sigma^2}\}, \\
q_n(y) &= \frac{1}{\sqrt{2\pi(CB)^2\sigma^2}}\exp\{-\frac{(y-CA_2x_{n-1})^2}{2(CB)^2\sigma^2}\}.
\end{aligned}
$$

So,

$$
\ln(\frac{p_n}{q_n}) = \frac{(y-CA_2x_{n-1})^2}{2(CB)^2\sigma^2} - \frac{(y-CA_1x_{n-1})^2}{2(CB)^2\sigma^2}
$$

Note $CB = 1$ and after taking an expectation with respect to p_n, we obtain

$$
\begin{aligned}
D_{KL}(p_n\|q_n) = \mathsf{E}_{p_n}\ln(\frac{p_n}{q_n}) &= \frac{(CA_2x_{n-1}-CA_1x_{n-1})^2}{2\sigma^2} \\
&= \frac{(CA_2-CA_1)(x_{n-1}x'_{n-1})(CA_2-CA_1)'}{2\sigma^2}.
\end{aligned} \tag{3.34}
$$

The right hand side is in fact proportional to the additional variance *that results due to the incorrect choice of the model (M_2 instead of M_1). Indeed at the n^{th} time-step, the variance of the prediction error with the assumed model M_2 is given by*

$$
\varepsilon_{2,n} = (CA_2x_{n-1}-CA_1x_{n-1})^2 + \sigma^2,
$$

so the right hand side of (3.34) is simply $\frac{\varepsilon_{2,n}-\sigma^2}{2\sigma^2}$*. Using (3.34), we also obtain*

$$\begin{aligned}\Delta\mathscr{H}(M_1,M_2) &= \lim_{n\to\infty} \mathsf{E}_{p(y_0^{n-1})} D_{KL}(p_n\|q_n) \\ &= \frac{C(A_2-A_1)\Sigma_{xx}(A_2-A_1)'C'}{2\sigma^2} \\ &= \frac{1}{2}\{\rho-1\},\end{aligned} \tag{3.35}$$

where Σ_{xx} *is the* $N\times N$ *auto-covariance matrix of the state* $\mathbf{x}_n$*. It is obtained as a solution of a Lyapunov equation:*

$$A\Sigma_{xx}A'-\Sigma_{xx}=-\sigma^2BB'.$$

It is worthwhile to note that the right hand side of (3.35) provides a formula for $\Delta\mathscr{H}$ *and for* $\frac{\rho-1}{2}$ *in terms of the parameters of the two models,* A_1 *and* A_2 *in this case. If* $N=1$*, this formula reduces to (3.18) for the scalar Example 3.2.2.*

■

From Corollary 3.3.3 and this example, we see that one of the parameter (ρ) in the expression of $\Delta\mathscr{H}$ is a measure of extra variance of the prediction error resulting due to the incorrect choice of the model. In the following section, we show that the other parameter r arises due to scaling and/or non-minimum phase zeros.

3.3.3 Frequency Domain Formula for the SISO Case

In order to obtain a frequency domain formula for the K-L rate, it is convenient to express the SISO linear model (3.22) as a transfer function

$$L_i(z)=\frac{z^{-k^i}(b_0^i+b_1^iz^{-1}+\cdots+b_{n_i}^iz^{-n_i})}{1+a_1^iz^{-1}+\cdots+a_{m_i}^iz^{-m_i}},$$

for $i=1,2$. We assume that $L_i(z)$ is stable and has no zeros on the unit circle. With the model i, the spectral density of the output process $\{\mathbf{y}_n\}$ is given by $S_i(e^{j\omega})=|L_i(e^{j\omega})|^2\sigma^2$. In (3.32), we expressed $\Delta\mathscr{H}$ in term of ρ, σ_1^2 and σ_2^2. These quantities have the following frequency domain formulae:

$$\frac{\sigma_i^2}{\sigma^2} = \exp\left(\frac{1}{2\pi}\int_{-\pi}^{\pi}\ln|L_i(e^{j\omega})|^2d\omega\right), \tag{3.36}$$

$$\rho = \frac{(\frac{1}{2\pi}\int_{-\pi}^{\pi}\frac{|L_1(e^{j\omega})|^2}{|L_2(e^{j\omega})|^2}d\omega)}{\exp(\frac{1}{2\pi}\int_{-\pi}^{\pi}\ln\frac{|L_1(e^{j\omega})|^2}{|L_2(e^{j\omega})|^2}d\omega)}. \tag{3.37}$$

Equation (3.36) is the Szego formula and (3.37) is due to T. Georgiou (see equation (9) in [130]). Using (3.36) in formula (3.31) for r, we have

$$r = \frac{\sigma_2^2}{\sigma_1^2} = \exp(\frac{1}{2\pi}\int_{-\pi}^{\pi} \ln \frac{|L_2(e^{j\omega})|^2}{|L_1(e^{j\omega})|^2} d\omega). \tag{3.38}$$

Using (3.32), we then get a frequency domain expression for the K-L rate

$$\begin{aligned} \Delta\mathscr{H}(L_1, L_2) &= \frac{1}{2}\left(\ln(r) + \frac{\rho}{r} - 1\right) \\ &= \frac{1}{2}\left(\frac{1}{2\pi}\int_{-\pi}^{\pi} \ln \frac{|L_2|^2}{|L_1|^2} d\omega + \frac{1}{2\pi}\int_{-\pi}^{\pi} \frac{|L_1|^2}{|L_2|^2} d\omega - 1\right), \end{aligned} \tag{3.39}$$

where the notation $\Delta\mathscr{H}(L_1, L_2)$ is used to draw attention to the fact that the right hand side gives a formula for the K-L rate in terms of the transfer functions L_1 and L_2. Note that all of the terms in this formula depend only upon the magnitude $|L_i(e^{j\omega})|$ of the two transfer functions. As a simple corollary, if $|L_1(e^{j\omega})| = |L_2(e^{j\omega})|$ then $\Delta\mathscr{H}(L_1, L_2) = 0$. This is consistent with the prediction (filtering) based nature of the metric. As already noted in [130], ρ is invariant to scaling either L_1 or L_2 by a constant. Unlike ρ, r varies with scaling. The following two examples are used to discuss the properties of r:

Example 3.3.5. *Let $L_1(z) = \tilde{L}(z)$ and $L_2(z) = k\tilde{L}(z)$ where $\tilde{L}(z)$ is assumed stable with no zeros on the unit circle. In this case, $\rho = 1$ and $\Delta\mathscr{H}$ arises only due to the scaling constant k. Using (3.36), we have $\sigma_2^2 = k^2\sigma_1^2$, i.e., $r = k^2$. Using the formula (3.32) in Corollary 3.3.3:*

$$\Delta\mathscr{H}(L_1, L_2) = \ln(|k|) + \frac{1 - k^2}{2k^2}. \tag{3.40}$$

Note that if $\tilde{L}(z) = 1$ then the process $\{\boldsymbol{y}_n\}$ is i.i.d. and the right hand side is in fact the Kullback-Leibler distance between the two stationary pdfs $p_{\boldsymbol{d}_n}(\cdot) = N(0, \sigma^2)$ and $p_{k\boldsymbol{d}_n}(\cdot) = \mathbf{N}(0, k^2\sigma^2)$.

■

In addition to capturing the effect due to scaling, $\Delta\mathscr{H}$ also accounts for non-minimum phase zeros. This is due to the Jensen's formula:

$$\frac{1}{2\pi}\int_{-\pi}^{\pi} \ln|L_i(e^{j\omega})| d\omega = \ln|b_0^i| + \sum_{|z_l|>1} \ln|z_l|, \tag{3.41}$$

where z_l denote the non-minimum phase zeros of the transfer function $L_i(z)$; cf., [136]. To illustrate the effect of non-minimum phase zeros on r and the K-L rate, we consider another example.

Example 3.3.6. *Consider*

$$L_1(z) = 1, \qquad L_2(z) = \frac{1 - kz^{-1}}{1 - \frac{1}{2}z^{-1}}, \tag{3.42}$$

where the zero k lies in $(0,1)$ (minimum phase) or in $(1,\infty)$ (non-minimum phase). We have $b_0^1 = b_0^2 = 1$, and using (3.41),

$$\begin{aligned} \textit{For} \quad k < 1 \quad &: \quad r = 1, \\ \textit{For} \quad k > 1 \quad &: \quad r = k^2. \end{aligned}$$

This means that for $k < 1$ the only contribution to $\Delta\mathscr{H}$ arises due to $\frac{1}{2}\{\rho - 1\}$. For values of $k > 1$ both r and ρ contribute and as $k \to \infty$, we have $r \to \infty$ and $\rho \to \frac{5}{4}$. Thus for values of $k \gg 1$, $\Delta\mathscr{H}$ is primarily due to the non-minimum phase zero. In particular, $\Delta\mathscr{H}(L_1, L_2) \to \infty$ as $k \to \infty$. Figure 3.2 depicts the graphs of $\frac{1}{2}(\rho - 1)$, $\Delta\mathscr{H}$ and the second term $\frac{1}{2}\{ln(r) + \frac{1}{r} - 1\}$ as functions of the zero at k.

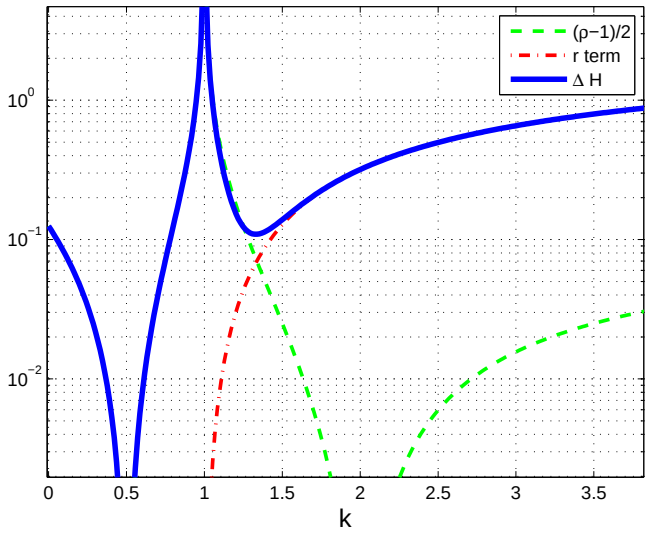

Figure 3.2: A plot of $\Delta\mathscr{H}(L_1, L_2)$ as a function of k.

Note that $\rho = 1$ for $k = \frac{1}{2}$ (minimum phase zero) and for $k = 2$ (non-minimum phase zero). For both these locations of zero, the transfer function L_2 is all-pass. At the value of $k = \frac{1}{2}$, $|L_2| = |L_1| = 1$ and $\Delta\mathscr{H} = 0$. At the value of $k = 2$, $|L_2| = 2|L_1|$ and $\Delta\mathscr{H} = \ln(k) + \frac{1-k^2}{2k^2}$. This is the same expression as the right hand side of (3.40) in Example 3.3.5.

■

In the prediction-based setting, the metrics ρ, r, and $\Delta\mathscr{H}$ only depend upon the magnitude $|L_i(e^{j\omega})|$ of the two transfer functions (see (3.37)-(3.39)). This is not surprising because optimal filtering of linear systems with Gaussian

noise input requires knowledge of only the spectral density of the output process $\{\mathbf{y}_n\}$ (see also [53]). So, a transfer function with non-minimum phase zero can be replaced by another transfer function that yields the same spectral density but has only minimum-phase zeros. For instance in the preceding example, for value of $k = 2$, $L_2 = \frac{1-2z^{-1}}{1-\frac{1}{2}z^{-1}}$ can be replaced by another transfer function $L_2 = 2$. The two are indistinguishable with respect to a prediction-based approach. This will lead one to conclude that the non-minimum phase zeros are not important in model comparison. With a spectral density based approach as in [53], this conclusion is essentially correct.

For a given transfer function model, however, the Jensen's formula (3.41) indicates dependence on log value of magnitude of non-minimum phase zeros *in addition* to $\ln|b_0^i|$. Note that the coefficient b_0^i represents the effect of direct feed through from noise to output. This issue is important because in certain cases (e.g., where the model represents the sensitivity transfer function of a feedback loop), b_0^i may be fixed a priori (to 1 in the case of sensitivity transfer function). In such cases, one must consider the effect of non-minimum phase zeros. For the particular example of sensitivity transfer functions, these zeros lead to fundamental performance limitations (the Bode formula).

For cases where one has the freedom to either arbitrarily scale the assumed model L_2 or to vary the variance of noise for the assumed model, one can indeed replace the non-minimum phase model with a minimum-phase one as long as the two models produce the same spectral density of the output process. It is interesting to note that in such a case, the K-L rate in fact equals the metric proposed in [130, 53] where the author used an approach based entirely on spectral densities. This is the subject of the following section.

3.3.4 Relationship to Georgiou's Metric

The K-L rate formula (3.32) depends upon both ρ and r. As already noted, ρ is invariant to scaling but $\Delta\mathscr{H}$ varies with it because r does. We denote the functional dependence of r on the scaling constant k as $r(k)$. Given two transfer functions $L_1(z)$ and $L_2(z)$, there exists an optimal scaling k^* that minimizes $\Delta\mathscr{H}(L_1, kL_2)$. The result is summarized with the aid of the following theorem.

Theorem 3.3.7. *Consider two stable SISO linear systems M_1 and M_2 as in (3.22) where (A_i, C_i) is observable, and $\{\boldsymbol{d}_n\} \sim \mathbf{N}(0, \sigma^2)$ is i.i.d Gaussian input with variance σ^2. L_i denotes the transfer function of model M_i. With respect to the scaling constant k, the minimal value of the K-L rate is given by*

$$\Delta\mathscr{H}^* = \min_{k\in\mathbb{R}} \Delta\mathscr{H}(L_1, kL_2) = \frac{1}{2}\ln(\rho). \tag{3.43}$$

At the minimizing value of the scaling constant k, denoted by $k = k^*$, we have

$$\rho = r(k^*). \tag{3.44}$$

Proof. Let $r_1 \doteq r(1)$ denote the value of r at $k = 1$. Using (3.37) and (3.38), ρ is invariant with respect to the scaling constant k and $r(k) = k^2 r_1$. We thus have

$$\Delta\mathscr{H}(L_1, kL_2) = \frac{1}{2}\left(\ln(k^2 r_1) + \frac{\rho}{k^2 r_1} - 1\right). \tag{3.45}$$

Differentiating with respect to k, we have

$$\frac{d\Delta\mathscr{H}(L_1, kL_2)}{dk} = \frac{1}{k} - \frac{\rho}{k^3 r_1}.$$

Setting the right hand side equal to zero, we obtain

$$\frac{1}{k^*} = \frac{\rho}{k^{*3} r_1} \qquad \Longrightarrow \qquad \rho = k^{*2} r_1 = r(k^*).$$

Substituting this in (3.45), we obtain the minimal K-L rate

$$\Delta\mathscr{H}^* = \Delta\mathscr{H}(L_1, k^* L_2) = \frac{1}{2}\ln(\rho).$$

□

The theorem shows that the metric ($\ln(\rho)$) proposed in [130] is proportional to the K-L rate provided one chooses the optimal value of scaling in computing the latter. In many applications involving model identification from experimental data, one needs to choose a noise model (see for e.g., [124] for identification of noise-driven models of combustion dynamics). With white (Gaussian and i.i.d) noise, this amounts to choosing the variance σ^2 of the noise or equivalently choosing the gain (scaling) of the model (transfer function L_2) for a nominally chosen value of variance. Since K-L rate is a measure of uncertainty, it makes sense to choose the noise model that minimizes the K-L rate. The resulting optimal K-L rate gives Georgiou's metric.

It is important to note that at the optimal scaling $k = k^*$, $\rho = r(k^*) = k^{*2} r_1$. This means that the value of the optimal gain k^* increases as the prediction performance degrades. In model reduction applications, this implies that noise should increase as one truncates states. The point is illustrated with the aid of the following example.

Example 3.3.8. *Suppose the true model is a first-order AR model:*

$$M_1: \quad \boldsymbol{y}_{n+1} = \alpha_1 \boldsymbol{y}_n + \boldsymbol{d}_n, \tag{3.46}$$

and the assumed model is its reduced order approximation

$$M_2: \quad \boldsymbol{y}_{n+1} = k\boldsymbol{d}_n,$$

where $\alpha_1 \in (-1,1)$, $\boldsymbol{d}_n \sim \mathbf{N}(0,\sigma^2)$ *is an i.i.d. input process, and the value of k needs to be chosen to minimize* $\Delta\mathscr{H}$. *From the Example 3.2.2, we have* $\rho = \frac{1}{1-\alpha_1^2}$, $\sigma_1^2 = \sigma^2$, $\sigma_2^2 = k^2\sigma^2$, *and* $r = k^2$.

Using (3.44), we know $\Delta\mathscr{H}$ *is minimized for the choice of*

$$\rho = r \qquad \Longrightarrow \qquad k^* = \sqrt{\frac{1}{1-\alpha_1^2}} > 1.$$

Thus, the "effective" noise increases from $\boldsymbol{d}_n \sim \mathbf{N}(0,\sigma^2)$ *to* $k^*\boldsymbol{d}_n \sim \mathbf{N}(0, \frac{\sigma^2}{1-\alpha_1^2})$ *as one reduces the model from first-order to zeroth-order.*

■

3.4 Application of K-L rate to Model Reduction

3.4.1 Optimal Prediction Model

In this section, we consider the model reduction problem for the general nonlinear system (3.5) where the model reduction objective is to write a reduced order model for the output coordinate $\mathbf{y}$. In particular, the true model is:

$$M_1: \quad \begin{aligned} \mathbf{x}_{n+1} &= T(\mathbf{x}_n, \mathbf{d}_n) \\ \mathbf{y}_n &= C(\mathbf{x}_n, \mathbf{d}_n), \end{aligned} \tag{3.47}$$

where n is the discrete time-step, $\mathbf{x}_n \in X \subset \mathbb{R}^m$ is the state, $\mathbf{y}_n \in Y \subset \mathbb{R}^{m_o}$ is the output, and $\mathbf{d}_n \in D \subset \mathbb{R}^{m_i}$ is an i.i.d. noise input. With respect to the coordinate $\mathbf{y}$, the model reduction objective is to construct a model

$$M_2: \quad \mathbf{y}_{n+1} = S(\mathbf{y}_n, \tilde{\mathbf{d}}_n) \tag{3.48}$$

where S is a dynamical system and $\{\tilde{\mathbf{d}}_n\}$ is an i.i.d. process (noise model). In applications, the coordinate $\mathbf{y}$ could denote a *coarse* coordinate and M_2 a first-order model for this coordinate [137].

There are two ideas in our work that are relevant to the solution of this problem. The first idea concerns *representation* of a nonlinear dynamical systems in terms of a Markov operator (see (3.6)). The model M_2 in (3.48) is transformed into a linear system by considering not the evolution of $\mathbf{y}_n$ but its distribution $p_{\mathbf{y}_n}(y)$. The evolution of

distributions is described by the Markov operator:

$$p_{\mathbf{y}_{n+1}}(y) \quad = \quad \int_Y s(y|\tilde{y}) p_{\mathbf{y}_n}(\tilde{y}) d\tilde{y} \tag{3.49}$$

where $s(y|\tilde{y})$ is the stochastic kernel for S. As a result of this representation, we convert the difficult problem of finding the map S and the noise model $\{\tilde{\mathbf{d}}_n\}$ into finding the transition kernel $s(y|\tilde{y})$.

The second idea concerns the use of the K-L rate for the purposes of approximation. In particular, the model reduction objective of finding a model M_2 is cast as an optimization problem:

$$\min_{s(y|\tilde{y})} \Delta\mathscr{H}(M_1, M_2). \tag{3.50}$$

The minimizing transition kernel, denoted as $s^*(y|\tilde{y})$, then describes the best Markov approximation of M_1. It turns out that linearity of the representation (4.5) together with convexity of the K-L rate (3.50) allows for a straightforward solution of the model reduction problem. This solution is summarized in the following:

Theorem 3.4.1. *Consider the problem of approximating a given nonlinear model M_1 in (3.47) by a first-order model (3.48). In terms of the Markovian representation (4.5) of the model M_2, the optimal solution to the model reduction problem in (3.50) is given by:*

$$\underset{s(y_1|y_0)}{argmin} \Delta\mathscr{H}(M_1, M_2) = \frac{p^2(y_0, y_1)}{p(y_0)} \doteq s^*(y_1|y_0), \tag{3.51}$$

where $p(y_0)$ is the invariant distribution of the process $\{\mathbf{y}_n\}$, and $p^2(y_0, y_1)$ is its bivariate distribution (provided these exist).

Proof. The starting point is the formula (3.12) for the K-L rate:

$$\Delta\mathscr{H}(M_1, M_2) = \lim_{n\to\infty} \mathsf{E}_{p(y_0^n)} \ln \frac{p(\mathbf{y}_n|\mathbf{y}_0^{n-1})}{q(\mathbf{y}_n|\mathbf{y}_0^{n-1})},$$

where $p(y_n|y_0^{n-1})$ is the belief process for the output $\{\mathbf{y}_n\}$ with the true model M_1 and $q(y_n|y_0^{n-1})$ is the belief process with the assumed model M_2 (see Sec. 3.2.1). The simplification arises due to the Markovian nature of the assumed model M_2. In particular, with model M_2 we have assumed that

$$\begin{aligned} \text{Prob}(\mathbf{y}_n|\mathbf{y}_0^{n-1}) &= \text{Prob}(\mathbf{y}_n|\mathbf{y}_{n-1}), \\ \therefore,\ q(y_n|y_0^{n-1}) &= q(y_n|y_{n-1}). \end{aligned}$$

Furthermore, the representation (4.5) implies that $q(y_n|y_{n-1}) = s(y_n|y_{n-1})$. So,

$$\begin{aligned}\Delta\mathscr{H}(M_1,M_2) &= \lim_{n\to\infty} \mathsf{E}_{p(y_0^n)} \ln \frac{p(\mathbf{y}_n|\mathbf{y}_0^{n-1})}{s(\mathbf{y}_n|\mathbf{y}_{n-1})} \\ &= \lim_{n\to\infty} \mathsf{E}_{p(y_0^n)} \left[\ln(p(\mathbf{y}_n|\mathbf{y}_0^{n-1})) - \ln(s(\mathbf{y}_n|\mathbf{y}_{n-1}))\right] \\ &= \mathscr{H}(\mathbf{y}) - \lim_{n\to\infty} \mathsf{E}_{p(y_{n-1},y_n)}[\ln(s(\mathbf{y}_n|\mathbf{y}_{n-1}))],\end{aligned}$$

where we have used the formula for the entropy rate (3.10) and the fact that the assumed model M_2 is first-order Markov. Now,

$$\mathsf{E}_{p(y_{n-1},y_n)}\left[\ln(s(\mathbf{y}_n|\mathbf{y}_{n-1}))\right] = \mathsf{E}_{p(y_{n-1})}\mathsf{E}_{p(y_n|y_{n-1})}\left[\ln(s(\mathbf{y}_n|\mathbf{y}_{n-1}))\right].$$

The crucial observation is that

$$\mathsf{E}_{p(y_n|y_{n-1})}[\ln(s(\mathbf{y}_n|\mathbf{y}_{n-1}))] \leq \mathsf{E}_{p(y_n|y_{n-1})}[\ln(p(\mathbf{y}_n|\mathbf{y}_{n-1}))],$$

where the equality is achieved if and only if $s(y_n|y_{n-1}) = p(y_n|y_{n-1})$. As a result,

$$\begin{aligned}\Delta\mathscr{H}(M_1,M_2) &= \mathscr{H}(\mathbf{y}) - \lim_{n\to\infty} \mathsf{E}_{p(y_{n-1},y_n)}[\ln(s(\mathbf{y}_n|\mathbf{y}_{n-1}))] \\ &\geq \mathscr{H}(\mathbf{y}) - \lim_{n\to\infty} \mathsf{E}_{p(y_{n-1},y_n)}[\ln(p(\mathbf{y}_n|\mathbf{y}_{n-1}))],\end{aligned}$$

where the equality holds if and only if $s(y_n|y_{n-1}) = p(y_n|y_{n-1})$. Assuming stationarity, we thus have the optimal transition kernel:

$$s^*(y_1|y_0) = p(y_1|y_0) = \frac{p^2(y_0,y_1)}{p(y_0)},$$

where $p(y_0)$ and $p^2(y_0,y_1)$ are the stationary and bivariate distribution of the process $\{\mathbf{y}_n\}$, and the final equality follows from the definition of conditional distribution. □

Remark 3.4.2. *The model (3.51) is in fact the same as the optimal prediction model that also appears in the recent work of Meyn [91]. In his paper, Meyn notes that the full order and the reduced order models share the exact one-dimensional and two-dimensional statistics. The term "optimal prediction model" is due to Chorin [90]. It reflects the property that the model exactly predicts the expectation* $\mathsf{E}[c(\mathbf{y}_n,\mathbf{y}_{n+1})]$ *for any arbitrary function c. In [138], Chorin shows that these concepts are closely related to the Mori-Zwanzig formalism for model reduction in physics [139].*

3.4.2 Model Reduction from $AR(N)$ to $AR(M)$

The K-L rate is particularly well-suited for the analysis of Markov models. For example, the optimal prediction model is a Markov model. In this section, we consider the problem of reducing an N^{th}-order Markov model $AR(N)$ to an M^{th}-order Markov model $AR(M)$. Although Theorem 3.4.1 provides a formula for the optimal reduced order model (with $M = 1$) in a more general setting, here we restrict ourselves to the case of linear systems with Gaussian noise. In this case, we obtain closed-form expression for the optimal model parameters.

The true model is assumed to be an $AR(N)$ model

$$M_1: \quad \mathbf{y}_{n+1} = a^1_{N-1}\mathbf{y}_n + a^1_{N-2}\mathbf{y}_{n-1} + \cdots + a^1_0\mathbf{y}_{n-N+1} + \mathbf{d}_n, \tag{3.52}$$

where $\{\mathbf{d}_n\} \sim \mathbf{N}(0,\sigma^2)$. The model reduction objective is to obtain a model

$$M_2(\{a^2_i\},k)\colon \mathbf{y}_{n+1} = a^2_{M-1}\mathbf{y}_n + a^2_{M-2}\mathbf{y}_{n-1} + \cdots + a^2_0\mathbf{y}_{n-M+1} + k\mathbf{d}_n, \tag{3.53}$$

such that the K-L rate $\Delta\mathscr{K}(M_1,M_2)$ is minimum. The optimization problem is to find the model parameters, coefficients $\{a^2_i\}_{i=0}^{M-1}$ and the gain k, that achieve this minimum.

Before presenting the solution of this problem, we recall notation and results of Example 3.3.4 where the formula for $\Delta\mathscr{K}$ is described in terms of the state-space matrices (see equation (3.35)). To extend this formula to models with different dimensions, we simply express $AR(M)$ as an $AR(N)$ model with some of the coefficients zero. Denoting the state $\mathbf{x}_n \doteq [\mathbf{y}_{n-N+1},\ldots,\mathbf{y}_{n-M},\mathbf{y}_{n-M+1}\ldots,\mathbf{y}_n]$, the state-space matrices for the two models M_1 and M_2 are:

$$A_1 = \begin{pmatrix} 0 & 1 & & 0 & 0 & \cdots & 0 \\ 0 & 0 & & 1 & 0 & \cdots & 0 \\ 0 & 0 & & 0 & 1 & \cdots & 0 \\ \vdots & & & \vdots & & \vdots & \\ a^1_0 & \cdots & a^1_{N-M-1} & a^1_{N-M} & \cdots & a^1_{N-1} \end{pmatrix}_{N\times N},$$

$$A_2 = \begin{pmatrix} 0 & 1 & 0 & 0 & \cdots & 0 \\ 0 & 0 & 1 & 0 & \cdots & 0 \\ 0 & 0 & 0 & 1 & \cdots & 0 \\ \vdots & & \vdots & & \vdots & \\ 0 & \cdots & 0 & a^2_0 & \cdots & a^2_{M-1} \end{pmatrix}_{N\times N}, \tag{3.54}$$

$$B_1 = [0,0,\cdots,1]'_{1\times N}, \qquad C_1 = [0,0,\cdots,1]_{1\times N},$$
$$B_2 = [0,0,\cdots,k]'_{1\times N} = kB_1, \qquad C_2 = C_1.$$

For notational convenience, we split the state $\mathbf{x}_n = [\tilde{\mathbf{v}}_n, \mathbf{v}_n]$ where $\mathbf{v}_n = [\mathbf{y}_{n-M+1}\cdots,\mathbf{y}_n]$, and $\tilde{\mathbf{v}}_n = [\mathbf{y}_{n-N+1},\ldots,\mathbf{y}_{n-M}]$. Along this splitting, we denote $a^{(1)} \doteq [a^1_{N-M},\cdots,a^1_{N-1}]'$, $a^{(2)} \doteq [a^2_0,\cdots,a^2_{M-1}]'$, $\tilde{a}^{(1)} \doteq [a^1_0,\cdots,a^1_{N-M-1}]'$, and $b = a^{(2)} - a^{(1)}$. Assuming stationarity, the covariance matrix of state $\mathbf{x}_n$ is expressed as

$$\Sigma_{xx} = \begin{pmatrix} \Sigma_{\tilde{v}\tilde{v}} & \Sigma_{\tilde{v}v} \\ \Sigma'_{\tilde{v}v} & \Sigma_{vv} \end{pmatrix}. \tag{3.55}$$

On substituting (3.55) in (3.35), we obtain

$$\begin{aligned} \frac{1}{2}\{\rho - 1\} &= \frac{C(A_2 - A_1)\Sigma_{xx}(A_2 - A_1)'C'}{2\sigma^2} \\ &= \frac{1}{2\sigma^2}\begin{bmatrix} \tilde{a}^{(1)'} & b' \end{bmatrix}\begin{pmatrix} \Sigma_{\tilde{v}\tilde{v}} & \Sigma_{\tilde{v}v} \\ \Sigma'_{\tilde{v}v} & \Sigma_{vv} \end{pmatrix}\begin{bmatrix} \tilde{a}^{(1)} \\ b \end{bmatrix} \end{aligned} \tag{3.56}$$

The variances for the two belief processes are given by $\sigma_1^2 = (C_1B_1)^2\sigma^2 = \sigma^2$, $\sigma_2^2 = (C_2B_2)^2\sigma^2 = k^2\sigma^2$, and $r = \frac{\sigma_2^2}{\sigma_1^2} = k^2$. As a result, the formula for the K-L rate (3.32) in this case is given by

$$\Delta\mathscr{H}(M_1, M_2(\{a_i^2\}, k)) = \frac{1}{2\sigma^2}\begin{bmatrix} \tilde{a}^{(1)'} & b' \end{bmatrix}\begin{pmatrix} \Sigma_{\tilde{v}\tilde{v}} & \Sigma_{\tilde{v}v} \\ \Sigma'_{\tilde{v}v} & \Sigma_{vv} \end{pmatrix}\begin{bmatrix} \tilde{a}^{(1)} \\ b \end{bmatrix} + \frac{1}{2}\left\{\ln(k^2) + \frac{1}{k^2} - 1\right\}. \tag{3.57}$$

The following theorem uses this formula to describe the solution to the model reduction optimization problem.

Theorem 3.4.3. *Consider the problem of approximating the AR(N) model (3.52) by an AR(M) model (3.53). Let $a^{(1)} \doteq [a^1_{N-M},\cdots,a^1_{N-1}]'$ and $\tilde{a}^{(1)} \doteq [a^1_0,\cdots,a^1_{N-M-1}]'$ denote coefficients of model M_1, and $a^{(2)} \doteq [a^2_0,\cdots,a^2_{M-1}]'$ denotes coefficients of model M_2. The coefficients of the optimal reduced order model M_2 are given by*

$$a^{(2)} = a^{(1)} + \Sigma_{vv}^{-1}\Sigma'_{\tilde{v}v}\tilde{a}^{(1)}, \tag{3.58}$$

where $\Sigma_{\tilde{v}\tilde{v}}$ and $\Sigma_{\tilde{v}v}$ are covariance sub-matrices in (3.55). At the optimal point,

$$\min_{\{a_i^2\}}\rho = 1 + \frac{1}{\sigma^2}\tilde{a}^{(1)'}\left[\Sigma_{\tilde{v}\tilde{v}} - \Sigma_{\tilde{v}v}\Sigma_{vv}^{-1}\Sigma'_{\tilde{v}v}\right]\tilde{a}^{(1)} \doteq \rho^* \tag{3.59}$$

The optimal gain

$$k = \sqrt{\rho^*} \tag{3.60}$$

for which one obtains the minimal value of the K-L rate:

$$\min_{\{a_i^2\},k} \Delta\mathscr{H}(M_1, M_2(\{a_i^2\},k)) = \frac{1}{2}\ln\rho^*. \tag{3.61}$$

Proof. The proof proceeds in two steps. In the first step, we find coefficients $\{a_i^2\}$ that minimize ρ. In the second step, we find the optimal gain k that together with optimal coefficients found in the first step minimize the K-L rate. Using (3.56),

$$\frac{\rho-1}{2} = \frac{1}{2\sigma^2}\left[b'\Sigma_{vv}b + \tilde{a}^{(1)'}\Sigma_{\tilde{v}\tilde{v}}\tilde{a}^{(1)} - 2b'\Sigma'_{\tilde{v}v}\tilde{a}^{(1)}\right], \tag{3.62}$$

where $b = a^{(2)} - a^{(1)}$. On taking derivative with respect to the vector b, we have

$$\frac{d}{db}\frac{\rho-1}{2} = \frac{1}{2\sigma^2}\left[2\Sigma_{vv}b - 2\Sigma'_{\tilde{v}v}\tilde{a}^{(1)}\right].$$

Setting this equal to zero, we have

$$\begin{aligned} \Sigma_{vv}b &= \Sigma'_{v\tilde{v}}\tilde{a}^{(1)}, \\ \therefore,\ a^{(2)} &= a^{(1)} + \Sigma_{vv}^{-1}\Sigma'_{\tilde{v}v}\,\tilde{a}^{(1)}. \end{aligned}$$

This proves (3.58). Substituting the optimal coefficients $a^{(2)}$ into (3.62) gives (3.59).

In the second step, we use Theorem 3.3.7 to obtain k that minimizes $\Delta\mathscr{H}$. At the optimal point, (3.44) gives

$$\rho = r = k^2,$$

and (3.43) gives

$$\min_{\{a_i^2\},k} \Delta\mathscr{H}(M_1, M_2(\{a_i^2\},k)) = \frac{1}{2}\ln\rho^*.$$

This proves (3.60) and (3.61). □

Example 3.4.4. *Consider the following AR(2) model*

$$M_1: \quad \boldsymbol{y}_{n+1} = \frac{5}{6}\boldsymbol{y}_n - \frac{1}{6}\boldsymbol{y}_{n-1} + \boldsymbol{d}_n \tag{3.63}$$

where $\{\boldsymbol{d}_n\} \sim \mathbf{N}(0,\sigma^2)$. *The objective is to find an* $AR(1)$ *model*

$$M_2(\alpha_2,k): \quad \boldsymbol{y}_{n+1} = \alpha_2 \boldsymbol{y}_n + k\boldsymbol{d}_n, \tag{3.64}$$

such that the K-L rate $\Delta\mathscr{H}(M_1,M_2)$ *is minimum. Here, the state coordinate* $\boldsymbol{x}_n = [\boldsymbol{y}_{n-1},\boldsymbol{y}_n]$, *and*

$$A_1 = \begin{pmatrix} 0 & 1 \\ -\frac{1}{6} & \frac{5}{6} \end{pmatrix}, \qquad A_2 = \begin{pmatrix} 0 & 1 \\ 0 & \alpha_2 \end{pmatrix}.$$

The Lyapunov equation is

$$A_1 \Sigma_{xx} A_1' - \Sigma_{xx} + \begin{pmatrix} 0 & 0 \\ 0 & \sigma^2 \end{pmatrix} = 0,$$

whose solution is given by

$$\Sigma_{xx} = \begin{pmatrix} 2.1 & 1.5 \\ 1.5 & 2.1 \end{pmatrix} \sigma^2.$$

We have $a^{(1)} = \frac{5}{6}$, $\tilde{a}^{(1)} = -\frac{1}{6}$, *and* $a^{(2)} = \alpha_2$. *Using (3.58),*

$$\alpha_2 = a^{(1)} + \Sigma_{vv}^{-1}\Sigma_{\tilde{v}v}' \tilde{a}^{(1)} = \frac{5}{6} - (\frac{1.5}{2.1})\frac{1}{6} = \frac{5}{7}.$$

Using (3.59) and (3.60), $\rho^* = 1.0286$ *and* $k = \sqrt{\rho^*} = 1.0142$. *The optimal* $AR(1)$ *model is thus given by*

$$\boldsymbol{y}_{n+1} = \frac{5}{7}\boldsymbol{y}_n + 1.0142\boldsymbol{d}_n. \tag{3.65}$$

The K-L rate $\Delta\mathscr{H}^* = \frac{1}{2}\ln\rho^* = 0.0141$. *This model is also the optimal prediction model (3.51) because assuming stationarity,*

$$\begin{aligned} p(y_0,y_1) &= \mathbf{N}(\begin{bmatrix} 0 \\ 0 \end{bmatrix}, \begin{bmatrix} 2.1 & 1.5 \\ 1.5 & 2.1 \end{bmatrix} \sigma^2), \\ p(y_0) &= \mathbf{N}(0, 2.1\sigma^2), \\ \therefore,\ s^*(y_1|y_0) &= \frac{p(y_0,y_1)}{p(y_0)} = \mathbf{N}(\frac{5}{7}y_0, 1.0286\sigma^2), \end{aligned}$$

the transition kernel for (3.65). A comparison of the power spectral densities of the two models M_1 *and* M_2 *appears in Figure (3.3).*

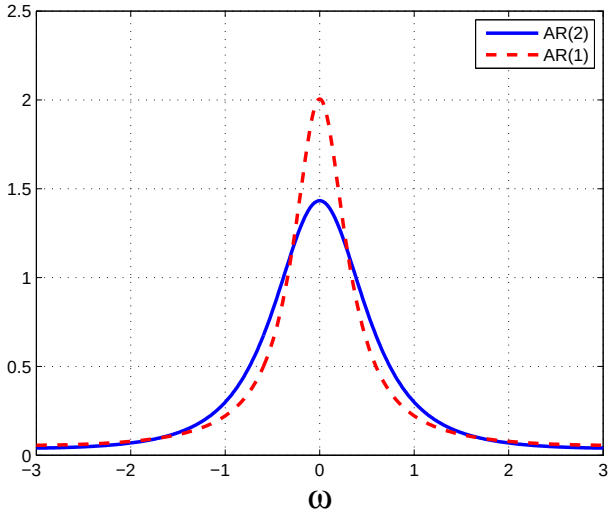

Figure 3.3: Power spectral density of models M_1 in (3.63) and M_2 in (3.65).

3.4.3 Stochastic Linearization

In this section, we utilize the metric $\Delta\mathscr{H}$ to approximate a nonlinear model M_1 by a linear model M_2. We consider

$$M_1(\alpha): \quad \mathbf{y}_{n+1} = \alpha(\mathbf{y}_n) + \mathbf{d}_n, \tag{3.66}$$

$$M_2(A): \quad \mathbf{y}_{n+1} = A\mathbf{y}_n + \mathbf{d}_n, \tag{3.67}$$

where $\mathbf{y}_n \in \mathbb{R}^m$, $\mathbf{d}_n \in \mathbb{R}^m$ and $\mathbf{d}_n \sim \mathbf{N}(0,R)$, $\alpha(\cdot): \mathbb{R}^m \to \mathbb{R}^m$ is a continuous nonlinear vector function, $A \in \mathbb{R}^{m\times m}$ is a constant but as yet unknown $m \times m$ Picard matrix (i.e. eigenvalues of A are strictly inside the unit circle). It is assumed that R is positive-definite (denoted by $R \succ 0$).

Given the nonlinear model $M_1(\alpha)$, the objective is to find the matrix A such that the linear model M_2 is *closest* to M_1. The metric $\Delta\mathscr{H}(M_1, M_2)$ is used to measure the distance between the two models. With the given structure (3.66)-(3.67), this leads to an optimization problem

$$\min_{A\in\mathbb{R}^{m\times m}} \Delta\mathscr{H}(M_1(\alpha), M_2(A)). \tag{3.68}$$

The best linear approximation corresponds to the Picard matrix $A = A^*$ that achieves this minimum. The following theorem presents the optimal model.

Theorem 3.4.5. *Consider the problem of approximating a given nonlinear model (3.66) by a linear model (3.67), where the noise $\boldsymbol{d}_n \sim \mathbf{N}(0,R)$ is i.i.d with covariance $R \succ 0$. For the stochastic linearization problem (3.68), the*

solution is given by

$$\underset{A\in\mathbb{R}^{m\times m}}{argmin}\,\Delta\mathscr{H}(M_1(\alpha),M_2(A)) = \mathsf{E}[\alpha(\boldsymbol{y})\boldsymbol{y}']\Sigma_{yy}^{-1} \doteq A^*,$$

where $\mathsf{E}[\cdot] = \int \cdot f(y)dy$ *is the expectation with respect to* $f(y)$*, the invariant density of* $\{\boldsymbol{y}_n\}$ *with the true nonlinear model* $M_1(\alpha)$*.* Σ_{yy} *denotes its covariance matrix.*

Proof. The two belief processes arise as

$$\begin{aligned} p_n &= p(y_n|y_{n-1}) = \mathbf{N}(\alpha(y_{n-1}),R), \\ q_n &= q(y_n|y_{n-1}) = \mathbf{N}(Ay_{n-1},R), \end{aligned}$$

where we have used the fact that both models are first-order Markov. For these processes,

$$D_{KL}(p_n\|q_n) = \frac{1}{2}(\alpha(y_{n-1}) - Ay_{n-1})'R^{-1}(\alpha(y_{n-1}) - Ay_{n-1}),$$

and

$$\begin{aligned} \Delta\mathscr{H}(M_1(\alpha),M_2(A)) &= \lim_{n\to\infty} \mathsf{E}_{p(y_{n-1})}\left[D_{KL}(p_n\|q_n)\right] \\ &= \frac{1}{2}\mathsf{E}\left[(\alpha(\mathbf{y}) - A\mathbf{y})'R^{-1}(\alpha(\mathbf{y}) - A\mathbf{y})\right], \end{aligned}$$

where $\mathsf{E}[\cdot] = \int \cdot f(y)dy$ is the expectation with respect to the invariant density $f(y)$.

Using (3.68), the optimization problem is

$$\min_A \mathsf{E}\left[(\alpha(\mathbf{y}) - A\mathbf{y})'R^{-1}(\alpha(\mathbf{y}) - A\mathbf{y})\right] \doteq F(A).$$

With respect to the matrix A, the differential is given by

$$dF(A)\cdot B = -2\mathsf{E}\left[(B\mathbf{y})'R^{-1}(\alpha(\mathbf{y}) - A\mathbf{y})\right],$$

where $B \in \mathbb{R}^{m\times m}$ is an arbitrary element of the tangent space. Setting the differential equal to zero gives the condition

$$\begin{aligned} &\mathsf{E}\left[R^{-1}(A\mathbf{y} - \alpha(\mathbf{y}))\mathbf{y}'\right] = 0, \\ &\therefore,\ A\mathsf{E}[\mathbf{y}\mathbf{y}'] = \mathsf{E}[\alpha(\mathbf{y})\mathbf{y}'], \end{aligned} \tag{3.69}$$

and $A = \mathsf{E}[\alpha(\mathbf{y})\mathbf{y}']\Sigma_{yy}^{-1} \doteq A^*$.

In order to show that A^* is Picard, first use (3.66) to deduce

$$\begin{aligned} & \Sigma_{yy} = \mathsf{E}[\alpha(\mathbf{y})\alpha(\mathbf{y})'] + R \\ \therefore, \qquad & v'\mathsf{E}[\alpha(\mathbf{y})\alpha(\mathbf{y})']v < v'\Sigma_{yy}v, \quad \forall v \in \mathbb{R}^m. \end{aligned} \tag{3.70}$$

Since $R \succ 0$, it also follows that $\Sigma_{yy} \succ 0$. We next apply the Cauchy-Schwarz inequality to (3.69). For $v \in \mathbb{R}^m$,

$$\begin{aligned} |v'A^*\Sigma_{yy}v|^2 &= |\mathsf{E}[v'\alpha(\mathbf{y})\mathbf{y}'v]|^2 \\ &\leq \mathsf{E}[(v'\alpha(\mathbf{y}))^2]\,\mathsf{E}[(\mathbf{y}'v)^2] \\ &= \left(v'\mathsf{E}[\alpha(\mathbf{y})\alpha(\mathbf{y})']v\right)\,\left(v'\mathsf{E}[\mathbf{y}\mathbf{y}']v\right). \end{aligned} \tag{3.71}$$

Using (3.70) with (3.71), we obtain the inequality

$$|v'A^*\Sigma_{yy}v|^2 < (v'\Sigma_{yy}v)^2,$$

from which the result follows. Suppose λ is an eigenvalue of A^* with left eigenvector w then

$$|w'A^*\Sigma_{yy}w|^2 = |\lambda|^2|w'\Sigma_{yy}w|^2 < |w'\Sigma_{yy}w|^2.$$

Thus $|\lambda| < 1$, where we have used the fact that $\Sigma_{yy} \succ 0$. □

Example 3.4.6. *Consider the scalar case*

$$M_1(\alpha): \quad \boldsymbol{y}_{n+1} = \alpha(\boldsymbol{y}_n) + \boldsymbol{d}_n, \tag{3.72}$$

$$M_2(a): \quad \boldsymbol{y}_{n+1} = a\boldsymbol{y}_n + \boldsymbol{d}_n, \tag{3.73}$$

where $\alpha(\cdot)$ is a continuous nonlinear function, a is a constant, $\boldsymbol{d}_n \sim \mathbf{N}(0,\sigma^2)$. In this case,

$$\Delta\mathscr{H}(M_1(\alpha), M_2(a)) = \frac{1}{2\sigma^2}\mathsf{E}\left[(\alpha(\boldsymbol{y}) - a\boldsymbol{y})^2\right]$$

where $\mathsf{E}[\cdot] = \int \cdot\, f(y)dy$. Differentiating with respect to the parameter a gives the optimal value of a as

$$a^* = \frac{\mathsf{E}[\alpha(\boldsymbol{y})\boldsymbol{y}]}{\mathsf{E}[\boldsymbol{y}^2]}.$$

This is consistent with a result that one would expect from using a describing function method [124]. Figure 3.4

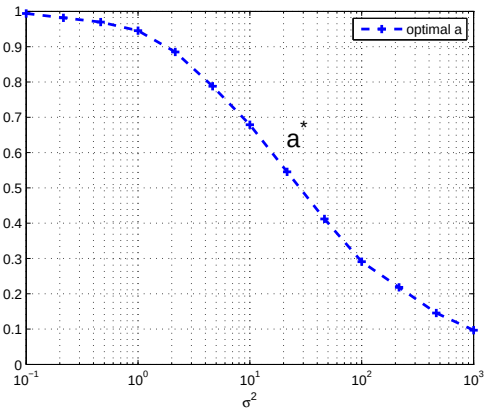

Figure 3.4: A plot of a^* as a function of σ^2.

depicts a^* *as a function of* σ *where* α *is taken to be a saturation nonlinearity*

$$\alpha(x) \quad = \quad \begin{cases} 2x & \textit{for } |x| < 1, \\ 2sgn(x) & \textit{otherwise}, \end{cases}$$

and σ^2 *is varied from* 0.1 *to* 100. *Figure 3.5 depicts the corresponding* $\Delta\mathscr{H}$. *Note the value of* a^* *decreases as the variance of input noise increases. Asymptotically as* $\sigma^2 \to \infty$, *the optimal gain* $a^* \to 0$. *The corresponding* $\Delta\mathscr{H}$ *also approaches zero monotonically indicating that the linear approximation gets better as the variance of the noise increases.*

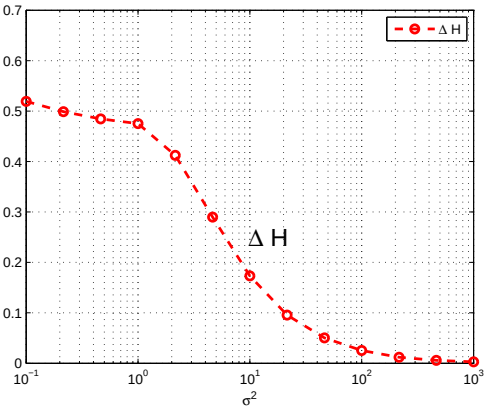

Figure 3.5: A plot of the optimal value of $\Delta\mathscr{H}(M_1, M_2)$ as σ^2 changes.

Algorithmically, we construct an estimate of $\mathsf{E}[\alpha(\boldsymbol{y})\boldsymbol{y}]$ *from a single realization* $\{y_n\}$ *of the output process, that is*

obtained from simulating the nonlinear system (3.72). In particular, note that

$$\begin{aligned} \mathsf{E}[\boldsymbol{y}_{n+1}\boldsymbol{y}_n] &= \mathsf{E}[\alpha(\boldsymbol{y}_n)\boldsymbol{y}_n] + \mathsf{E}[\boldsymbol{y}_n\boldsymbol{d}_n] \\ &= \mathsf{E}[\alpha(\boldsymbol{y}_n)\boldsymbol{y}_n]. \end{aligned}$$

Therefore, an estimate of $\mathsf{E}[\alpha(\boldsymbol{y})\boldsymbol{y}]$ *is constructed by taking an average*

$$\mathsf{E}[\alpha(\boldsymbol{y})\boldsymbol{y}] = \frac{1}{N}\sum_{n=0}^{N-1} y_{n+1}y_n,$$

from a trajectory y_0^{N-1} *obtained from simulating (3.72). Alternatively,* $\mathsf{E}[\boldsymbol{y}_{n+1}\boldsymbol{y}_n]$ *can be obtained by taking an inverse Fourier transform of the spectral density of the process* $\{\boldsymbol{y}_n\}$.

3.5 Conclusion

In this chapter, we presented a prediction based framework for comparing linear and nonlinear dynamical systems. Our work is inspired by and closely related to [130] who proposed to use variance of the prediction error to compare spectral densities. Instead, we based our considerations in terms of additional uncertainty (entropy) that results for the prediction problem with an incorrect choice of the model. Detailed comparison to the variance based metric is presented together with three separate examples describing the approach.

In all of the examples, Markov formalism together with the K-L rate is used to carry out model reduction. The only difference is in the specification of the constraint: in the first example, optimization is carried out over the set of first-order Markov models; in the second example, the optimization is carried out over the set of linear $AR(M)$ models. The framework is not necessarily limited to model reduction but can help with a range of modeling issues. In the third example, we employed the framework to carry out stochastic linearization of a random dynamical system. The constraint here was the set of linear systems with Gaussian noise.

One of the advantages of using the K-L rate as the metric is that it provides a measure of degradation in prediction performance due to model reduction. Because these models have minimal uncertainty of prediction, we believe that they are ideal for nonlinear estimation and control problems. This will be a subject of future investigations.

Chapter 4

Performance Limitation with Kullback -Leibler Type Control Cost

4.1 Introduction

In Seron *et. al.* [38], fundamental limitations in control of continuous-time nonlinear systems are investigated using the so-called *cheap control* approach. The cheap control problem for a stabilizable and detectable linear time-invariant (LTI) system

$$\begin{aligned} \dot{x}(t) &= Ax(t)+Bu(t), \quad x\in\mathbb{R}^n,\ u\in\mathbb{R}^m \\ y(t) &= Cx(t), \quad y\in\mathbb{R}^m,\ x(0)=x_0 \end{aligned} \tag{4.1}$$

consists of finding a state feedback control that minimizes

$$J_\varepsilon = \frac{1}{2}\int_0^\infty (y(t)^T y(t)+\varepsilon u(t)^T u(t))dt, \tag{4.2}$$

where $\varepsilon > 0$ is small. The minimum value is denoted as J_ε^*.

As $\varepsilon \to 0$, the limit of J_ε^* is denoted as J_0^*. The fundamental limitations are expressed in terms of the value of J_0^*. The value depends upon non-minimum phase zeros, and is related to a Bode-type integral formula for the complementary sensitivity function (see [38] and Qiu-Davison [71]).

In [38], the focus is on characterizing fundamental limitations due to unstable zero dynamics in nonlinear systems. Using a singular perturbation analysis in the small parameter ε, it is shown that in the limit $\varepsilon \to 0$ the cheap control problem reduces to a minimum energy (L^2) problem. The optimal control works by stabilizing the unstable zero dynamics in the nonlinear case.

An optimal control analogue of the Bode's integral formula for the sensitivity function appears in a technical report by Seron [37]. For a single-input LTI system (4.1), the optimal control problem is to find a state-feedback

control which minimizes the functional:

$$J_\varepsilon = \frac{1}{2}\int_0^\infty (\varepsilon x(t)^T x(t) + u(t)^2)dt, \tag{4.3}$$

where $\varepsilon > 0$ is small. The minimal values is denoted as J_ε^*. The fundamental limitations are expressed in terms of the limit J_0^*. When x_0 is set by a unit impulse at the input (i.e. $x_0 = B$),

$$J_0^* = \sum_k p_k,$$

where p_k are the right-half plane poles of (4.1).

Just as the value of J_0^* for the cheap control problem is related to the Bode-type integral for the complementary sensitivity function, the value of J_0^* for (4.3) is the same as the right hand-side of Bode integral formula (2.2) for the sensitivity function. The optimal control in this case works by stabilizing the unstable open-loop dynamics. The two problems are seen to be dual to each other [37].

The objective of this chapter is to investigate fundamental limitations in control of nonlinear systems within an optimal control framework. The inspiration comes from the cheap control problem, and its analogy to the Bode formula. Vis-a-vis the work of Seron [38, 37], there are two differences:

1. The fundamental limitations are considered for the discrete time system.

2. The quadratic control cost metric (the term u^2) in (4.3) is replaced by an information theoretic Kullback-Leibler (K-L) divergence metric.

The K-L metric is motivated by the recent work of Todorov [74, 140].

In [74], Todorov introduces a class of the so-called *linearly solvable* Markov Decision Processes (MDP). The main idea is to replace the control cost, term u^2, in (4.3) by a certain K-L divergence:

$$\mathrm{KL}(q\|p) = \mathsf{E}[\ln(\frac{q}{p})],$$

where $q = q(x'|x)$ is the stochastic kernel (conditional probability density function (pdf)) for the closed-loop dynamics, and $p = p(x'|x)$ is the conditional pdf for the open-loop dynamics. The advantage of using such a cost metric is that the optimal control problem (Bellman equation) is solvable in closed-form [74]. The disadvantage is that the optimal control solution is given *not* in terms of the optimal control law but instead in terms of the entire closed-loop dynamics (conditional pdf $q(\mathbf{x}'|\mathbf{x})$). With a particular (say affine) structure of control, the optimal closed-loop dynamics may not even be realizable. The framework, however, can be used to obtain fundamental limitations for a given open-loop

dynamics $p(x'|x)$. This is the focus of the present chapter.

The fundamental limitations are considered with respect to an average cost optimal control problem. The control objective is to find closed-loop $q(x'|x)$ that minimizes

$$J_\varepsilon = \lim_{N\to\infty} \frac{1}{N} \mathsf{E}[\sum_{t=0}^{N-1} \{\varepsilon c(\mathbf{x}_t) + \mathrm{KL}(q(\mathbf{x}_{t+1}|\mathbf{x}_t) \| p(\mathbf{x}_{t+1}|\mathbf{x}_t))\}], \tag{4.4}$$

where $\varepsilon > 0$ is small. For the LTI system, $c(x) = x^2$. The minimal average cost is denoted as J_ε^* and J_0^* denotes the limit as $\varepsilon \to 0$. As in the cheap control case, the fundamental limitation is expressed in terms of the value of J_0^* . Of particular interest is to

1. relate J_0^* to unstable aspects of open-loop dynamics, and

2. find conditions on open-loop dynamics so that there are no fundamental limitations, i.e., $J_0^* = 0$.

The main contribution of this chapter is to show that the fundamental limitation, value of J_0^*, can be obtained via analysis of a linear eigenvalue problem. The important point is that the eigenvalue problem depends only upon the open-loop dynamics $p(x'|x)$. For an LTI system, the limitations are given by

$$J_0^* = \sum_k \ln|p_k|,$$

which p_k are the unstable poles as in the Bode formula. As a corollary, $J_0^* = 0$ if the open-loop LTI system is asymptotically stable.

The analysis of the eigenvalue problem shows that for the general case, $J_0^* = 0$ if the open-loop dynamics are ergodic. For nonlinear systems, the limitations thus arise only if the open-loop dynamics are non-ergodic. The results are illustrated with several examples.

Apart from the papers of Seron and Todorov, there are close parallels of our work with the risk sensitive optimal control literature, and the control of chaos literature.

The eigenvalue problem considered in this chapter is related to the eigenvalue problem that arises in the risk sensitive optimal control problem [76]. In Fleming and McEneaney [77] and Fleming and Sheu [78], asymptotic formulae for the principle eigenvalue of a certain linear operator are considered in the small-noise limit. The linear operator arises via consideration of a risk sensitive optimal control problem and the value of the principal eigenvalue is related to the optimal cost. Via a logarithmic transformation, the eigenvalue is also seen as an optimal cost for an average cost optimal control problem; cf., Chapter VI in [79][1].

The fact that there are no fundamental limitations in control of ergodic open-loop dynamics is consistent with the

[1] A detailed comparison with the risk sensitive control literature and the logarithmic transform is a subject of future work.

control of chaos literature in dynamical systems [93]. There have been studies such as the Ott-Grebogi-Yorke (OGY) method of controlling chaos which seek to exploit nonlinear dynamics for the purpose of stabilization: "*Assuming the motion of the free-running (uncontrolled) chaotic orbit to be ergodic, eventually the chaotic wandering of an orbit trajectory will bring it close to the chosen unstable periodic orbit or steady state. When this occurs, we can apply small controlling perturbations to direct the orbit to the desired periodic motion or steady state [93].*" Implicit in the OGY quote is the idea of using nonlinear dynamics to ones advantage to minimize control effort.

For LTI systems, open-loop dynamics are ergodic if and only if they are asymptotically stable (i.e., all the Lyapunov exponents are negative). For nonlinear systems, the two notions are quite different. As shown with the aid of mod 2 example in Section 4.3.3, open-loop dynamics can be ergodic even with positive Lyapunov exponents. The fundamental limitations analysis shows that the conclusions with linear assumption can be rather misleading in this case. The differences arise not only in the value of J_0^* but also in the nature of optimal control solution.

The outline of this chapter is as follows. The optimal control problem is introduced in Section 4.2. In Section 4.3, the main fundamental limitations result is presented and illustrated with examples including both ergodic and non-ergodic cases.

4.2 Problem formulation

Consider a discrete-time nonlinear system

$$\mathbf{x}_{t+1} = T(\mathbf{x}_t, u_t, \mathbf{d}_t),$$

where $\mathbf{x}_t, \mathbf{x}_{t+1} \in X \subset R^n$, u_t is the control input, and $\mathbf{d}_t$ is i.i.d. noise. The map T is assumed to be continuous with respect to its arguments. The system is said to be open-loop if $u_t = 0$ for all time t.

For the open-loop system, the evolution of distributions is described by the Markov operator $\mathbb{P} : L^1(X) \to L^1(X)$:

$$\rho_{\mathbf{x}_{t+1}}(x') \quad = \quad \int_X p(x'|x)\rho_{\mathbf{x}_t}(x)dx \doteq \mathbb{P}[\rho_{\mathbf{x}_t}](x'), \tag{4.5}$$

where $\mathbf{x}_t \sim \rho_{\mathbf{x}_t}(\cdot)$ and $\mathbf{x}_{t+1} \sim \rho_{\mathbf{x}_{t+1}}(\cdot)$. We reserve the notation $p(x'|x)$ to denote the stochastic transition kernel for the open-loop dynamics[2].

In the setting of Markov Decision Processes (MDP), the optimal control objective is to find a state-feedback control law $u = k(x)$ so as to minimize a suitably defined infinite-horizon objective functional. We reserve the notation $q(x'|x)$

[2]We will require some form of continuity and boundedness properties for the kernel $p(x'|x)$. For example, consider $\mathbf{x}_{t+1} = \alpha(\mathbf{x}_t) + \mathbf{d}_t$, where $\mathbf{d}_t \sim g(\cdot)$. In this case $\mathbb{P}[\rho](x') = \int_X g(x' - \alpha(x))\rho(x)dx$. In certain cases, X may be assumed to be compact.

to denote the stochastic transition kernel of the closed-loop system

$$\mathbf{x}_{t+1} = T(\mathbf{x}_t, k(\mathbf{x}_t), \mathbf{d}_t).$$

Following Todorov [74], the difficult problem of finding control $u = k(x)$ is replaced by the problem of finding the transition kernel $q(x'|x)$ directly. The only assumption made on $q(x'|x)$ is that it be absolutely continuous with respect to $p(x'|x)$. This means $q(x'|x) = 0$ whenever $p(x'|x) = 0$[3].

We will refer to $p(x'|x)$ and $q(x'|x)$ as the open-loop and the closed-loop dynamics, respectively.

Example 4.2.1. *Consider a scalar linear system with Gaussian noise*

$$\mathbf{x}_{t+1} = a\mathbf{x}_t + u_t + \mathbf{d}_t,$$

where t is the discrete time, $\mathbf{x}_t \in \mathbb{R}$, $\mathbf{d}_t \sim N(0, \sigma^2)$. The open-loop dynamics are obtained by setting $u_t = 0$:

$$p(x'|x) = N(ax, \sigma^2).$$

There are no assumptions made on closed-loop dynamics: for a given $x \in X$, $q(x'|x)$ is an arbitrary pdf with support on X.

Note that an arbitrary $q(x'|x)$ may not be realizable with an affine structure of control as in (4.2). For example, consider a deterministic control law $u = k(x)$. The closed-loop in this case is $q(x'|x) = N(ax + k(x), \sigma^2)$, which is always Gaussian with variance σ^2.

In this chapter, following Todorov [74], the cost of control is defined in terms of the Kullback-Leibler (K-L) divergence between $q(x'|x)$ and $p(x'|x)$:

$$\mathrm{KL}(q(x'|x)||p(x'|x)) \doteq \mathsf{E}_{x' \sim q(x'|x)}[\ln \frac{q(x'|x)}{p(x'|x)}], \tag{4.6}$$

where q is assumed to be absolutely continuous with respect to p.

4.2.1 Infinite Horizon Optimal Control Problem

We consider an infinite horizon optimal control problem where the control objective is to minimize the functional

$$J_\varepsilon = \lim_{N \to \infty} \frac{1}{N} \mathsf{E}[\sum_{t=0}^{N-1} \{\varepsilon c(\mathbf{x}_t) + \mathrm{KL}(q(\mathbf{x}_{t+1}|\mathbf{x}_t)||p(\mathbf{x}_{t+1}|\mathbf{x}_t))\}], \tag{4.7}$$

[3]This assumption is somewhat restrictive and one of the objective of future work is to consider formulations where this is not necessary.

where $\mathsf{E}[\cdot]$ denotes the expectation under a given control law, and $c(x) \geq 0$ is a continuous function that is used to penalize the state. The KL term serves as a measure of control cost. If no additional control is used then $p = q$ and $\mathrm{KL}(q\|p) = 0$. In general, the term measures the discrepancy between the transition kernels of the open and closed-loop systems. The parameter $\varepsilon > 0$ is small.

The solution of (4.7) is obtained by writing the Bellman equation. We denote the minimum average cost as J_ε^* and $v(x)$ as the relative value function. The Bellman equation is given by:

$$J_\varepsilon^* + v(x) \quad = \quad \min_{q(x'|x)} \{\varepsilon c(x) + \mathrm{KL}(q(x'|x)||p(x'|x)) + \mathsf{E}_{x' \sim q(x'|x)}[v(x')]\}, \tag{4.8}$$

where $v(x)$ is the relative cost function [141]. Denote the N-step cost-to-go function at state x as $V_\varepsilon^N(x)$, then $v(x)$ represents the deviation of $V_\varepsilon^N(x)$ from NJ_ε^* for large N:

$$v(x) = \lim_{N \to \infty} \{V_\varepsilon^N(x) - NJ_\varepsilon^*\}.$$

Following Todorov [74], we express

$$\begin{aligned} \mathrm{KL}(q(x'|x)\|p(x'|x)) + \mathsf{E}_{x' \sim q(x'|x)}[v(x')] \quad &= \quad \mathsf{E}_{x' \sim q(x'|x)} \left(\ln \frac{q(x'|x)}{p(x'|x)e^{-v(x')}} \right) \\ &= \quad -\ln(k(x)) + \mathrm{KL}\left(q(x'|x) \| \frac{p(x'|x)e^{-v(x')}}{k(x)} \right), \end{aligned} \tag{4.9}$$

where $k(x)$ is a normalization term defined as

$$k(x) = \mathsf{E}_{x' \sim p(x'|x)}[\mathsf{E}(-v(x'))] = \int_X p(x'|x)e^{-v(x')}dx'. \tag{4.10}$$

The Bellman equation (4.8) is now expressed as

$$J_\varepsilon^* + v(x) - \varepsilon c(x) = -\ln(k(x)) + \min_{q(x'|x)} \mathrm{KL}(q(x'|x)||\frac{p(x'|x)e^{-v(x')}}{k(x)}). \tag{4.11}$$

The K-L divergence is a non-negative metric that is zero if and only if the two distributions are equal. This gives the optimal control law in terms of closed-loop dynamics:

$$q^*(x'|x) = \frac{p(x'|x)e^{-v(x')}}{k(x)} = \frac{p(x'|x)e^{-v(x')}}{\int_X p(x'|x)e^{-v(x')}dx'}. \tag{4.12}$$

Using the optimal control, the Bellman equation is given by

$$e^{-(J_\varepsilon^* + v(x))} = e^{-\varepsilon c(x)} E_{x' \sim p(x'|x)}[e^{-v(x')}] \tag{4.13}$$

Denote $\lambda_\varepsilon = e^{-J_\varepsilon^*}$ and define a non-negative auxiliary function $Z_\varepsilon(x) \doteq e^{-v(x)}$ to express (4.13) as

$$\lambda_\varepsilon Z_\varepsilon(x) = e^{-\varepsilon c(x)} \mathsf{E}_{p(x'|x)}[Z_\varepsilon(x')]. \tag{4.14}$$

As $\varepsilon \to 0$, the limiting problem is formally given by

$$\lambda_0 Z_0(x) = \mathsf{E}_{p(x'|x)}[Z_0(x')], \tag{4.15}$$

where $\lambda_0 = e^{-J_0^*}$.

4.2.2 Example

To make these ideas precise, we consider the scalar system first introduced in Example 4.2.1. The scalar system is given by

$$\mathbf{x}_{t+1} = a\mathbf{x}_t + u_t + \mathbf{d}_t, \tag{4.16}$$

where t is the discrete time, $\mathbf{x}_t \in \mathbb{R}$, $u_t \in \mathbb{R}$ is control and $\mathbf{d}_t \sim N(0, \sigma^2)$. We assume $c(x) = x^2$. The average cost optimal control problem is to minimize

$$J_\varepsilon = \lim_{N\to\infty} \frac{1}{N} \mathsf{E}[\sum_{t=0}^{N-1} \varepsilon \mathbf{x}_t^2 + \mathrm{KL}(q(\mathbf{x}_{t+1}|\mathbf{x}_t) \| p(\mathbf{x}_{t+1}|\mathbf{x}_t))]. \tag{4.17}$$

For $\varepsilon > 0$, the solution to this problem is given by the following Lemma. The proof appears in Appendix B.1.

Lemma 4.2.2. *Consider the optimal control problem with dynamics (4.16) and the cost functional (4.17). For $\varepsilon > 0$, the optimal closed-loop dynamics are given by*

$$q^*(x'|x) = p(x'|x) e^{-\varepsilon x^2} e^{\kappa(x^2 - x'^2)} \sqrt{2\sigma^2\kappa + 1}.$$

The optimal average cost

$$J_\varepsilon^* = \frac{1}{2} \ln(2\sigma^2\kappa + 1),$$

and the eigenfunction $Z_\varepsilon(x) = e^{-\kappa x^2}$ *where* κ *is a non-negative solution of*

$$\kappa - \varepsilon = \frac{\kappa a^2}{2\sigma^2\kappa + 1}.$$

In the limit as $\varepsilon \to 0$, we have the following fundamental limitation result. The proof appears in Appendix B.2.

Theorem 4.2.3. *For the optimal control problem with dynamics (4.16) and the cost functional (4.17),*

$$J_0^* = \begin{cases} \ln|a| & \text{for } |a| > 1, \quad \text{(Non-ergodic case)} \\ 0 & \text{for } |a| < 1 \quad \text{(ergodic case)} \end{cases} \tag{4.18}$$

Before closing this section, we make two remarks. The first remark concerns the nature of control. For $\varepsilon = 0$, the open-loop dynamics are given by $p(x'|x) \sim N(ax, \sigma^2)$ and the optimal closed-loop dynamics are given by

$$q^*(x'|x) \sim N(\frac{x}{a}, \frac{\sigma^2}{a^2}).$$

One important observation is that this transition kernel is not realizable using an affine control as in Example (4.2.1). As already noted in the Example, an additive control can not affect the variance. With any additive control $u = k(x)$, the closed-loop dynamics would be of the form $N(ax + k(x), \sigma^2)$.

So the assumption on the nature of control is rather strong. Theorem 4.2.3 shows that there are fundamental limitations on achievable performance inspite of this.

The other remark concerns fundamental limitations for the classical optimal control problem:

$$J_\varepsilon = \lim_{N\to\infty} \frac{1}{N} \mathsf{E}[\sum_{t=0}^{N-1} \varepsilon \mathbf{x}_t^2 + u_t^2]. \tag{4.19}$$

In this case, it is a straightforward calculation to obtain the following result:

Theorem 4.2.4. *For the optimal control problem with dynamics (4.16) and the cost functional (4.19),*

$$J_0^* = \begin{cases} |a|^2 - 1 & \text{for } |a| > 1, \\ 0 & \text{for } |a| < 1. \end{cases} \tag{4.20}$$

One thus sees that limitations equal the right hand side of the Bode formula for the problem (4.17) but not for (4.19).

4.3 Fundamental limitations in control

Fundamental limitations are obtained via analysis of the eigenvalue problem (4.14) for $\varepsilon > 0$ and the eigenvalue problem (4.15) for the limiting case $\varepsilon = 0$. We define a Markov operator $\mathbb{U} : L^\infty(X) \to L^\infty(X)$:

$$\mathbb{U}Z(x) \doteq \mathsf{E}_{p(x'|x)}[Z(x')] = \int_X p(x'|x)Z(x')dx'.$$

This operator is the dual to the Markov operator $\mathbb{P}$ with respect to the standard inner-product

$$< Z(x), \rho(x) > \doteq \int_X Z(x)\rho(x)dx,$$

where $\rho(x) \in L^1(X)$ and $Z(x) \in L^\infty(X)$. In deterministic settings, $\mathbb{U}$ is called the Koopman operator.

The two eigenvalue problems (4.14) and (4.15) can be expressed as:

$$\begin{aligned} &\text{For} \quad \varepsilon > 0: \quad e^{-\varepsilon c(x)}\mathbb{U}Z_\varepsilon(x) = \lambda_\varepsilon Z_\varepsilon(x) \\ &\text{For} \quad \varepsilon = 0: \quad \mathbb{U}Z_0(x) = \lambda_0 Z_0(x), \end{aligned} \tag{4.21}$$

where $c(x) \geq 0$ is assumed to be a continuous function. Recall $Z_\varepsilon(x) = e^{-v_\varepsilon(x)}$, so $Z_\varepsilon(x) > 0$ on X[4].

There are two important points to be made here:

1. The fundamental limitations depend upon the open loop dynamics – stochastic kernel $p(x'|x)$. For $\varepsilon > 0$, the limitations also depend upon the nature of performance requirement – cost function $c(x)$.

2. As $\varepsilon \to 0$, $e^{-\varepsilon c(x)} \to 1$ on compact subsets of X in the sup-norm topology. We thus have $\lambda_\varepsilon \to \lambda_0$ and $Z_\varepsilon(x) \to Z_0(x)$ in a point-wise sense [142][5]. We have $Z_0(x) \geq 0$ on X.

As a result, we can obtain fundamental limitations by considering non-negative bounded eigenfunctions of (4.21). One such eigenfunction is known to be the unity eigenfunction, denoted as $1(x)$. The associated eigenvalue $\lambda_0 = 1$ and $J_0^* = -\ln(\lambda_0) = 0$.

Definition 4.3.1. *The open-loop dynamics $p(x'|x)$ is said to be ergodic if every non-negative eigenfunction of (4.21) is of the form $c \cdot 1(x)$ where $c > 0$.*

We thus have the following two cases to consider:

1. If $p(x'|x)$ is ergodic then $J_0^* = 0$ and $J_\varepsilon^* \to J_0^*$ for any choice of $c(x) \geq 0$[6].

[4] Regularity properties of the eigenfunction $Z_\varepsilon(x)$ will depend upon assumptions on $p(x'|x)$. These properties need to be further investigated.

[5] Under suitable assumptions, one can perhaps obtain stronger conclusions on convergence and on regularity properties of limiting function $Z_0(x)$. This is a subject of future work.

[6] A perturbation analysis may be used to obtain an asymptotic formula for fundamental limitation J_ε^* as $\varepsilon \to 0$.

2. If $p(x'|x)$ is not ergodic then the $\lim_{\varepsilon\to 0} J_\varepsilon^*$ depends upon the choice of $c(x)$.

4.3.1 Example 1: Linear Dynamics with Gaussian Noise

Consider the SISO LTI system

$$\mathbf{x}_{t+1} = A\mathbf{x}_t + Bu_t + \mathbf{d}_t, \tag{4.22}$$

where t is the discrete time, $\mathbf{x}_t \in \mathbb{R}^n$, $u_t \in \mathbb{R}$ is control and $\mathbf{d}_t \sim N(0,R)$ with $R \succ 0$. For the open-loop dynamics, the stochastic kernel $p(x'|x) = N(Ax,R)$ is used to define the two Markov operator $\mathbb{P}$ and $\mathbb{U}$.

We first assume that A is Picard, i.e., has all its eigenvalues inside the unit circle. For this case, we have:

1. The Markov operator $\mathbb{P}$ has a unique eigenvalue at 1. The eigenfunction is the invariant density $\pi(x) = N(0,\Sigma_{xx})$, where Σ_{xx} solves the following Lyapunov equation

$$A\Sigma_{xx}A^T - \Sigma_{xx} + R = 0.$$

2. The Markov operator $\mathbb{U} : L^\infty(X) \to L^\infty(X)$ also has a unique eigenvalue at 1. The only bounded eigenfunction is $1(x)$.

Let $Z(x)$ be a bounded eigenfunction of $\mathbb{U}$ with eigenvalue λ then

$$< Z(x), \pi(x) >=< Z(x), \mathbb{P}\pi(x) >=< \mathbb{U}Z(x), \pi(x) >= \lambda < Z(x), \pi(x) > . \tag{4.23}$$

If $\lambda \neq 1$ then $< Z(x), \pi(x) >= 0$, and $Z(x)$ must change sign. So, the open-loop dynamics are ergodic.

Theorem 4.3.2 (Ergodic)**.** *Consider the optimal control problem (4.17) for the LTI system (4.22) where A is assumed Picard. Then*

$$J_0^* = 0.$$

We next consider the LTI system (4.22) where A has all its eigenvalues outside the unit circle. For this case, the fundamental limitations depend upon the choice of $c(x)$. We have the following theorem. The proof appears in Appendix B.3.

Theorem 4.3.3 (Non-ergodic)**.** *Consider the optimal control problem (4.17) with $c(x) = x^2$. The dynamics are given by the LTI system (4.22) where A has all its eigenvalues outside unit circle. Then*

$$J_0^* = \lim_{\varepsilon\to 0} J_\varepsilon^* = \ln|A|.$$

4.3.2 Example 2: Nonlinear Dynamics with Gaussian Noise

For nonlinear systems, the property of ergodicity crucially depends upon the nature of noise. With Gaussian noise, a very general class of nonlinear systems are known to be ergodic. Consider, for example, the system

$$\mathbf{x}_{t+1} = T(\mathbf{x}_t) + \mathbf{d}_t \tag{4.24}$$

where $\mathbf{d}_t \sim N(0,R)$ with $R \succ 0$. $T : \mathbb{R}^n \to \mathbb{R}^n$ is a continuous map that additionally satisfies

$$\|T(x)\| \leq \gamma \|x\|, \qquad \text{for } \|x\| \geq M,$$

with $|\gamma| < 1$ for some $M > 0$. For this system, ergodicity follows from the Corollary 10.5.2 in [126]:

Theorem 4.3.4 (Corollary 10.5.2 in [126])**.** *Consider the discrete-time system (4.24) on $X = \mathbb{R}^n$. The Markov operator $\mathbb{P} : L^1(X) \to L^1(X)$ given by*

$$\mathbb{P}\rho(x') = \int_X \rho(x) \frac{1}{(2\pi)^{d/2}|R|^{1/2}} e^{-\frac{1}{2}(x'-T(x))'R^{-1}(x'-T(x))} dx,$$

has a unique invariant density that is asymptotically stable.

The fundamental limitation result is expressed in the following conjecture.

Conjecture 4.3.5. *Consider the optimal control problem (4.17) for open-loop dynamics (4.24). Then*

$$J_0^* = \lim_{\varepsilon \to 0} J_\varepsilon^* = 0.$$

As a result, the fundamental limitations expressed in Theorem 4.3.3 for LTI dynamics are very fragile. For example, suppose

$$T(x) = \begin{cases} Ax & \text{for} \quad \|x\| \leq M_1 \\ \text{sat}(Ax) & \text{otherwise,} \end{cases}$$

where A has its eigenvalues outside unite circle and $\text{sat}(\cdot)$ is saturation function. Even though $J_0^* = \ln|A|$ for LTI dynamics, $J_0^* = 0$ provided there is suitable nonlinearity such as the saturation nonlinearity for large x.

Such a conclusion is not very useful or unexpected for $\varepsilon = 0$. The important point is that for small value of ε, $J_\varepsilon^* = \ln|A| + O(\varepsilon)$ for LTI dynamics while $J_\varepsilon^* = O(\varepsilon)$ provided there is suitable nonlinearity for large x. The nature of optimal control is expected to be very different for linear and nonlinear case. This needs to be investigated.

4.3.3 Example 3: Ergodic Dynamics with Positive Lyapunov exponents

For LTI systems, ergodicity is equivalent to all Lyapunov exponents being negative. For nonlinear systems, the two notions can be quite different. Consider, for example, the system defined by mod-2 map (dyadic map) $T(x) \doteq \mathrm{mod}(2x,1)$ on $X = [0,1]$:

$$x_{t+1} = T(x_t) \quad \text{for} \quad x \in X. \tag{4.25}$$

The Lyapunov exponent is $\ln(2)$. The dynamics are ergodic with a unique invariant density given by the Lebesgue (uniform) density on X [126]. Suppose $Z(x)$ is any eigenfunction of $\mathbb{U}$ with eigenvalue $\lambda < 1$ then by repeating the argument in (4.23), we have

$$\int_X Z(x)dx = 0.$$

Conjecture 4.3.6. *Consider the optimal control problem (4.7) for mod-2 dynamics (4.25). In this case,*

$$J_0^* = \lim_{\varepsilon \to 0} J_\varepsilon^* = 0.$$

In the remainder of this Section, we summarize results of the numerical solution of the eigenvalue problem (4.14). We consider a perturbed version of the mod-2 dynamics:

$$\mathbf{x}_{t+1} = \mathrm{mod}(2\mathbf{x}_t + \mathbf{d}_t, 1) \doteq T^{(d)}(\mathbf{x}_t), \quad \text{for } \mathbf{x}_t \in X, \tag{4.26}$$

where $\mathbf{d}_t$ is uniform disturbance in the interval $[-w,w]$ with $w = 0.05$. By construction, $T^{(d)} : X \to X$. For the optimal control problem (4.7), we choose $c(x) = \sin(\pi x)$ for $x \in X$.

In order to obtain numerical solution of the eigenvalue problem, we discretize X into $N = 600$ equi-spaced points. The eigenfunction $Z(x)$ is discretized as a $N \times 1$ vector. Figure 4.1 depicts $J_\varepsilon^* = -\ln(\lambda_\varepsilon)$ as a function of ε. As $\varepsilon \to 0$, $J_\varepsilon^* \to 0$.

We next discuss the nature of optimal control solution for a fixed value of $\varepsilon = 0.01$. Figure 4.2 depicts the eigenfunction $Z_\varepsilon(x)$, and $v_\varepsilon(x) = -\ln(Z_\varepsilon(x))$ for $\varepsilon = 0.01$. The eigenfunction $Z_\varepsilon(x)$ achieves local maximum at the following set of points:

$$\mathbb{S} \doteq \{0, \frac{1}{8}, \frac{1}{4}, \frac{3}{8}, \frac{1}{2}, \frac{5}{8}, \frac{3}{4}, \frac{7}{8}, 1\}.$$

It is conjectured that the optimal control works by directing trajectory towards these local maximum points of the

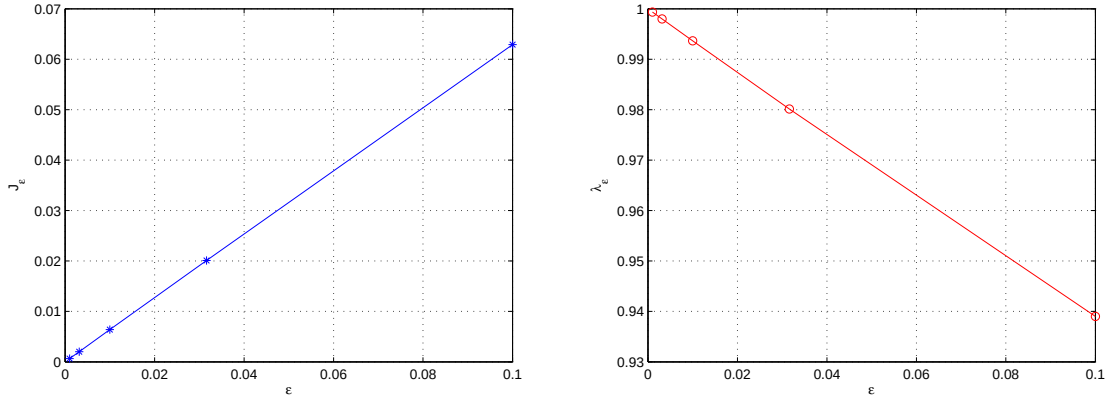

(a) (b)

Figure 4.1: Plots of (a) J_ε^* and (b) λ_ε as function of ε

eigenfunction $Z_\varepsilon(x)$. We recall that the optimal closed loop dynamics are given by (see (4.12)):

$$q^*(x'|x) = \frac{p(x'|x)Z_\varepsilon(x')}{k(x)}. \tag{4.27}$$

For a fixed $x \in X$,

$$\begin{aligned} \operatorname*{argmax}_{x' \in X} q^*(x'|x) &= \operatorname*{argmax}_{x' \in supp(p(x'|x))} Z_\varepsilon(x'), \\ \operatorname*{argmin}_{x' \in X} q^*(x'|x) &= \operatorname*{argmin}_{x' \in supp(p(x'|x))} Z_\varepsilon(x'), \end{aligned}$$

because $p(x'|x)$ is uniform. As a result, control works by increasing the probability of transition to a local maximum in the support of $p(x'|x)$.

The points in the set $\mathbb{S}$ are significant because mod-2 map sends these points to $0/1$ in the smallest number of transitions: $T^0(0) = T^0(1) = 0$, $T(\frac{1}{2}) = 0$, $T^2(\frac{1}{4}) = T^2(\frac{3}{4}) = 0$, $T^3(\frac{1}{8}) = T^3(\frac{3}{8}) = T^3(\frac{5}{8}) = T^3(\frac{7}{8}) = 0$[7]. The optimal control thus works by causing the trajectory to go towards these points from where it is easy to reach 0.

It is conjectured that the number of local maximum points of eigenfunction $Z_\varepsilon(x)$ depend upon the spread w of uniform disturbance. In the limit as $w \to 0$, the set $\mathbb{S}$ is given by

$$\mathbb{S} = \{x \in X : x = \frac{k}{2^n} \quad \text{for } 0 \le k \le 2^n - 1, \quad n, k \in \mathbb{N}\}$$

For the unperturbed map, these points in $\mathbb{S}$ reach 0 in at most n iterations.

[7]Here, $T^2(x) \doteq T(T(x))$, $T^3(x) \doteq T(T(T(x)))$ and T^0 is the identity map.

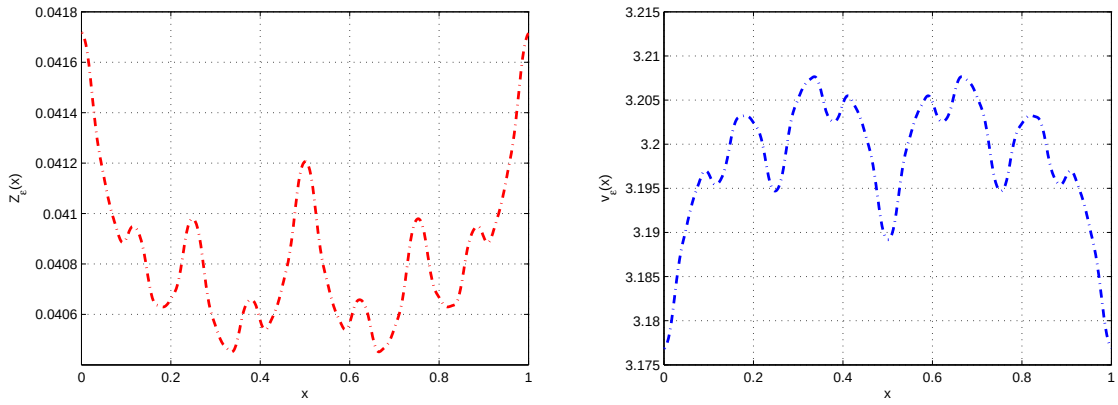

(a) (b)

Figure 4.2: Plot of (a) $Z_\varepsilon(x)$ and (b) $v_\varepsilon(x)$ for $c(x) = 0.01\sin(\pi x)$.

A detailed analysis of this optimal control as a function of w and ε is a subject of future investigation.

4.3.4 Example 4: Non-ergodic Dynamics

The fundamental limitations in control arise on account of non-ergodic open-loop dynamics. In this section, we revisit the example discussed in Section 1.3.1:

$$\mathbf{x}_{t+1} = \alpha(\mathbf{x}_t) + \mathbf{d}_t \doteq T^{(d)}(\mathbf{x}_t),$$

where

$$\alpha(x) = \begin{cases} a \cdot x & \text{for } |x| < L, \\ \text{sgn}(x) aL & \text{otherwise}, \end{cases} \tag{4.28}$$

where $a > 1$. The disturbance $\mathbf{d}_t$ is uniform in the interval $[-w, w]$. We set $X \doteq [-(aL+w), aL+w]$, so $T^{(d)} : X \to X$. We have two limiting cases to consider:

1. In the limit of $w \to 0$, the dynamics are non-ergodic with two attractors near $-L$ and L.

2. In the limit of $w \to \infty$, the dynamics are ergodic.

In the remainder of this section, we summarize results of the numerical solution of the eigenvalue problem (4.15). We fix $a = 2$ and $L = 6.4$ and solve for possible λ_0 and $Z_0(x)$ as the width w of the uniform disturbance varies. For each fixed value of w, the discretization of Markov operator $\mathbb{U}$ is obtained by dividing X into $N = 600$ equi-spaced points. Figure 4.3 depicts eigenfunctions for the two limiting case, where $w = 0.4$ and $w = 4.0$, respectively.

It is observed that the spectrum of the Markov operator is qualitatively different in the two limits:

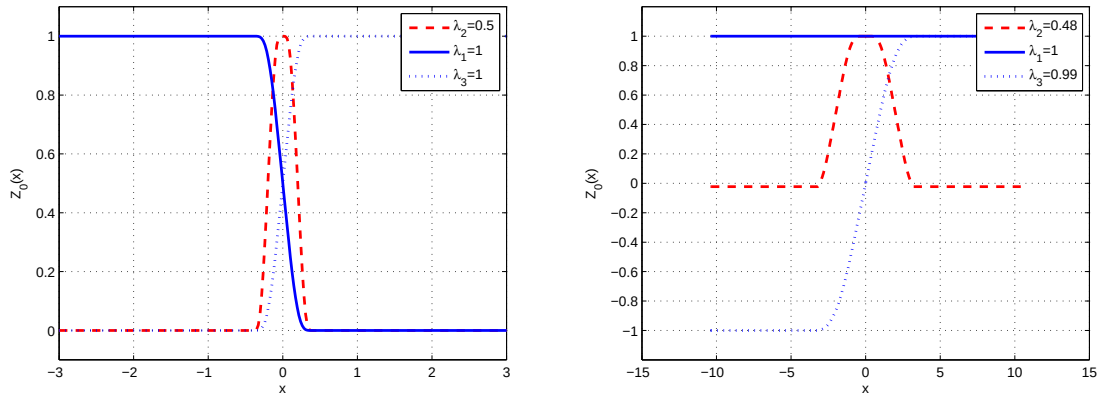

(a) $w = 0.4$ (b) $w = 4.0$

Figure 4.3: (a) For $w = 0.4$, there are three non-negative eigenfunctions with eigenvalues $\lambda_0 = 1, 1, \frac{1}{2}$. (b) For $w = 4.0$, there is only one non-negative eigenfunction with eigenvalue $\lambda_0 = 1$. The other two eigenfunctions change sign on X.

1. If w is very small, there are three non-negative eigenfunctions, two for eigenvalue $\lambda_0 = 1$ and one for eigenvalue $\lambda_0 = 0.5$. The corresponding $J_0^* = -\ln(\lambda_0) = \ln 2$.

2. If w is very large, there is only one non-negative eigenfunction $\lambda_0 = 1$. The other two eigenfunctions change sign on X. The corresponding $J_0^* = -\ln(\lambda_0) = 0$.

Further analysis on this problem is a subject of future work.

4.4 Conclusion

The main conclusions of the Chapter are:

1. The fundamental limitations arise only if the open-loop dynamics are non-ergodic. In particular, $J_0^* = 0$ if the open-loop dynamics are ergodic.

2. For LTI systems with Gaussian noise, the limitations are given by $J_0^* = \sum_k \ln|p_k|$, where $\ln|p_k|$ are the positive Lyapunov exponents, as in the Bode formula. In particular, $J_0^* = 0$ if the open-loop LTI system is asymptotically stable.

3. For nonlinear systems with Gaussian noise, $J_0^* = 0$ under rather mild assumption on dynamics (contractivity for large x). This suggests that the fundamental limitation result for the LTI case is fragile with respect to certain types of nonlinearities.

4. With the aid of mod-2 example in Section 4.3.3, we show that positive Lyapunov exponents may not be central to the analysis of fundamental limitations in the nonlinear case. The optimal control solution in these case is reminiscent of the control of chaos literature where similar points have been made.

Chapter 5

Optimal Sensor Location Design for Tracking Agents with Uncertain Dynamics

5.1 Introduction

Surveillance and monitoring systems with spatially distributed sensors are becoming increasingly common [143, 144, 145, 99]. A prototypical application is the estimation of location of mobile agents during emergency evacuation (egress) in a building; Figure (5.1) describes the layout of a single office floor in a building with sensors (video cameras) in the corridors. The feed from a number of video cameras as well as the measurements from light, CO_2, and motion sensors in a building can be used to monitor the movement of the building occupants [94]. Similar monitoring systems are also being put to use in tracking the traffic in large street networks [146, 145]. Complexity is a common feature in such applications, arising from both the uncertain dynamic nature of agent movement, and the large number of sensors [95, 96]. This makes the task of finding an "optimal" locations of the sensors a challenging problem.

Historically, the problem of choosing a sensor configuration which delivers best performance was studied by the chemical process control community in the 70's (see [147, 148] and references therein). Their focus was on processes with linear dynamics, with performance measures such as process observability and robustness to sensor faults. In recent years, this problem is of interest to the wireless sensor networks community [97, 98, 99]. In [98], the authors propose an approach to optimize sensor locations for localization of a target at a fixed location. In [97], certain heuristics are proposed for choosing sensor location that leads to maximum entropy reduction of the posterior target location distribution. In [100, 99], combinatorial optimization based approaches are considered for choosing sensor locations in order to maximize mutual information while maintaining constraints on communication quality among sensors.

In much of this recent work, the focus has been on sensing processes that are either in steady- or near steady-state (say temperature distribution over a given area) or have simple linear models of dynamics. There are several important surveillance and monitoring applications, however, where transient nonlinear and uncertain dynamics are central to the performance objective. For example, in estimation of agents during building evacuation, *only* the transient dynamics of agent movement during egress are useful. In the steady-state, the building is empty so there is nothing to monitor.

Motivated by the estimation of agent movement in the building evacuation problem, we consider models of dy-

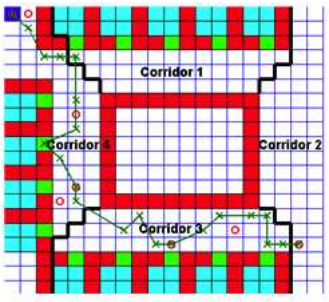

Figure 5.1: A floor of a building with four hallways discretized into 400 cells. The motion of a mobile agent through the building is modeled as a Markov chain evolving over 400 states, each cell being a possible state of the process.

namics as a Markov chain on a finite graph. Figure 5.1 depicts a single realization of the Markov process that gives the trajectory of the agent as she exits the building. Apart from models of agent movement [101, 94], such Markov models have been used for simulating traffic in buildings, planes, and outdoor walkways [101, 102, 103, 104, 105]. Markov chains on finite graphs are also obtained after discretizing a nonlinear dynamical system over a bounded domain [106], and as such represent a useful paradigm for modeling nonlinear dynamics.

Given system dynamics (a Markov model) and sensor configuration (sensor locations in this chapter), Bayesian estimation can be used to obtain an estimate on the agent location given the history of past observations from sensor readings. The locations of the sensors crucially affects the information-content of the sensor readings and thus the quality of the estimates obtained. We measure the quality of an estimate at a certain time in terms of uncertainty – conditional entropy of the state given the history of past observations. To measure the performance of a given choice of sensor locations, we propose the time-cumulative uncertainty in the state estimates. One important feature of this metric is that it is algorithm-independent: it provides a lower bound on uncertainty for any algorithmic implementation of the estimator. Computation cost of this metric, however, is in general high since it involves entropy rates of Hidden Markov Model (HMM)s, which are costly to compute [107]. To address this issue, we derive certain upper bounds that are much easier to compute. These bounds are tight under certain conditions on the dynamics that are relevant to the building evacuation problem. Numerical investigations show that even when the bounds are not tight, they are close to the true metric, so that optimal sensor locations can be designed by optimizing over the bound. Computation of the bound takes a fraction of the time needed to estimate the true metric using Monte Carlo simulations.

The remainder of this chapter is organized as follows. In section 5.2, an abstraction of the problem in terms of Markov chain on finite graphs is described. The performance metric J is proposed and its bound $\bar{J}$ constructed for the single-sensor case on arbitrary graphs, along with extension to multi-sensor case on a 1-D graph. In section 5.3 design of sensor locations with the aid of these bounds is illustrated using examples. Conclusions and directions for future work appear in Section 5.4.

5.2 Discrete Graph Formulation

We consider dynamics that can be described by a Markov chain over finite state space. To further reduce the complexity, we only consider binary sensors such that a sensor's output is either 1 or 0. This model of dynamics and sensing is general enough to cover a wide variety of situations, such as agent movement in buildings monitored by wireless sensor networks [149], monitoring of highway traffic from loop detectors [145], etc.

Dynamics over a graph: The building is divided into a finite number of cells, each cell is called a node. We denote the successive locations of the agent by $\{x(0), x(1), \ldots, x(t)\}$. Let the sequence $\{1, 2, \ldots, N\}$ denote the nodes in the building that can be occupied by the agent ($N = 400$ states for the model shown in Figure 5.1). The behavior of the agent is assumed to be Markovian: for each i, j, and each $k \geq 0$,

$$P(i, j) = \Pr(x_{k+1} = j \mid x_k = i) = \Pr(x_{k+1} = j \mid x_0^{k-1};\ x_k = i). \tag{5.1}$$

The Markov transition matrix is used to model the preference of a typical agent. The building is now a *graph* $\mathscr{G} = (\mathscr{V}, \mathscr{E})$, where each element of the set $\mathscr{V} = \{1, 2, \ldots, N\}$ corresponds to a value that the state x can take, and each element (i, j) of $\mathscr{E}$ corresponds to a possible transition from i to j in one time step. The elements of $\mathscr{V}$ are called *nodes* and those of $\mathscr{E}$ are called *edges* of the graph. As a result, the dynamics now evolves over the nodes of the graph $\mathscr{G}$. Equation (5.1) represents an approximation of true agent dynamics.

We assume that the graph has a well-defined *entrance* node – whose index is usually taken as node 1 – and an *exit* node – whose index is usually taken as N. The agent enters the graph via the entrance node, so that $x_0 = 1$. The fact that the agent eventually exits the graph is ensured by requiring the exit node N to be an absorbing state. The remaining nodes are assumed to be transient. For any sample trajectory, we have $\lim_{k\to\infty} x_k = N$. For the Markov chain P, $e_N \doteq [0, \ldots, 0, 1]$ is the unique steady state distribution.

Sensing: The possible locations of a sensor are the nodes of the graph $\mathscr{G}$, and the number of sensors is denoted by m. The sensors are assumed to be binary: the reading of the j^{th} sensor at time k – denoted by $y_k^{(j)}$ (where $y_k^{(j)} \in \{0, 1\}$ for $j \in \{1, \ldots, m\}$ for every k) – is 1 if and only if the agent at time k is at the node where the sensor j is located. The node of $\mathscr{G}$ where the j^{th} sensor is located is denoted by $\ell(j) \in \mathscr{V}$. We further assume the sensors are reliable that do not have false readings. We denote the vector of sensor observations at time k as $y_k \doteq (y_k^{(1)}, \ldots, y_k^{(m)})$.

For a given sensor locations, we are interested in estimating the state based on history of past observations from sensor readings. The design objective is to obtain the locations of the sensors so that the *estimation performance* is the best possible.

Performance metric: For a given graph $\mathscr{G} = (\mathscr{V}, \mathscr{E})$, dynamics P, and *sensor locations* $\{\ell(1), \ldots, \ell(m)\} \subset \mathscr{V}$, we

propose the following performance metric

$$J := \sum_{k=0}^{\infty} H(x_k|y_0^k, x_0 = 1) \tag{5.2}$$

where x_k denotes the agent location at time k, and $y_0^k = \{y_0, \ldots, y_k\}$ denotes the history of past observations. $H(x_k|y_0^k, x_0 = 1)$ denotes the conditional entropy [150]. It is obtained by considering the so-called belief process which is denoted by $\pi_k(x) \doteq p(x_k|y_0^k)$. It represents one's belief in the current state given the history of past observations [16]. The conditional entropy $H(x_k|y_0^k) \doteq \mathsf{E}_{p(y_0^k)}[-\ln \pi_k]$ is a measure of the average uncertainty at time k. Hence, J is a measure of the cumulative uncertainty regarding the agent's location summed over all times. The series (5.2) converges because the Markov chain is assumed to be absorbing.

Since the entropy $H(x_k|y_0^k)$ reflects the uncertainty in the optimal estimate of the state. When additional constraints are present, such as bandwidth limitations and delay in transmitting data from sensors to a fusion center, or due to distributed processing of data, the resulting estimate will have a higher uncertainty (in an expected sense) at every time k, no matter what estimation algorithm is used. As a result, the metric defined in (5.2) represents an algorithm-independent lower bound on the cumulative uncertainty associated with the estimate $\hat{x}_k$ of the state x_k over time.

5.2.1 Entropy Bound for a Single Sensor

In this section, we describe an upper bound on J, and an algorithm to compute it, when there is a single sensor ($m = 1$). The location (node index) of the sensor is denoted by ℓ. The bound will be exact for a certain class of Markov chains. The bound uses the concept of first hitting time of a Markov chain [151].

Let τ_1 be the first hitting time of the sensor location ℓ, i.e., τ_1 is the minimum k such that $x_k = \ell$. We denote the distribution of τ_1 as $p(\tau_1)$. For a Markov chain P over any connected graph, this distribution can be computed in a straightforward manner. We omit the details in the interest of brevity. The bound is provided in Theorem 5.2.2, which requires the computation of two quantities that are described below.

1. Define

$$\mathscr{H}_1(\tau_1 = k') \doteq \sum_{k=1}^{k'-1} h(\mu_k) \tag{5.3}$$

where $\mu_0 = e_1$ and μ_k is the conditional distribution of x_k given that $\tau_1 > k$, i.e., conditioned on the event that the sensor hasn't detected the agent until time k. In other words, for $i = 1, \ldots, N$, $\mu_k(i) = \Pr(x_k = i|y_0^k = \mathbf{0}, x_0 = 1)$, where

0 is the vector of all 0's. Also define

$$\tilde{\mu}_k(i) \doteq \Pr(x_k = i | y_0^{k-1} = \mathbf{0}, x_0 = 1) = \Pr(x_k = i | x_0 = 1, x_1 \neq \ell, \ldots, x_{k-1} \neq \ell).$$

Let us first compute μ_1. Clearly, $\mu_1(\ell) = 0$. For $i \neq \ell$,

$$\mu_1(i) = \Pr(x_1 = i | x_1 \neq \ell, x_0 = 1) = \frac{\Pr(x_1 = i, x_1 \neq \ell | x_0 = 1)}{\Pr(x_1 \neq \ell | x_0 = 1)} = \frac{\tilde{\mu}_1(i)}{1 - \tilde{\mu}_1(\ell)}.$$

It is now straightforward to see that μ_k can be computed recursively with the following algorithm:

1. $\mu_0 = e_1$, $\tilde{\mu}_0 = e_1$.
2. $\tilde{\mu}_r = \mu_{r-1} P$.
3. $\mu_r(\ell) = 0$ and for $i \neq \ell$, $\mu_r(i) = \frac{\tilde{\mu}_r(i)}{1 - \tilde{\mu}_r(\ell)}$.

2. Consider one sample path of the process and let $\tilde{k}$ denote the time at which the agent leaves the sensor node for the first time. That is,

$$\tilde{k} = \min k \text{ such that } x_k = \ell, x_{k+1} \neq \ell.$$

Denote $z_r \doteq x_{\tilde{k}+r}$ for $r \geq 0$. Define

$$\mathscr{H}_{\text{exit}} \doteq \sum_{k=\tilde{k}}^{\infty} H(x_k) = \sum_{r=0}^{\infty} H(z_r) = \sum_{r=0}^{\infty} h(\pi_r) \tag{5.4}$$

where $\pi_r = \theta P^r$, where θ denotes the probability distribution of z_0. To determine θ, note that $\theta(\ell) = 0$. For $i \neq \ell$, we have

$$\theta(i) \doteq \Pr(x_{\tilde{k}} = i | x_{\tilde{k}} \neq \ell) = \frac{\Pr(x_{\tilde{k}} = i, x_{\tilde{k}} \neq \ell)}{\Pr(x_{\tilde{k}} \neq \ell)} = \frac{\Pr(x_{\tilde{k}} = i)}{1 - \Pr(x_{\tilde{k}} = \ell)}$$

where we have used the fact that $\{x_{\tilde{k}} = i\} \cap (\{x_{\tilde{k}} = \ell\})^c = \{x_{\tilde{k}} = i\}$ since the events $x_{\tilde{k}} = i$ and $x_{\tilde{k}} = \ell$ are mutually exclusive for $i \neq \ell$. The unconditional probabilities $\Pr(x_{\tilde{k}} = i)$ are simply the entries of $e_\ell P$. Thus we have

$$\theta(i) = \begin{cases} 0 & \text{if } i = \ell, \\ \frac{P(\ell,i)}{1 - P(\ell,\ell)} & \text{otherwise} \end{cases} \tag{5.5}$$

Before we present the result, we need to define strongly biased Markov chains for D graphs. A 1-dimensional (1-

D) graph with node set $\mathscr{V} = \{1, \ldots, N\}$ as shown in Figure 5.2. Such graphs describe spatial discretization of single routes. The entrance node represents the start of the route and the exit represents the end of the route. For egress type applications mentioned in the introduction, there is a particularly important class of Markov chains in which the movement is always towards the exit (e.g. egress problem in a building):

Definition 5.2.1. *Consider a Markov chain P on a one-dimensional graph $\mathscr{V} = \{1, \ldots, L\}$ where 1 is the entrance node and L is the exit node. We say P is* strongly biased *if $P(i, j) = 0$ whenever $i < j$.*

The next theorem provides a bound on J in terms of the quantities defined above that is useful for choosing the location of the sensor ℓ.

Theorem 5.2.2. *Consider a graph $\mathscr{G} = (\mathscr{V}, \mathscr{E})$ with dynamics P and a single sensor at location $\ell \in \mathscr{V}$. Let τ_1 denote the first hitting time for this sensor and $p(\tau_1)$ denote its distribution. Define*

$$\bar{J} \doteq \mathsf{E}_{p(\tau_1)}[\mathscr{H}_1] + \mathscr{H}_{exit} \tag{5.6}$$

where $\mathscr{H}_1$ and $\mathscr{H}_{exit}$ are defined by (5.3) and (5.4). We then have

$$J \leq \bar{J}$$

where the equality holds when $\mathscr{G}$ is a 1-D strongly biased Markov chain. □

Remark 5.2.3. *Note that $\mathscr{H}_{exit}$ can be approximated by $\sum_{r=0}^{R} H(\pi_r)$ for sufficiently large R. Similarly, $\mathsf{E}_{p(\tau_1)}[\mathscr{H}_1]$ can be approximated by $\sum_{k'=1}^{K} \mathscr{H}_1(\tau_1 = k')Pr(\tau_1 = k')$ for sufficiently large K. Thus, Theorem 5.2.2 offers a way of evaluating an upper bound on J that is computationally more tractable than computing J directly.*

Remark 5.2.4. *This tightness shows that for strongly biased Markov chains, we can exactly capture the overall uncertainty about agent position using the bound. Design of optimal sensor placement can now be carried out by optimizing over the bound $\bar{J}$ which is easier to compute than J. Thus, numerical search algorithms can be effectively utilized for optimal sensor placement. Although currently we define strongly biased chains only for 1D graphs, extensions to more general graphs where the motion is predominantly towards a certain direction, seems feasible.*

Proof. Using (5.2), we have

$$J = \sum_{k=0}^{\infty} H(x_k | y_0^k, x_0 = 1) = \sum_{k=0}^{\infty} \mathsf{E}_{p(\tau_1)}[H(x_k | y_0^k, x_0 = 1; \tau_1 = k')] = \sum_{k=0}^{\infty} \{ \sum_{k'=1}^{\infty} H(x_k | y_0^k, x_0 = 1; \tau_1 = k') p(\tau_1 = k') \} \tag{5.7}$$

Now,

$$\sum_{k=0}^{\infty} H(x_k|y_0^k, x_0 = 1, \tau_1 = k') = \sum_{k=0}^{k'-1} H(x_k|y_0^k, x_0 = 1, \tau_1 = k') \quad + \sum_{k=k'}^{\infty} H(x_k|y_0^k, x_0 = 1, \tau_1 = k') \tag{5.8}$$

Reversing the order of summation in (5.7), plugging (5.8) into it, and using (5.3), we get

$$J = \mathsf{E}_{p(\tau_1)}[\mathscr{H}_1] + \mathsf{E}_{p(\tau_1)}[\sum_{k=k'}^{\infty} H(x_k|y_0^k, x_0 = 1, \tau_1 = k')] \tag{5.9}$$

The sum $\sum_{k=k'}^{\infty} H(x_k|y_0^k, x_0 = 1)$ is equal to $\sum_{k=\tilde{k}}^{\infty} H(x_k|y_0^k, x_0 = 1)$ since when $k' \leq k < \tilde{k}$ we have $y_k \equiv 1$ which means $x_k = \ell$. For this case, $H(x_k|y_0^k, x_0 = 1) = 0$. Next

$$\sum_{k=\tilde{k}}^{\infty} H(x_k|y_0^k, x_0 = 1) \leq \sum_{k=\tilde{k}}^{\infty} H(x_k) = \mathscr{H}_{\text{exit}}$$

where the inequality holds because conditioning always serve to reduces uncertainty. Now 5.9) gives us

$$J \leq \mathsf{E}_{p(\tau_1)}[\mathscr{H}_1] + \mathsf{E}_{p(\tau_1)}[\mathscr{H}_{\text{exit}}] = \mathsf{E}_{p(\tau_1)}[\mathscr{H}_1] + \mathscr{H}_{\text{exit}} = \bar{J}$$

where the equality follows since H_{exit} is a constants with respect to τ_1 (which can be seen from the last series in (5.4)). The equality $J = \bar{J}$ holds when the chain is strongly biased, which concludes the proof. ■

5.2.2 Entropy Bound for Multiple Sensors

For multiple sensor location design case, we limit ourselves to 1-D graphs in this chapter. Extensions to more general graphs will be carried out in the future. We assume m sensors with locations $(\ell(1), \ldots, \ell(m))$ and an ordering whereby $\ell(j) < \ell(j')$ whenever $j < j'$. The m sensor readings at time step k form a vector y_k. To obtain a bound, we first define τ_j with respect to the sensor location $\ell(j)$. τ_1 is the first hitting time of the sensor 1. For $j > 1$, τ_j is defined as the time elapsed after the agent first leaves the sensor node $\ell(j-1)$ and the sensor $\ell(j)$ first detects the agent. The assumption that an agent is always detected by each sensor together with the ordering of sensors ensure that $\tau_j \geq 0$.

Due to the ordering , the considerations of multi-sensor case are analogous to the single sensor case. We reserve the notation k'_j to denote time of first detection by sensor j (for one sample path), and $\tilde{k}_j$ to denote time of agent first leaving sensor j. The distribution of τ_j is denoted by $p(\tau_j)$. Computing $p(\tau_j)$ is straightforward, but we omit the details for the sake of brevity. Similar to the 1-sensor case, derivation of a bound on J requires defining $\mathscr{H}_1$ and $\mathscr{H}_{\text{exit}}$, which are described below.

1. Define

$$\mathscr{H}_j(\tau_j = k') \doteq \sum_{k=0}^{k'-1} h(\mu_k) \tag{5.10}$$

where μ_k is the conditional distribution of $x_{\tilde{k}_{j-1}+k}$ given all past sensor readings. It can be computed using a recursive algorithm quite similar to the one described preceding Theorem 5.2.2, which we omit due to space limitations.

2. Define

$$\mathscr{H}_{exit} \doteq \sum_{k=\tilde{k}_m}^{\infty} H(x_k) = \sum_{k=0}^{\infty} h(\pi_k) \tag{5.11}$$

where $\pi_k = \theta P^k$, and θ here is defined as the probability distribution of agent at time $\tilde{k}_m$. The distribution π_k can be computed in a manner similar to that described earlier for the 1-sensor case.

The following theorem gives a bound on J for the multi-sensor case. The proof is provided in the appendix.

Theorem 5.2.5. *Consider a one-dimensional graph $\mathscr{G} = (\mathscr{V}, \mathscr{E})$ with dynamics given by P and m sensors located at $\{\ell(1), \ell(2), \cdots, \ell(m)\} \subset \mathscr{V}$. Denote*

$$\bar{J} = \sum_{j=1}^{m} \mathsf{E}_{p(\tau_j)}[\mathscr{H}_j] + \mathscr{H}_{exit} \tag{5.12}$$

where $\mathscr{H}_j$ and $\mathscr{H}_{exit}$ are defined by (5.10) and (5.11), respectively. We then have

$$J \leq \bar{J} \tag{5.13}$$

with equality if P is strongly biased. □

Proof. The proof follows the same line as in 1-sensor case. We first obtain bounds of accumulated uncertainty for a given sample path of observation sequence $\{\hat{y}_0^k\}$, and take expectation at the end. A key observation is that, after agent reach sensor $j-1$ for the first time (at k'_{j-1}), there is no uncertainty until it leaves at $\tilde{k}_j$. To evaluate the sum $\sum_{k=0}^{\infty} H(x_k | y_0^k = \hat{y}_0^k, x_0 = 1)$, only non-zero terms need to be considered. We then have

$$\sum_{k=0}^{\infty} H(x_k | y_0^k = \hat{y}_0^k, x_0 = 1) = \sum_{j=1}^{m} \{ \sum_{k=\tilde{k}_{j-1}}^{k'_j - 1} H(x_k | y_0^k = \hat{y}_0^k, x_0 = 1) \} + \sum_{\tilde{k}_m}^{\infty} H(x_k | y_0^k = \hat{y}_0^k, x_0 = 1)$$

For each j, using Markov property, we get

$$\sum_{k=\tilde{k}_{j-1}}^{k'_j - 1} H(x_k | y_0^k = \hat{y}_0^k, x_0 = 1) = \sum_{k=\tilde{k}_{j-1}}^{k'_j - 1} H(x_k | y_{\tilde{k}_{j-1}-1}^k = \hat{y}_{\tilde{k}_{j-1}-1}^k)$$

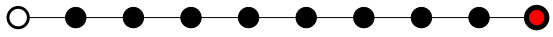

Figure 5.2: A 1 dimensional graph with 10 nodes. Node 1 on the left is the entrance and node 10 on the right is the exit. Two nodes are connected by an edge if and only if the transition probability between them is non-zero.

because when $k'_{j-1} \le k \le \tilde{k}_{j-1} - 1$, sensor $j-1$ always reads '1', indicating $x_k = \ell(j-1)$.

For the convenience of notation, we define $\{y(j)\}_k^r$ to be the reading of sensor j from time k to time r. From definition of $\mathscr{H}_j$, it can be shown that

$$\mathscr{H}_j(\tau_j = k') = \sum_{k=\tilde{k}_{j-1}}^{k'_j-1} H(x_k | \{y(j)\}_{\tilde{k}_{j-1}}^{k} = \mathbf{0}) \ge \sum_{k=\tilde{k}_{j-1}}^{k'_j-1} H(x_k | y_{\tilde{k}_{j-1}-1}^{k} = \hat{y}_{\tilde{k}_{j-1}-1}^{k})$$

The inequality hold because for any sample path, $\hat{y}_{\tilde{k}_{j-1}-1}^{k}$ must satisfy $\{\hat{y}(j)\}_{\tilde{k}_{j-1}}^{k} = \mathbf{0}$ when $k < k'_j$ (meaning sensor j does not detect the agent during this period). However, other elements of y_k can be 1, which serve to provide information about x_k and further reduce uncertainty.

Recall we also have

$$\sum_{\tilde{k}_m}^{\infty} H(x_k | y_0^k, x_0 = 1) \le \sum_{\tilde{k}_m}^{\infty} H(x_k) = \mathscr{H}_{exit}$$

Put these together, for any given sample path of $\{y_0^k\}$,

$$\sum_{k=0}^{\infty} H(x_k | y_0^k = \hat{y}_0^k, x_0 = 1) \le \sum_{j=1}^{m} \mathscr{H}_j + \mathscr{H}_{exit}$$

by arguments similar to that used in 1-sensor case, on taking expectation w.r.t $p(\tau_j)$, $1 \le j \le m$, (5.12) is obtained.

■

This bound comes as a natural extension of the bound in 1-sensor case: first divide the movement of agent into m stages, then bound the uncertainty in each stage. We now provide several examples using the bound $\bar{J}$ for sensor location design.

5.3 Design Using Bounds

5.3.1 Single Sensor Location Design

Example 5.3.1.

The first example involves designing the location of a single sensor in the 1-D graph with 10 nodes shown in Figure 5.2. The transition probability matrix for this graph is

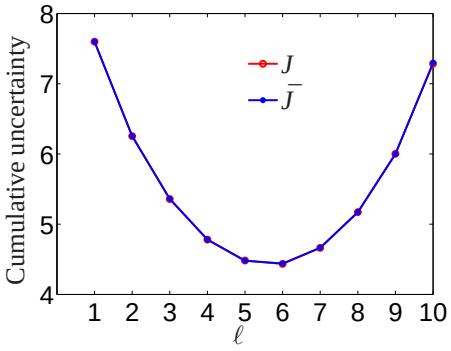

Figure 5.3: Designing a sensor's location in a 1-D graph by minimizing J. The performance metric J (estimated from 8000 MC simulations) and the bound $\bar{J}$ (computed from the formula (5.6)) are plotted against the 10 possible sensor locations. We see that the bound $\bar{J}$ closely matches the true value J, and is minimized by placing the sensor at the 6th node (the entrance at the left is node 1).

$$P = \begin{bmatrix} 0.1 & .9 & \cdots & \cdots & 0 \\ 0 & 0.1 & .9 & \cdots & 0 \\ \vdots & \vdots & \vdots & \vdots & \vdots \\ 0 & 0 & \cdots & 0.1 & .9 \\ 0 & 0 & \cdots & 0 & 1 \end{bmatrix}_{10\times 10} \tag{5.14}$$

This Markov chain is strongly biased, with node 1 as the entrance and node 10 as the exit. We compute the J and $\bar{J}$ for the 10 possible sensor locations. The value of the performance metric J is estimated using Monte Carlo simulation of 8000 runs. Figure 5.3 shows that:

1. $\bar{J} = J$ for every choice of sensor location. This is consistent with Theorem 5.2.2 since the chain is strongly biased.

2. The choice of sensor location that minimizes estimation uncertainty according to the metric J is node 6, so the optimal sensor location is node 6.

Example 5.3.2.

This example is on selecting a sensor's location in a 2-D graph. A single floor of a building can be realistically modeled as a 2-D graph. The uncertain motion of an agent is now described by a Markov chain that is defined over this graph. Consider the 2-D graph $\mathscr{G}$ and corresponding transition matrix P as in Fig. 5.4. Assume node 1 as entrance and node 9 as exit. For the 9 possible sensor locations, we computed performance metric J by Monte Carlo simulation of 4000 runs and its bound $\bar{J}$ following Theorem 5.2.2.

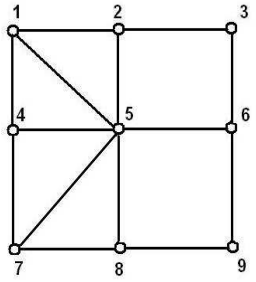

(a) $\mathscr{G}$

$$\begin{bmatrix} .1 & .3 & 0 & .3 & .3 & 0 & 0 & 0 & 0 \\ 0 & .1 & .4 & 0 & .5 & 0 & 0 & 0 & 0 \\ 0 & 0 & .1 & 0 & 0 & .9 & 0 & 0 & 0 \\ 0 & 0 & 0 & .1 & .5 & 0 & .4 & 0 & 0 \\ 0 & 0 & 0 & 0 & .1 & .5 & 0 & .4 & 0 \\ 0 & 0 & 0 & 0 & 0 & .1 & 0 & 0 & 0.9 \\ .1 & .3 & 0 & .3 & .3 & 0 & 0 & 0 & 0 \\ 0 & 0 & 0 & 0 & 0 & 0 & 0 & .1 & .9 \\ 0 & 0 & 0 & 0 & 0 & 0 & 0 & 0 & 1 \end{bmatrix}_{9\times 9}$$

(b) P

Figure 5.4: A 2-D graph with 9 nodes and the associated transition probability matrix P.

Algorithm	Example 5.3.2	Example 5.3.3
Monte Carlo	15.0977	$>$300
Bound J-bar	0.0556	0.0528

Table 5.1: Average running time comparison for computing J and $\bar{J}$

Figure 5.5 shows that:

1. $\bar{J} > J$ for every choice of sensor location.
2. The choice of sensor location that minimizes estimation uncertainty according to the metric J (and he bound $\bar{J}$) is node 5, which complies with intuition.

These two examples show that in many cases, the bound $\bar{J}$ can serve as a criterion for sensor location design instead of the true metric J. Of course, a more extensive comparison with larger graphs is needed before general conclusions can be drawn. The advantage of using the bound $\bar{J}$ instead of J lies in the low computation cost. In table 5.1, the average time required for computing J and $\bar{J}$ for all possible sensor locations on the given 2-D graph are compared. These results are obtained from 10 repeated runs of MATLAB simulation of each algorithm. It can be observed that using Monte Carlo method to get a reasonable approximation of J requires much more time than computing the bound $\bar{J}$.

5.3.2 Design of Multiple Sensors' Locations

Example 5.3.3.

Consider an 1-D graph of 10 nodes shown in Figure 5.2, where the task is now to choose the locations of two sensors. We consider the same transition matrix (5.14), so that the chain is strongly biased. The initial position of the agent is at node 1 and the exit node (node 10) is an absorbing state. We compute the values of J and $\bar{J}$ for every

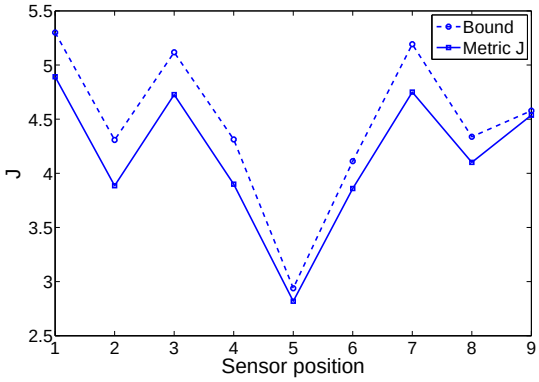

Figure 5.5: Designing a sensor's location in a 2-D graph by minimizing J. The performance metric J (estimated from 4000 MC simulations) and the bound $\bar{J}$ (computed from the formula (5.6)) are plotted against the 9 possible sensor locations. We see that $\bar{J}$ closely bounds the true value J, and they are both minimized by placing the sensor at the 5th node.

possible configuration of these two sensors in the graph. $\bar{J}$ is computed through Monte Carlo simulation of 8000 runs. Figure 5.6 shows the surfaces of J and $\bar{J}$ as a function of sensor configuration. Consistent with Theorem 5.2.5, J and $\bar{J}$ gives the same surfaces (since the chain is strongly biased). We see from the figure that the optimal design is to put the two sensors at nodes 4 and 8, respectively. Monte Carlo simulation gives the minimum $J = 2.3108$ while the value of the bound computed as $\bar{J} = 2.3117$.

The computation times for this simulation are given in table 5.1. Again using Monte Carlo method to get a reasonable approximation of J requires much more time than computing the bound $\bar{J}$.

5.4 Conclusion

In this chapter we presented a entropy-based metric J to quantify the algorithm-independent performance limit of multi-sensor systems used to monitor processes with complex dynamics. A stochastic framework was used to represent the dynamics as a Markov chain on a finite graph. Since computation of the performance metric involves computing the entropy rate of a HMM, which is intractable for all but the simplest cases, we obtained upper bounds $\bar{J}$ on J that are easier to compute. Illustrative numerical examples show the effectiveness of the proposed methodology.

There are several aspects of the problem that need further work, such as extension of the definition of strongly biased Markov chains to general graphs. For an extension of the bound $\bar{J}$ to general graphs with multiple sensors, we can find the order by which agent hit each sensor (along with the corresponding probability) and obtain $\bar{J}$. For graphs with a large number of nodes, choosing sensor locations by optimizing over all possible sensor configurations might be prohibitive. In that case we can use state aggregation techniques for Markov chains (see, e.g., [152]) to do

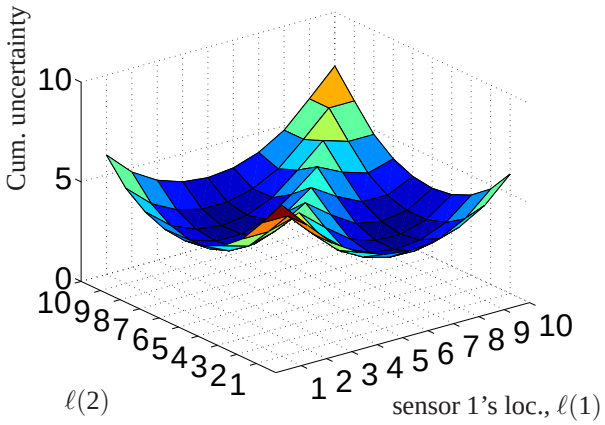

Figure 5.6: The performance metric J and its upper bound $\bar{J}$ for the 2-sensor case in an 1-D graph. The minimum J is achieved for the sensor locations as nodes 4 and 8. Since the chain is strongly biased, as predicted by Theorem 5.2.5, both J and $\bar{J}$ produces the same surface.

the design in a coarse scale and then successively refine it. Another possibility is to start with an initial design and refine it by developing numerical search algorithms to optimize $\bar{J}$. In practice, there are constraints on where sensors can be placed. This limits the search space for optimal sensor placement, which helps in such numerical search based methods.

Chapter 6

Convergence Rate For Distributed Optimization Methods: Novel Bounds and Distributed Step Size Computation

6.1 Introduction

In this chapter we consider the following convex optimization problem defined on a network of n agents:

$$\min_{x\in C} \frac{1}{n}\sum_{i=1}^{n} f_i(x)\,, \tag{6.1}$$

where $x \in \mathbb{R}^m$ is the decision variable, C is a convex constraint set, and all the functions $f_i : \mathbb{R}^m \to \mathbb{R}$ are assumed to be convex. Each $f_i(x)$ is associated to a particular agent i in the network, and is unknown to all other agents. We refer to $f_i(x)$ as the local objective function of agent i. The global objective function is defined as their summation $f(x) = \sum_{i=1}^{n} f_i(x)$ and the optimal value is $f(x^*)$. The optimal solution set in C is denoted as X^* and assumed to be non-empty, so that $x^* \in X^*$. The topology of the network is specified by an undirected graph $G = (V,E)$, where $V = \{1,2\ldots,n\}$ represents agents and $E \subseteq V \times V$ represents the communication links between them.

Such networked optimization problem arises in a broad range of applications, e.g., in distributed estimation [112, 113, 114], resource allocation in communication networks [115, 116, 117, 118], distributed Model Predictive Control [119], etc. There has been considerable interest in devising distributed algorithm for solving (6.1). With a distributed algorithm, agents can find the optimizer utilizing local computation and local communication only – thus such algorithms are scalable as the number of agents grows, feature that is desirable when operating in large-scale networked environments. On the contrary, a centralized algorithm tends to overburden the central nodes/fusion centers, and is less resilient to node failures.

One popular algorithm for solving (6.1) is to use subgradient methods. It is easy to implement and can handle non-differentiable objective functions. There are two types of subgradient algorithms: 1) the incremental subgradient algorithm [153, 154, 155, 156], where an estimate of the optimal solution is passed around the network, either on a deterministic path or in some random fashion. 2) the consensus subgradient one [108, 109, 110, 111], where each agent maintains an estimate of the solution and updates it iteratively by exchanging messages with neighbors. In this chapter we focus on the latter.

In the consensus subgradient algorithm, the update is essentially a combination of a subgradient iteration and an averaging algorithm (that is governed by a Markov chain on the graph). In this regard it is closely related to the consensus averaging, where the goal is for all agents to reach consensus on the average of their initial values (see Vicsek et al. [157], Jadbabaie et al. [158], Olfati-Saber and Murray [159]). A well-known result in consensus averaging literature is that the convergence rate to consensus is determined by the spectral properties of the graph. Therefore, for consensus subgradient algorithm, it is natural to expect similar results.

Our goal here is to understand and explore the impact of graph topology on the convergence rate of consensus subgradient algorithm. In a recent work on distributed dual averaging algorithm [120], Duchi *et. al.* obtained a bound for the convergence rate explicitly in terms of the spectral gap of the network. In this chapter we establish similar results for unconstrained consensus subgradient algorithm, where the step size is constant. We start by following the proof techniques in [120] and split the error in distributed subgradient iterations into two parts, one related to subgradient update, the other related to consensus averaging. A tighter bound on the second term is then provided using the spectral gap of the graph.

This tighter bound is used to determine a suitable value of the step size in a distributed fashion by the agents. This of course requires the estimation of the spectral gap of the graph in a distributed fashion. Although there are algorithms for the computation of the eigenvalues (and thus of the spectral graph) of a symmetric matrix, see for example [160], they rely on consensus based approaches and thus are slow to converge (proportional to the mixing time of the Markov chain). In order to speed up the computation of the step size, we describe a novel distributed algorithm based on the simulation of the wave equation on a graph. This algorithm is in general much faster than consensus based algorithms, and provides provably correct estimates of the spectrum of a graph [121, 122].

Although the proposed bound compares favorably to previous results [108, 109], it still tends to be quite conservative, especially for large networks with poor connectivity. In such situations, the common practice of bounding the ℓ_1-norm distance between the stationarity and the current probability distribution[1]:

$$\|A^t(i,\cdot) - \mathbb{1}/n\|_1 \leq \sqrt{n}\lambda_2^t$$

is overly conservative (c.f. Section 6.2.3). Based on the observation that such Markov chains usually mix faster for small t, we proposed to use an alternative expression to approximate the ℓ_1-norm distance (it actually bounds the ℓ_1-norm distance for very general situations). Using this result the slackness in our bound is greatly reduced and more importantly, the dependence on n is eliminated.

Despite the fact that the choice of the step size is based on a conservative bound, the proposed approach is a simple and viable way to fully distribute computation over a multi-agent system.

[1] Refer to the Notation subsection below for an explanation of the notation.

The rest of the chapter is organized as follows. In Section 6.2 we describe the consensus subgradient algorithm and provide an estimate of the convergence rate for fixed step size case. The sources of conservativeness in our result are analyzed. We discuss a refined heuristic in Section 6.2.3. Section 6.3 describes the wave propagation based algorithm for distributed computation of the proposed bound. In particular, we show that the distributed computation of the second eigenvalue of the Markov chain, provides a way to estimate the overall instantaneous error by each agent, as well as compute in a distributed way a suitable step size value. Examples and simulation results are provided in Section 6.4.

Notation We denote with $\mathbb{1}$ the vector with all entries equal to 1. For a matrix A, we use a_{ij} or $[A]_{ij}$ to denote the (i,j) entry of the matrix. The ith row and the jth column of a matrix A are denoted $A(i,\cdot)$ and $A(\cdot,j)$, respectively. We also use $[A]_i$ and $[A]_j$ when there is no risk of confusion. A square matrix A is said to be stochastic if $A\mathbb{1} = \mathbb{1}$ and doubly stochastic if $\mathbb{1}^T A = \mathbb{1}^T$. For such matrix A we denote with $\lambda_j(A)$ the j-th eigenvalue, ordered in descending value so that $1 \geq \lambda_2(A) \geq \cdots \geq \lambda_j(A) \geq \ldots$. For a convex function $f : \mathbb{R}^m \to \mathbb{R}$, we use $\partial f(x)$ to represent its subgradients at x. A vector $g \in \partial f(x) \in \mathbb{R}^m$ is a subgradient of f at x if $f(x) + g(x)^T(y-x) \leq f(y)$ for all y.

6.2 Problem Formulation

Let $C = \mathbb{R}^m$, then the problem (6.1) becomes

$$\min_{x \in \mathbb{R}^m} \frac{1}{n} \sum_{i=1}^{n} f_i(x)\,. \tag{6.2}$$

In the following, we focus on the analysis of the consensus subgradient method for solving this problem.

6.2.1 Consensus Subgradient Method

At time step $k = 1$, each agent i starts from its initial estimate of an optimal solution of problem (6.2), denoted as $x_i(1)$. At every subsequent discrete time instance, this estimate is updated according the following iteration, generating a sequence of estimates $x_i(1), \ldots, x_i(k), \ldots$

$$x_i(k+1) = \sum_{j \in \mathcal{N}_i} a_{ij}(k) x_j(k) - \alpha g_i(k)\,, \tag{6.3}$$

where $\mathcal{N}_i$ is the set of neighboring agents of agent i. The matrix $\{a_{ij}(k)\} = A(k) \in \mathbb{R}^{n \times n}$ is a doubly stochastic matrix, $\alpha \in \mathbb{R}$ is the constant scalar step size, and $g_i(k) \in \partial f_i(x_i(k))$. The matrices $A(k)$ respect the structure of the underlying network model G, i.e. $a_{ij} = a_{ji} = 0$ whenever (i,j) is not an edge in E. In the following discussion, we assumes that $A(k) \equiv A$ is time-invariant, although our results can be extended to time-varying matrix case with little extra effort,

under proper conditions to enforce "average" connectivity over time.

At each time step, the estimates of agent i is updated by combining two parts: the estimates x_j it received from its neighbors through averaging algorithm, and the local subgradient information of $f_i(x)$ evaluated at x_i. Intuitively, the subgradient step optimizes the local objective function whereas the averaging algorithm "diffuse" information about local objective functions to the other agents, and bring estimates of all agents together.

The evolution of estimates $x_i(k)$ at each agent can be represented with the help of a transition matrix, which is defined as

$$\Phi(k,s) = A(k-1)A(k-2)\cdots A(s)\,, \quad \Phi(s,s) = I$$

which for a constant matrix A reduces to $\Phi(k,s) = A^{k-s}$. Using transition matrices, we can write $x_i(k+1)$ in terms of previous estimates $x_1(s),\ldots,x_n(s)$ for any $s \leq k$, as follows

$$x_i(k+1) = \sum_{j=1}^{n} [\Phi(k+1,s)]_{ij} x_j(s) - \alpha g_i(k) - \sum_{r=s}^{k-1} \sum_{j=1}^{n} [\Phi(k+1,r+1)]_{ij} \alpha g_j(r)\,. \tag{6.4}$$

To obtain estimate of convergence rate, it is important to understand the evolution of $x_i(k)$ given in (6.4). For constant A, $[\Phi(k+1,s)]_{ij} = [A^{k-s+1}]_{ij}$ and $[\Phi(k+1,r+1)]_{ij} = [A^{k-r}]_{ij}$. Not surprisingly, the asymptotic behavior of $x_i(k)$ is closely related to the spectral properties of the double stochastic matrix A.

The spectral gap of A is defined as[2] $1-\lambda_2(A)$. In a consensus averaging setup it is well known that the spectral gap controls the rate of exponential decay to the stationary distribution [161]. We are interested in establishing a connection between the convergence rate (bound) of algorithm (6.3) and the spectral gap of matrix A.

6.2.2 Convergence Rate Analysis

The following assumptions are made on the set of subgradients of function $f_i(x)$.

Assumption 6.2.1. *For any $x \in \mathbb{R}^m$ and for any $f_i(x)$, the subgradient $g_i \in \partial f_i(x)$ is bounded*

$$\|g_i\| \leq L\,,$$

where $\|.\|$ is the ℓ_2-norm. ■

At time step k, we define the average estimate among all agents as $\overline{x}(k) = \frac{1}{n}\sum_{i=1}^{n} x_i(k)$. For agent i, the running local average up to time T is define as $\hat{x}_i(T) = \frac{1}{T}\sum_{k=1}^{T} x_i(k)$. Under the assumption on subgradient bound, we have the following result.

[2] We assume that $\lambda_2(A)$ is a simple eigenvalue of A.

Lemma 6.2.2. *Let Assumption 6.2.1 hold, and let us further assume that the set X^* of optimal solutions is nonempty, then at any node $i \in V$, the sequence $\{x_i(k)\}_{k=1}^{\infty}$ generated by recursion* (6.3) *with step size $\alpha > 0$ satisfies*

$$f(\hat{x}_i(T)) - f(x^*) \leq \frac{L}{T}\sum_{k=1}^{T}\|x_i(k) - \bar{x}(k)\| + \frac{\|\bar{x}(1) - x^*\|^2}{2\alpha T} + \frac{\alpha L^2}{2}, \tag{6.5}$$

where $\|.\|$ indicates the Euclidean ℓ_2-norm.

Proof. See appendix. □

The following theorem improves an earlier result in [109] and the convergence bound is expressed explicitly in terms of spectral gap of the matrix A.

Theorem 6.2.3. *Under the conditions of Lemma 6.2.2, we have*

$$f(\hat{x}_i(T)) - f(x^*) \leq \frac{\alpha L^2(\log n + 1)}{1 - \lambda_2(A)} + \frac{\|\bar{x}(1) - x^*\|^2}{2\alpha T} - \frac{3\alpha L^2}{2}. \tag{6.6}$$

Proof. See appendix. □

Note the right hand side of inequality (6.6) is always positive because

$$\frac{(\log n + 1)}{1 - \lambda_2(A)} > \frac{3}{2},$$

for any $n \geq 2$. The first term of the bound is proportional to the reciprocal of spectral gap $1 - \lambda_2(A)$. When the number of agents in the network n is large, the bound in (6.6) scales as $\log n$, thus dominating over the other terms.

6.2.3 An Approximate Bound Independent of n

Examining the proof of Theorem 6.2.3, we can see the dependence on n arises from inequality (C.11):

$$\|\Phi(k+1, r+1)_i - \frac{1}{n}\|_1 \leq \sqrt{n}(\lambda_2(A))^{k-r},$$

which results from the following inequalities (recall the fact $\Phi(k+1, r+1)_i = A^{k-r}(i, \cdot)$):

$$\|A^t(i,\cdot) - \mathbb{1}/n\|_1 \leq \sqrt{n}\|A^t(i,\cdot) - \mathbb{1}/n\|_2 \leq \sqrt{n}\lambda_2^t.$$

Note that $\|A^t(i,\cdot) - \mathbb{1}/n\|_1 \leq \sqrt{n}\lambda_2^t$ is a good bound asymptotically, but when t is small it is very conservative, especially for large n.

This conservativeness is not desirable when we have to bound the term $\sum_{r=1}^{k-1} \|[\Phi(k+1,r+1)]_i - \mathbb{1}/n\|_1$ in (C.10). In our proof of Theorem 6.2.3, we break the above sum at the cutoff time into two addends, and bound them separately. Although this helps improving the scaling from $\sqrt{n}$ to $\log n$, it is still a major source of conservativeness in the bound (6.6).

Therefore, we need a sharper estimate on the convergence rate of $\|A^t(i,\cdot) - \mathbb{1}/n\|_1$ than $\sqrt{n}\lambda_2^t$. Essentially, bounding $\|A^t(i,\cdot) - \mathbb{1}/n\|_1$ is equivalent to bounding the total variance mixing time of the Markov chain A, which is a topic that has attracted a lot of research interest, see for example [162] and references therein. It is well known that asymptotically in t the spectral gap provides a good bound, whereas for small t it is in general difficult to get a tight bound. Many techniques has been proposed to give sharper bounds: average conductance, Nash inequality, log-Sobolev, evolving set method, spectral profile, etc (for more details see [162, 161]). Several of these techniques use the fact that the Markov chain usually mixes faster in the early state. They can provide much tighter bound but usually not easy to compute.

In the following we propose to use $2\lambda_2^t$ as a heuristic of the ℓ_1-norm, so that

$$\|A^t(i,\cdot) - \mathbb{1}/n\|_1 \sim 2\lambda_2^t,$$

where 2 is the upper bound on $\|A^t(i,\cdot) - \mathbb{1}/n\|_1$ for any x and t. This heuristic is much easier to compute in practice and it provides a large improvement over $\sqrt{n}\lambda_2^t$.

As we will see in the following, for many cases, it can serve as a practical bound. This is because of the following fact:

1. Asymptotically the convergence rate of $\|A^t(i,\cdot) - \mathbb{1}/n\|_1$ is given by λ_2 [161].

2. Convergence at the beginning is often much faster than the rate characterized by λ_2 [162].

Example 6.2.4. *Consider the lazy random-walk on a n-cycle. The transition probability of the Markov Chain is*

$$A(i,j) = \begin{cases} 1/4 & \text{if} \quad j = i \pm 1 \mod n \\ 1/2 & \text{if} \quad j = i \\ 0 & \text{otherwise} \end{cases}$$

Let $n = 14$, the plot in Figure 6.1(a) shows the convergence of $\|A^t(1,\cdot) - \mathbb{1}/n\|_1$ as compared to $\sqrt{n}\lambda_2^t$ and $2\lambda_2^t$. It can be observed that $2\lambda_2^t$ is indeed a better bound here. Note the fast decrease of $\|A^t(1,\cdot) - \mathbb{1}/n\|_1$ for $t < 10$; Figure 6.1(b) is for $n = 50$, it can be observed that $2\lambda_2^t$ is a much tighter bound than $\sqrt{n}\lambda_2^t$. The instantaneous decrease rate of

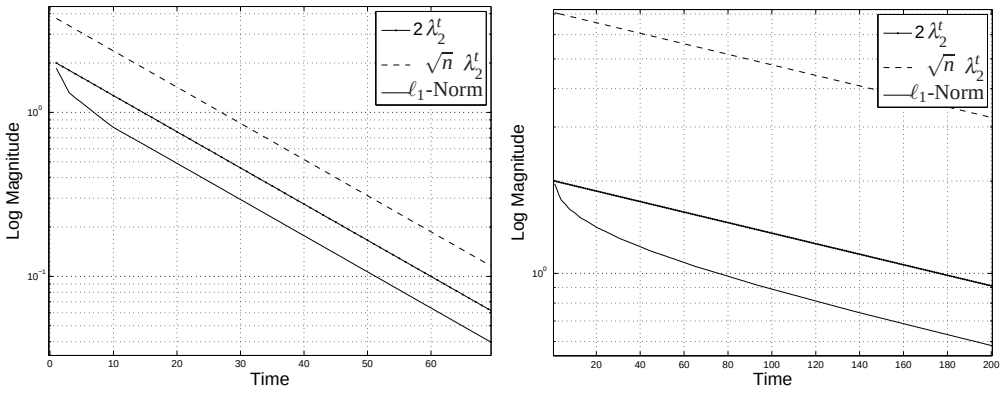

(a) $n = 14$ (b) $n = 50$

Figure 6.1: Bounds comparison for graph with ring-topology

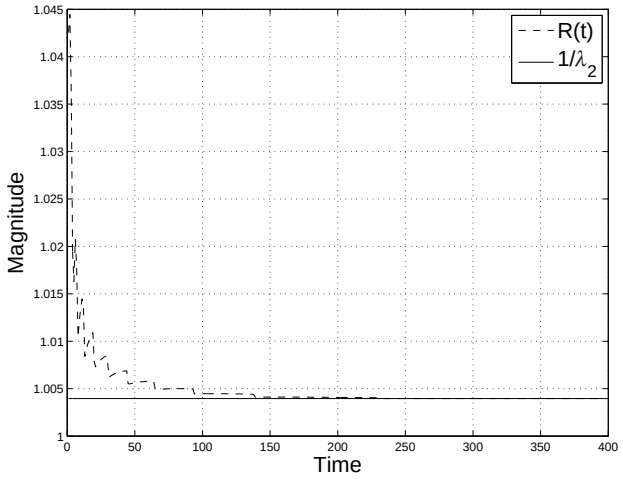

Figure 6.2: Instantaneous decrease rate profile for a ring with $n = 50$.

$\|A^t(1,\cdot) - \mathbb{1}/n\|_1$ *is defined as*

$$R(t) = \frac{\|A^{t-1}(1,\cdot) - \mathbb{1}/n\|_1}{\|A^t(1,\cdot) - \mathbb{1}/n\|_1}, \quad t \geq 1.$$

For the ring with $n = 50$ *it is depicted in Figure 6.2. At early stage of the random walk (*$t < 150$*),* $R(t)$ *is much larger than its asymptotic value* $1/\lambda_2$*, indicating a faster convergence. These plots are generated for* $x_1(1) = 1$ *and* $x_{j\neq 1}(1) = 0$*. Other initial states lead to similar plots.*

Example 6.2.5. *Consider a "dumbbell" graph where two complete graphs of the same size* $n/2$ *are connected by an edge. Let A be a Markov chain associated with the graph. For a random walk starting from any point i on the graph, we expect a fast local mixing and very slow global mixing.*

Let $n = 5$ *and with a randomly generated A, the plot of* $\max_i\{\|A^t(i,\cdot) - \mathbb{1}/n\|_1\}$ *are compared to* $\sqrt{n}\lambda_2^t$ *and* $2\lambda_2^t$ *in Figure 6.3.*

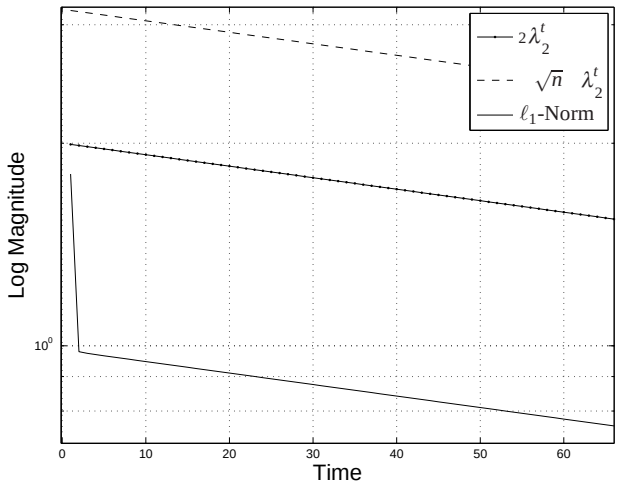

Figure 6.3: Bounds comparison for graph with "dumb-bell" topology.

Note that the convergence of $\max_i\{\|A^t(i,\cdot)-\mathbb{1}/n\|_1\}$ *demonstrates two time scales, as expected. The slow global convergence rate is characterized by* λ_2 *and* $2\lambda_2^t$ *is indeed a bound. More generally, we can consider graphs where nodes form clusters with strong intra-connection and weak inter-connections. Such graphs always have two time-scales: fast local convergence and slow global convergence. For such cases* $2\lambda_2^t$ *usually serve as a practical bound.*

A real world example could be the sensor networks, which comprises a large number of nodes, with interactions that are local because of the limited communication range of each node. This can lead to a local diffusion that is faster than global convergence given by λ_2^t.

With the proposed heuristic

$$\|A^t(i,\cdot)-\mathbb{1}/n\|_1 \sim 2\lambda_2^t,$$

we can provide, in the following lemma, an estimate of the convergence of the subgradient method. Its proof is similar to that of Theorem 6.2.3 and is omitted here.

Lemma 6.2.6. *Under the conditions of Lemma 6.2.2, we further assume the bound* $\|A^t(i,\cdot)-\mathbb{1}/n\|_1 \le 2\lambda_2^t$ *hold for any initial state* $x(0)$*, then the following inequality hold:*

$$f(\hat{x}_i(T)) - f(x^*) \le \frac{2\alpha L^2}{1-\lambda_2(A)} + \frac{\|\bar{x}(1)-x^*\|^2}{2\alpha T} + \frac{\alpha L^2}{2}. \tag{6.7}$$

Remark 6.2.7. *This estimate does not explicitly scale with network size n.*

The bound (6.6) and approximation result (6.7) characterizes a trade-off between the accuracy of the solution and the convergence speed, i.e. the number of iterations needed to achieve a certain accuracy. It is thus desirable to choose the step-size α such that the best accuracy is achieved within a pre-set number of iterations.

For example, the optimal step-size α for T iterations would be

$$\alpha^*(T) = \sqrt{\frac{\|\bar{x}(1) - x^*\|^2(1-\lambda_2(A))}{4TL^2}} = \frac{\sqrt{1-\lambda_2(A)}}{2L\sqrt{T}}\|\bar{x}(1) - x^*\|. \tag{6.8}$$

6.3 Distributed Computation of the Bound

As mentioned before, the advantage of consensus based subgradient algorithm (6.3) is that it provides a distributed solution to the optimization problem (6.1). Therefore it is desirable that the bound (6.6) and approximation (6.7) are computed in a distributed manner. This could be important for each agent to evaluate how good its current estimate of x^* is, or decide when to stop in the absence of a fusion/command center[3]. It is also possible to choose the optimal step size α^* as in equation (6.8) at each agent[4].

We consider the distributed computation of the approximation (6.7). To simplify the discussion, we assume that L, the bound of subgradients, can be obtained from a priori knowledge of the target function $f(x)$. Also assume that a bound of $\|\bar{x}(1) - x^*\|$, denoted as M, is known a priori. Clearly, depending on the problem these values could be conservative. Note however that the term depending on the initial condition becomes smaller as the time increases and, for large networks where agents have very limited communication ranges, the first term dominates. To estimate the first term, the second largest eigenvalue $\lambda_2(A)$ needs to be computed.

Distributed algorithms for computing the eigenvalues and eigenvectors of an undirected graph has been reported in many previous works [160, 163]. In a recent paper [121, 122], the authors proposed a wave-equation based method for distributed computation of eigenvalues and eigenvectors of a graph. The idea is to simulate, in a distributed fashion, the propagation of a wave over a graph and capture the frequencies at which the graph "resonates". From such frequencies, the eigenvalues and eigenvectors of the graph Laplacian can be recovered using local frequency estimators. This method is faster than the diffusion based eigenvalue/eigenvector computation by order of magnitudes.

We employ this wave-equation method to compute $\lambda_2(A)$. After each agent obtained their local estimate of $\lambda_2(A)$, the convergence bound (6.6) or approximation (6.7) can be computed. The wave-equation method is described as follows, for more details see [121, 122]. Consider the normalized Laplacian

$$\mathscr{L} \triangleq I - D^{-1}A,$$

in which, in our case, the normalizing diagonal matrix $D^{-1} = I$, as A is a doubly stochastic matrix. Consider the wave

[3] Note, however, that all agents needs to stop at the same time, otherwise those who stop late will get biased results

[4] This is always conservative since we are optimizing according to the bound.

equation

$$\frac{\partial^2 u}{\partial t^2} = c^2 \Delta u\,, \quad u \in \mathbb{R},$$

its discretization on the graph G is given by

$$u_i(t) - 2u_i(t-1) + u_i(t-2) = -c^2 \sum_{j \in \mathbb{N}(i)} \mathscr{L}_{ij} u_j(t-1).$$

In the RHS of the equation, $\sum_{j\in\mathbb{N}(i)} \mathscr{L}_{ij} u_j(t-1)$ comes from the discretization of Δu. On the LHS the terms are the discretization of $\partial^2 u/\partial t^2$. Note that node i only requires the value of $u_j(t-1)$ at its neighbors, weights on its edges $\mathscr{L}_{ij}$ and previous values of u_i to update its current state. The initial conditions are such that $u_i(-1) = u_i(0)$, chosen randomly in the interval $[0,1]$. Each agent run the wave equation iteration and collects the values $u_i(1), \ldots, u_i(T_{max})$. On this time series an FFT is performed and from the frequencies eigenvalues of $\mathscr{L}$ are recovered solving

$$\omega_j^2 = -c^2/4(c^2\tilde{\lambda}_j^2 - 4\tilde{\lambda}_j)$$

where ω_j is the j-th frequency. The time T_{max} is the time (iterations) needed to compute the eigenvalues. It turns out that

$$T_{max} = O\left(\arccos\left(\frac{2 + c^2(e^{-1/\tau} - 1)}{2}\right)^{-1}\right) \approx O(\sqrt{\tau}/c)\,,$$

where $c < \sqrt{2}$ and where τ is the mixing time of the random walk on the graph specified by the Markov chain A.

The algorithm is summarized in the following table.

Algorithm 1 Wave equation based eigenvalue computation for node i

$u_i(0) \leftarrow$ **Random**$([0,1])$
$u_i(-1) \leftarrow u_i(0)$
$t \leftarrow 1$
while $t < T_{max}$ **do**
  $u_i(t) \leftarrow 2u_i(t-1) - u_i(t-2) - c^2 \sum_{j\in\mathbb{N}(i)} \mathscr{L}_{ij} u_j(t-1)$
  $t \leftarrow t+1$
end while
$Y \leftarrow$ **FFT**$([u_i(1), \cdots, u_i(T_{max})])$
for $j \in [1, \cdots, k]$ **do**
  $\omega_j \leftarrow$ **FrequencyPeak**(Y, j)
end for
$\tilde{\lambda}_i \leftarrow$ **Solve**$(\omega_j^2 = \frac{-c^2}{4(c^2\tilde{\lambda}_j^2 - 4\lambda_j})$

The second largest eigenvalue $\lambda_2(A)$ of A is then obtained as $\lambda_2 = 1 - \tilde{\lambda}_2$.

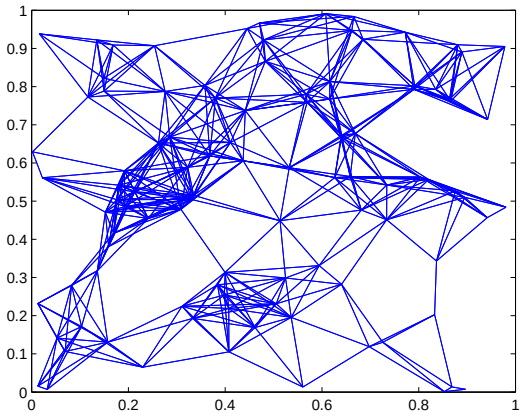

Figure 6.4: Random graph with 100 nodes

6.4 Simulations

Example 6.4.1. *Figure. 6.4 shows a randomly generated graph G in the square* $[0,1]\times[0,1]$ *with 100 nodes. We generate the double stochastic Markov chain A on G with second largest eigenvalue equal to* 0.975*, implying very slow mixing. To each agent we associate a quadratic function of the following form* $f_i(x) = a_i x + b_i(x-c_i)^2$*, where coefficients* a_i *and* c_i *are randomly chosen from interval* $[-1.5,1.5]$*,* b_i *is randomly chosen from interval* $[0,1.5]$*. The*

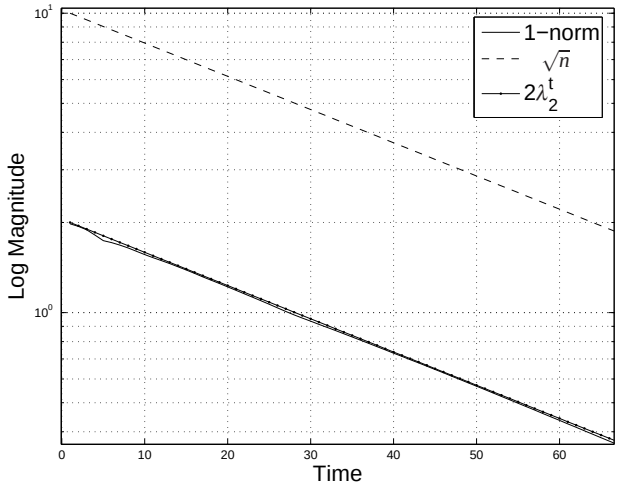

Figure 6.5: Comparison of our approximate and the $\sqrt{n}\lambda_2^t$ bound

plot in Figure. 6.5 compares $\sqrt{n}\lambda_2^t$ *and* $2\lambda_2^t$ *to the point-wise maximum of* $\|A^t(i,\cdot)-\frac{\mathbb{1}}{n}\|_1$ *over all x. It can be observed that* $2\lambda_2^t$ *indeed serves as a tighter bound of* $\|A^t(i,\cdot)-\frac{\mathbb{1}}{n}\|_1$ *in this case.*

The bounds in Theorem 6.2.3 and Lemma 6.2.6 for a typical agent i are shown in Figure 6.6, where $f(\hat{x}_i)-f(x^*)$ *is also plotted as ground truth for comparison. It demonstrates the improvement of Lemma 6.2.6 over Theorem 6.2.3*

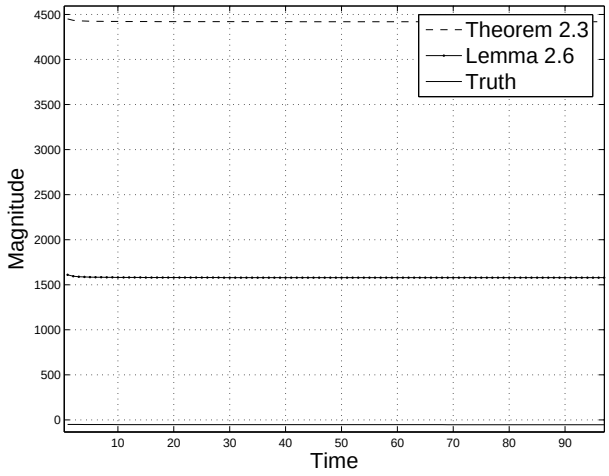

Figure 6.6: Comparison of our results in Theorem 6.2.3, Lemma 6.2.6 and the ground truth

and the conservativeness for both results. As illustrated in Figure 6.5, our approximation of $\|A^t(i,\cdot) - \frac{\mathbb{1}}{n}\|_1$ *is already good. One source of the conservativeness in the final result is that we replaced subgradients of any agent at any time by their upper bound L in inequality (C.10). For some special choices of function, our bound is less conservative, as we will see in the next example.*

Example 6.4.2. *Let us consider another A for the same example as before with second largest eigenvalue equal to* 0.911. *The plot in Figure 6.7 shows that* $2\lambda_2^t$ *is a much better approximation of* $\|A^t(i,\cdot) - \frac{\mathbb{1}}{n}\|_1$ *in this case.*

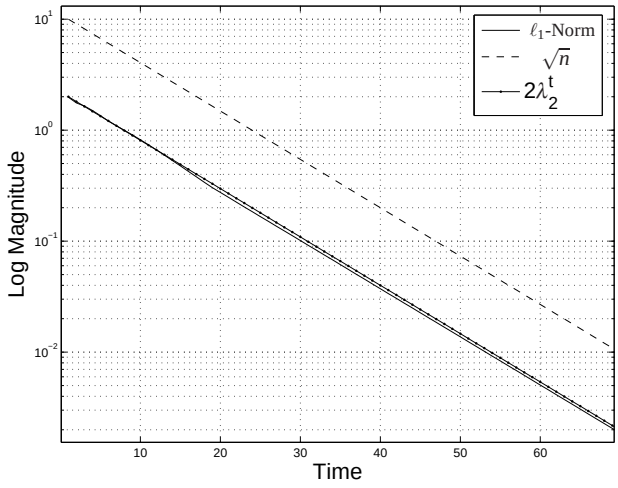

Figure 6.7: Comparison of our results in Theorem 6.2.3, Lemma 6.2.6 and the ground truth

To each agent we associate a scalar function of the following form $f_i(x) = |x - s_i|$ *and coefficients* s_i *is the shift amount randomly chosen from interval* $[-1.5, 1.5]$. *Note that for any* $x \neq s_i$, *the subgradient of* $f_i(x)$ *is always* 1 *or*

-1.

The bounds in Theorem 6.2.3 and Lemma 6.2.6 are plotted in Figure 6.8. For this example our bounds are less conservative.

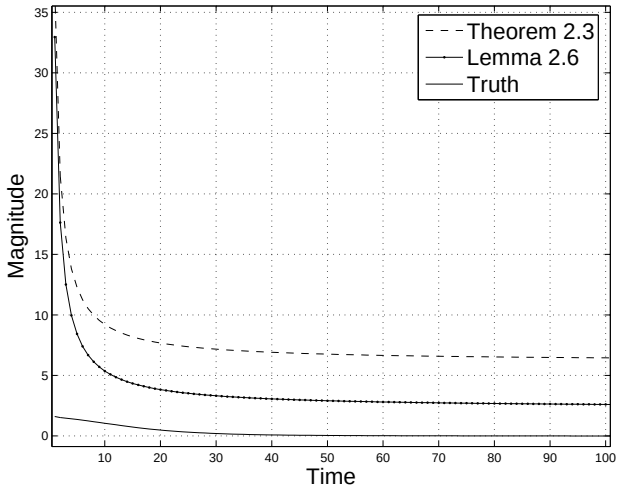

Figure 6.8: Comparison of our results in Theorem 6.2.3, Lemma 6.2.6 and the ground truth

6.5 Conclusion

In this chapter we derived a new bound on the convergence of a consensus based subgradient algorithm. This bound explicitly captures the spectral property of the underlying graph, and compare favorably to previous results. Exploring the source of conservativeness in our bound, we proposed an approximate of the optimization error that does not scale with the size of the graph. We also described an algorithm, based on the wave equation over graphs, to compute our bound in a distributed manner useful to: 1) chose the step size in a distributed fashion and 2) estimate the current error. Some simulations results show the comparison of the proposed bound with ground truth data.

Appendix A

Proofs and Numerical Examples in Chapter 2

A.1 Application

The classical Bode formula (2.1) for LTI systems is given in terms of sensitivity function. Depending upon whether the noise affects the input *or* the output, the sensitivity can be defined with respect the input or the output. In our setup, we have considered noise at the output. The motivation for us arises from problems in flow and combustion control where performance of output signals (such as pressure response in ACIC [124], or acoustic velocity perturbations in cavity flow [125]) is of primary interest:

Example A.1.1. *Figure A.1 depicts a feedback inter-connection of the active combustion instability control (ACIC) problem; cf., [124]. A lumped model for this can be expressed as*

$$\begin{aligned} \boldsymbol{x}_{n+1}^{(a)} &= \alpha_1(\boldsymbol{x}_n^{(a)}) + q(\boldsymbol{x}_n^{(c)}), \\ \boldsymbol{x}_{n+1}^{(c)} &= \alpha_2(\boldsymbol{x}_n^{(c)}) + \boldsymbol{u}_n, \\ \boldsymbol{y}_n &= c_1(\boldsymbol{x}_n^{(a)}) + \boldsymbol{d}_n, \end{aligned}$$

where $\boldsymbol{x}_n^{(a)}$ are the states of the thermoacoustic model, $\boldsymbol{x}_n^{(c)}$ are the states of the combustion model, $\boldsymbol{y}_n$ is the pressure response output, $\boldsymbol{d}_n$ is a model of noise due to to turbulence, and $\boldsymbol{u}_n$ is a fuel control input. Denoting $\boldsymbol{x}_n \doteq [\boldsymbol{x}_n^{(a)}, \boldsymbol{x}_n^{(c)}]$, one obtains the form (2.3)-(2.5) for any static nonlinear control $\boldsymbol{u}_n = k(\boldsymbol{y}_n)$. If one has a dynamic controller instead, one would augment the controller states into $\boldsymbol{x}_n^{(c)}$ and again obtain the same form – as long as the additive structure of control input is preserved.

The analysis and results of Chapter 2 can also be easily extended if one considered input noise *instead of* the output noise (so, $\mathbf{y}_n = c(\mathbf{x}_n)$ and $\mathbf{u}_n = k(\mathbf{y}_n) + \mathbf{d}_n$). For example, in the contractive case (see Section 2.3) with input noise alone, one would obtain $\mathscr{H}(\mathbf{u}) = \mathscr{H}(\mathbf{d})$.

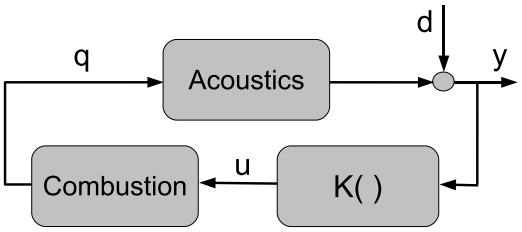

Figure A.1: Schematic of the active combustion instability control problem.

A.2 Entropic stability of LTI system with general disturbance

Consider a LTI system

$$\mathbf{x}_{n+1} = A\mathbf{x}_n + B\mathbf{u}_n \tag{A.1}$$

$$\mathbf{y}_n = C\mathbf{x}_n + \mathbf{d}_n \tag{A.2}$$

where $\mathbf{x}_n \in \mathbb{R}^m$, $\mathbf{u}_n$, $\mathbf{y}_n$ and $\mathbf{d}_n \in \mathbb{R}^1$, and (A,C) is observable. We assume that all the eigenvalues of A are outside unit circle, the disturbance has bounded uncertainty ($\mathscr{H}(\mathbf{d}) < \infty$), and u_n is stabilizing control. Denote

$$\begin{aligned}
\mathscr{T} &\doteq \begin{bmatrix} 0 & 0 & \cdots & & \\ CB & 0 & 0 & \cdots & \\ \vdots & & & & \\ CA^{m-2}B & CA^{m-3}B & \cdots & CB & 0 \end{bmatrix} \\
\mathscr{O} &\doteq [C, CA, \ldots, CA^{m-1}]' \\
\mathbb{y} &\doteq [\mathbf{y}_{n-m+1}, \mathbf{y}_{n-m+2}, \ldots, \mathbf{y}_n]' \\
\mathbb{u} &\doteq [\mathbf{u}_{n-m+1}, \mathbf{u}_{n-m+2}, \ldots, \mathbf{u}_n]' \\
\mathbb{d} &\doteq [\mathbf{d}_{n-m+1}, \mathbf{d}_{n-m+2}, \ldots, \mathbf{d}_n]'.
\end{aligned}$$

We have

$$\underbrace{\mathscr{O}\cdot}_{\text{invertible}} \mathbf{x}_{n-m+1} = \overbrace{\mathbb{y} - \mathscr{T}\cdot\mathbb{u}}^{\text{known}} - \underbrace{\mathbb{d}}_{\text{uncertain}},$$

where $\mathscr{O}$ is invertible because (A,C) is observable. Since $\mathbb{y}$ is observed and $\mathbb{u}$ is control (depends deterministically on $\mathbb{y}$), uncertainty in state arises only due to disturbance and can be bounded as:

$$H(\mathbf{x}_{n-m+1}|\mathbf{y}_1^n) \le H(\mathbf{x}_{n-m+1}|\mathbf{y}_{n-m+1}^n) \le m \cdot H(\mathbf{d}) + \ln|\mathscr{O}^{-1}|$$

for $n > m$. Using (A.1), we have

$$H(\mathbf{x}_n|\mathbf{y}_1^n) \leq \ln|A|^m + m \cdot H(\mathbf{d}) + \ln|\mathscr{O}^{-1}| < \infty,$$

i.e., asymptotic uncertainty of the state can be apriori bounded.

A.3 Calculations for Theorem 2.2.4

The Markov operator (corresponding to Π) first introduced in (2.19) is obtained by considering the conditional pdf

$$\begin{aligned}
&\text{if } d \geq r: \\
&p(\hat{r}|r) = \begin{cases} \frac{2\hat{r}}{a^2 dr}, & 0 \leq \hat{r} < ar \\ (1-\frac{r}{d})\delta(\hat{r}-ar), & \hat{r} = ar \\ 0, & \text{otherwise} \end{cases} \qquad \text{(A.3)} \\
&\text{if } r \geq d: \\
&p(\hat{r}|r) = \begin{cases} \frac{2\hat{r}}{a^2 dr}, & 0 \leq \hat{r} < ad \\ (1-\frac{d}{r})\delta(\hat{r}-ad), & \hat{r} = ad \\ 0, & \text{otherwise} \end{cases} \qquad \text{(A.4)}
\end{aligned}$$

The invariant density (corresponding to μ) is the fixed-point:

$$\begin{aligned}
\rho(\hat{r}) &= \int_0^{ad} p(\hat{r}|r)\rho(r)dr \\
&= \hat{r}\int_{\frac{\hat{r}}{a}}^{ad} \frac{2}{a^2 d}\frac{\rho(r)}{r}dr + \frac{1}{|a|}\rho(\frac{\hat{r}}{a})(1-\frac{\hat{r}}{ad}) + \delta(\hat{r}-ad)\int_d^{ad}(1-\frac{d}{r})\rho(r)dr, \qquad \text{(A.5)}
\end{aligned}$$

where

$$\int_0^{ad} \rho(r)dr = 1. \qquad \text{(A.6)}$$

To obtain the solution, we consider a decomposition:

$$\rho(r) = s(r) + b_0\delta(r-ad), \qquad \text{(A.7)}$$

where $c \in [0,1]$ is a constant and $s(r)$ denotes the regular part. In this co-ordinate, the integral equation (A.5) leads to a coupled set of equations:

$$s(\hat{r}) = \frac{2c}{a^3 d^2}\hat{r} + \frac{1}{|a|}s(\frac{\hat{r}}{a})(1-\frac{\hat{r}}{ad}) + \frac{2\hat{r}}{a^2 d}\int_{\frac{\hat{r}}{a}}^{ad}\frac{s(r)}{r}dr \tag{A.8}$$

$$b_0 = a\int_a^{ad}(1-\frac{d}{r})s(r)dr. \tag{A.9}$$

Now, one can verify that the regular solution $s(r)$ to the integral equation (A.8) can be expressed as series

$$s(r) = \sum_{n=1}^{\infty} b_n r^n \tag{A.10}$$

where the coefficients b_n satisfy the iteration

$$b_{n+1} = -\frac{n+2}{nd(a^{n+2}-1)}b_n.$$

One can thus express b_n in terms of b_1 as

$$b_n = (-1)^{n-1}\frac{n(n+1)}{2d^{n-1}\prod_{i=1}^{n-1}(a^{i+2}-1)}b_1 \quad \text{for } n \geq 2. \tag{A.11}$$

Substituting the series for $s(r)$ in (A.9) gives the value of b_0 in terms of b_1. The normalization constant b_1 is determined from using (A.6).

Next, we describe calculations for the entropy rate. From (2.22)

$$\mathscr{H}(y) = \int_0^{ad} h(r,d)\rho(r)dr, \tag{A.12}$$

where $\rho(r)$ is the invariant density and $h(r,d)$ is given by (2.21). Substituting (A.7)-(A.9) in (A.12) gives:

$$\mathscr{H}(y) = \ln(a) + \ln(d) + E, \tag{A.13}$$

where,

$$E = \int_0^d \frac{r}{2d}s(r)dr + \int_d^{ad}\frac{s(r)}{2}dr + \int_d^{ad}\frac{\int_0^r s(u)du}{r}dr. \tag{A.14}$$

On substituting the series expression (A.10) in the right-hand side of Eq. (A.14), we have

$$E = \sum_{n=1}^{\infty} b_n d^{n+1}\left[\frac{1}{2(n+2)} - \frac{a^{n+1}-1}{n+1}(\frac{1}{n+1}-\frac{1}{2})\right]$$

and using (A.11), we have $E = 0$. The Bode entropy (2.23) formula follows.

To use the integral formula (A.12), the invariant density $\rho(r)$ must be unique. This is true here because $V(r) = \frac{1}{r}$ is a Lyapunov function on $[0, ad]$. Using (A.3)-(A.4), it is readily verified that

$$\int_0^{ad} p(\hat{r}|r)V(\hat{r})dr = \frac{1}{a}V(r) + \frac{1}{ad}.$$

Since $\frac{1}{a} < 1$, $V(r)$ is a Lyapunov function. The existence of a Lyapunov function implies that the Markov operator (A.5) has a unique invariant density, $\rho(r)$ in this case [126].

A.4 Calculations for part (1) in the Proof of Theorem 2.4.2

Suppose λ is a simple eigenvalue of matrix A with an eigenvector v so $Av = \lambda v$. If $P \succeq 0$ is a semi positive-definite solution of the DARE (2.36) then

$$(1 - |\lambda|^2)v'P\bar{v} = -|\lambda|^2 v'(PC'(CPC' + r)^{-1}CP)\bar{v}$$

Now if $|\lambda| < 1$ then this implies $v'P\bar{v} \leq 0$. By positive semi-definiteness of P, we have $Pv = 0$. Thus the restriction of P to stable eigenspace $\mathbb{R}^{m_s}$ is 0 and on account of symmetry,

$$P = \begin{pmatrix} O & O \\ O & P_u \end{pmatrix},$$

where P_u satisfies the DARE

$$P_u = A_u(P_u - P_uC'(CP_uC' + rI)^{-1}CP_u)A_u'.$$

For repeated eigenvalues, a proof may be constructed in a standard manner by constructing an appropriate sequence.

A.5 Calculation for Theorem 2.5.1

We denote the general distribution $f(x)$ in (2.48) as a tuple (p_1, r, p_2). The distribution can be one of the four types: (p_1, L, p_2), $(p_1, r, 0)$, $(0, r, p_2)$, $(0, r, 0)$, where $0 < r < L$ (see Fig. A.2 (b)). For these four types, the entropy function $h_y(\pi)$ is as follows:

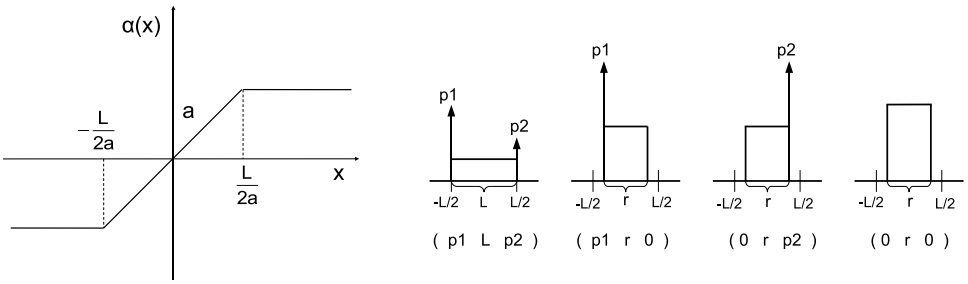

(a) Non-uniform dynamics $\alpha(x)$ (b) 4 types of belief states $f(x)$

Figure A.2: Non-uniform dynamics and belief types

1. For $f = (p_1, L, p_2)$,

$$h_y(\pi) = -\int_0^L (\frac{p_1}{d} + \frac{p_3}{dL}x)\ln(\frac{p_1}{d} + \frac{p_3}{dL}x)dx - (1-\frac{L}{d})\ln\frac{1}{d} - \int_0^L (\frac{p_2}{d} + \frac{p_3}{dL}x)\ln(\frac{p_2}{d} + \frac{p_3}{dL}x)dx, \tag{A.15}$$

2. For $f = (p_1, r, 0)$,

$$h_y(\pi) = -\int_0^r (\frac{p_1}{d} + \frac{p_3}{dr}x)\ln(\frac{p_1}{d} + \frac{p_3}{dr}x)dx - (1-\frac{r}{d})\ln\frac{1}{d} - \int_0^r (\frac{p_3}{dr}x)\ln(\frac{p_3}{dr}x)dx, \tag{A.16}$$

3. For $f = (0, r, p_2)$, the formula is symmetric to the case 1) with $f = (p_1, r, 0)$,

4. For $f = (0, r, 0)$, we have

$$h_y(\pi) = \ln(d) + \frac{r}{2d}, \tag{A.17}$$

where d is assumed to be large and in particular larger than L.

We show the estimate (2.49) for (A.16):

$$\begin{aligned} h_y(\pi) \;&=\; -\frac{1}{d}\left[\int_0^r (p_1+\frac{p_3}{r}x)\ln(p_1+\frac{p_3}{r}x)dx + \int_0^r (\frac{p_3}{r}x)\ln(\frac{p_3}{r}x)dx\right] + \frac{\ln(d)}{d}\left[\int_0^r (p_1 + \frac{p_3}{r}x)dx + \int_0^r \frac{p_3}{r}xdx - r\right] + \ln(d) \\ &= -\frac{C_1}{d} + C_2\frac{\ln(d)}{d} + \ln(d). \end{aligned}$$

For other cases, the calculation is entirely analogous.

A.6 Entropy rate formula for the discrete counterpart of Theorem 2.2.4

In discrete settings, the spaces $\underline{X}$ and $\underline{Y}$ are discrete and obtained by discretizing (quantizing) X and Y respectively; the underline notation is used to distinguish discrete and continuous variables. The setup is as follows:

1. The partition $\underline{X} = \{D_i\}_1^L$ is obtained by taking a uniform partition of X, where each $D_i = [(2i-2-L)\frac{\varepsilon}{2}, (2i-L)\frac{\varepsilon}{2}]$ has length ε. ε is positive but otherwise arbitrary. As $\varepsilon \downarrow 0$, one obtains a finer partition of the state space X and a better approximation of the (continuous) Markov operator $\mathbb{P}_c$ [49].

2. The dynamics are given by (2.15) where a is assumed to be odd. In this case, $\underline{X}$ defines a Markov partition for the dynamics (see Sec. 15.1 in [47]). This ensures that one can obtain an accurate estimate of entropy by considering the discrete problem.

3. The counterpart of uniform i.i.d. disturbance is defined with respect to the partition: For $\mathbf{x}_n \in D_i$, the output $\mathbf{y}_n \in D_j$ with probability (w.p.) $\frac{1}{d}$ if $|j-i| < \frac{d}{2}$. Here, d is taken to be a positive odd integer and represents the spread of the disturbance (see Fig. A.3).

4. The discrete output $\underline{\mathbf{y}}_n \in \underline{Y} \doteq \{0, \pm\varepsilon, \pm 2\varepsilon, \ldots\}$ is obtained by quantizing $\mathbf{y}_n$.

5. The control $\underline{\mathbf{u}}_n = k(\underline{\mathbf{y}}_n)$, where the control space $\underline{U} = \{0, \pm\varepsilon, \pm 2\varepsilon, \ldots\}$.

We assume a control $k(\cdot)$ is chosen so $T_c : X \to X$. $\underline{\pi}_n$ denotes the belief (now a probability vector) at time n and $\underline{f}_n$ denotes its marginal on $\underline{X}$. $\underline{f}_0$ is assumed uniform and $\mathbf{r}_n$ and $\hat{\mathbf{r}}_n$ denote the number of cells in the support of $\underline{f}_n$ and $\hat{\underline{f}}_n$ respectively. One can verify that these are also uniform probability vectors. We have $\hat{\mathbf{r}}_n < \min(\mathbf{r}_n, d)$ so $\hat{\mathbf{r}}_n$ can take d possible values $\{1, 2, \ldots, d\}$ and

$$\mathbf{r}_n = |a|\hat{\mathbf{r}}_{n-1},$$

so $\mathbf{r}_n$ can also take d possible values $\{a, 2a, \ldots, ad\}$. This results in d possible *types* of $\underline{f}_n$ and hence of $\underline{\pi}_n$. We partition the support of limiting measure $\underline{\mu}$ (in $\nabla_{\underline{S}}$) into d disjoint sets $\{\mathscr{D}_1, \mathscr{D}_2, \cdots \mathscr{D}_d\}$ according to these types. Note that the entropy $h_y(\underline{\pi})$ is determined entirely by the type and we use

$$h_i \doteq h_y(\underline{\pi}) = \frac{i|a| - d + 1}{i|a|} \ln(i|a|) - 2\sum_{n=1}^{d-1} \frac{n}{i|a|d} \ln(\frac{n}{i|a|d}) \tag{A.18}$$

to denote entropy for all $\underline{\pi} \in \mathscr{D}_i$, where $i = 1, 2, \ldots, d$. Using the integral formula (2.14):

$$\mathscr{H}(\underline{\mathbf{y}}) = \int_{\nabla_{\underline{S}}} h_y(\underline{\pi}) d\mu(\underline{\pi}) = \sum_{i=1}^{d} h_i \mu_i, \tag{A.19}$$

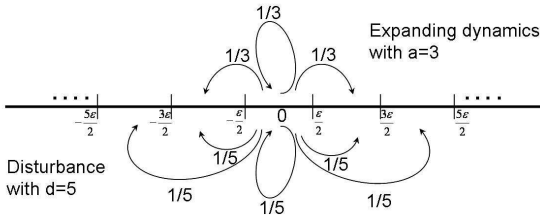

Figure A.3: The discrete uniform partition of $X \subset \mathbb{R}^1$. The arrows indicate transition probabilities (for initial state in cell $[-\frac{\varepsilon}{2}, \frac{\varepsilon}{2}]$) due to dynamics and disturbance for $\alpha(x) = 3x$ ($a = 3$) and $d = 5$.

where $\mu_i = \underline{\mu}(\mathscr{D}_i)$. The invariant measure is obtained by considering the Markov operator $\underline{\Pi}$ (now a matrix) with entries

$$\underline{\Pi}_{ij} = \text{Prob}(\underline{\pi}_{n+1} \in \mathscr{D}_j | \underline{\pi}_n \in \mathscr{D}_i)$$

giving transition probability between types. The calculation of these probabilities is entirely analogous to the calculation in the continuous case. With $d \leq a$,

$$\text{Prob}(\underline{\pi}_{n+1} \in \mathscr{D}_j | \underline{\pi}_n \in \mathscr{D}_i) \quad = \quad \begin{cases} \frac{2j}{iad}, & j < d \\ \frac{(ia-d+1)}{ia}, & j = d \end{cases},$$

and the invariant measure is

$$\underline{\mu} = (e, 2e, \ldots, (d-1)b, \mu_d), \tag{A.20}$$

where $e = \frac{2}{(|a|-1)d^2+d}$ and $\mu_d = \frac{(|a|-2)d^2+2d}{(|a|-1)d^2+d}$. Using (A.19), one obtains

$$\mathscr{H}(\underline{\mathbf{y}}) = \sum_{i=1}^{d} h_i \mu_i = \ln(|a|) + \ln(d).$$

We omit the case $d \geq a$ because even though the approach is the same, the calculations for the Markov matrix and the invariant measure are a bit more involved.

Next, we employ stochastic simulations to verify the results of the discrete formulation with the choice of $\alpha(x) = 3x$ ($a = 3$) and $d = 5$. The uniform partition along with transition probabilities is shown in Fig. A.3. We summarize the results with two choice of control. In the first case, we assume a stabilizing linear control

$$\underline{\mathbf{u}}_n = -3\underline{\mathbf{y}}_n.$$

After $10,000$ iterations, the belief process converges to a set $\mathscr{A} \in \nabla_{\underline{S}}$ with six distinct points, denoted as $\{\underline{\pi}^1, \ldots, \underline{\pi}^6\}$. Since $d = 3$, these are split into three types as follows:

$$\begin{aligned} h_y(\underline{\pi}^4) = h_y(\underline{\pi}^5) = h_y(\underline{\pi}^6) = h_1 &= 2.1972, \\ h_y(\underline{\pi}^2) = h_y(\underline{\pi}^3) = h_2 &= 2.8911, \\ h_y(\underline{\pi}^1) = h_3 &= 3.3740 \end{aligned}$$

consistent with formula (A.18). Note that the distinct distributions (say $\underline{\pi}^4, \underline{\pi}^5, \underline{\pi}^6$) with the same type have the same width r but different supports in $\underline{X}$. The invariant measure of the belief process was numerically verified to be

$$\underline{\mu} = (0.0952, 0.1905, 0.7143),$$

that is consistent with (A.20). Finally,

$$\mathscr{H}(\underline{\mathbf{y}}) = \sum_i \mu_i h_i = 3.1699 = \ln(a) + \ln(d).$$

One important observation is that $h_y(\underline{\pi}) < \ln(a) + \ln(d)$ for types 1 and 2, and $h_y(\underline{\pi}) > \ln(a) + \ln(d)$ for type 3. So the entropy rate is really a measure of average uncertainty.

In the second set of simulations, we chose a control

$$\underline{\mathbf{u}}_n = \begin{cases} 0, & 0 < |\underline{\mathbf{y}}_n| < 4\varepsilon \\ -3\underline{\mathbf{y}}_n, & \text{otherwise} \end{cases}$$

that is not locally stabilizing but keeps the trajectories bounded. For this choice of control, the belief process converges to a set $\mathscr{A} \in \nabla_{\underline{S}}$ with 21 distinct distributions. Even though the invariant attracting set $\mathscr{A}$ depends upon the choice of control, the invariant measure $\underline{\mu}$ is only a function of d types that are independent of control. Numerically, we obtained the same entropy rate.

A.7 Entropy estimates for a GES stable control Markov chain example

Consider three control Markov chains shown in Figure A.4. The state space $\underline{X} = \{0,-1,1\}$ and control space $\underline{U} = \{0,-1,1\}$. The three Markov chains are given by

$$\underline{P}^{(0)} = \begin{bmatrix} 1 & 0 & 0 \\ \frac{1}{2} & \frac{1}{2} & 0 \\ \frac{1}{2} & 0 & \frac{1}{2} \end{bmatrix}, \quad \underline{P}^{(-1)} = \begin{bmatrix} 0 & 0 & 1 \\ 1 & 0 & 0 \\ 0 & 0 & 1 \end{bmatrix},$$
$$\underline{P}^{(1)} = \begin{bmatrix} 0 & 1 & 0 \\ 0 & 1 & 0 \\ 1 & 0 & 0 \end{bmatrix}.$$

The observation space $\underline{Y} = \{0,-1,1\}$ is the same as $\underline{X}$ and $C = \text{Prob}(\underline{\mathbf{y}}_n|\underline{\mathbf{x}}_n)$ is used to denote the 3×3 emission matrix. With no disturbance, $\underline{C} = I$, the identity matrix.

A stabilizing control law is taken to be:

y	$u = k(y)$
0	0
1	-1
-1	1

(A.21)

In the absence of disturbance, $\{\underline{\mathbf{x}}_n\}$ is Markov with the closed-loop matrix

$$\underline{P}_c = \begin{bmatrix} 1 & 0 & 0 \\ 1 & 0 & 0 \\ 1 & 0 & 0 \end{bmatrix}.$$

We note that both the open-loop dynamics ($\underline{P}^{(0)}$) and the closed-loop dynamics ($\underline{P}_c$) are exponentially stable with the invariant measure supported on $0 \in \underline{X}$. Now, lets assume that observations are noisy modeled by

$$\underline{C} = \begin{bmatrix} 1-\gamma & \gamma & 0 \\ 0 & 1-\gamma & \gamma \\ \gamma & 0 & 1-\gamma \end{bmatrix}.$$

In effect, the disturbance has entropy $\mathscr{H}(\underline{\mathbf{d}}) = -\gamma\ln(\gamma) - (1-\gamma)\ln(1-\gamma)$. Clearly, $\mathscr{H}(\underline{\mathbf{y}}) \geq \mathscr{H}(\underline{\mathbf{d}})$. Figure A.5 shows that the inequality is in fact strict for $\gamma > 0$.

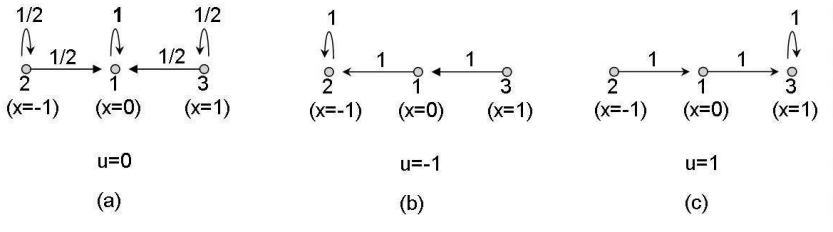

Figure A.4: The three control Markov chains

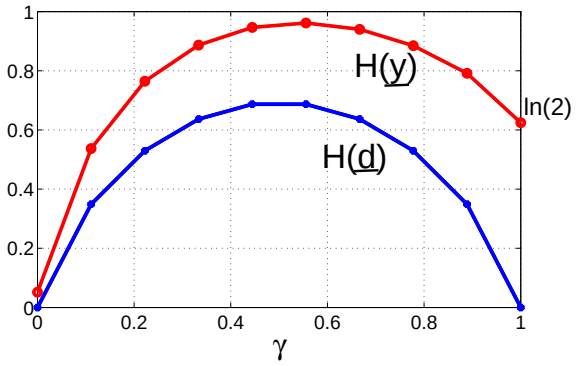

Figure A.5: Plot of numerically computed entropy rate $\mathscr{H}(\underline{\mathbf{y}})$ as a function of γ (for comparison $\mathscr{H}(\underline{\mathbf{d}})$ is also shown).

An explanation of this is as follows. For any observation sequence $\underline{\mathbf{y}}_0^{n-1}$, $H(\underline{\mathbf{y}}_n|\underline{\mathbf{y}}_0^{n-1}) = H(\underline{\mathbf{y}}_n|\underline{f}_n)$ where $\underline{f}_n$ is the belief at time n. Now, the latter $H(\underline{\mathbf{y}}_n|\underline{f}_n) \geq \mathscr{H}(\mathbf{d})$ with equality if and only if $\underline{f}_n$ is a delta function (i.e., one has perfect knowledge of the state). With out observation noise, this is indeed asymptotically the case. With observation noise, control can cause state to go into a region of state-space where positive uncertainty results. For the particular case at hand, one can verify that if $\underline{f}_{n-1} = \delta(\underline{x}-1)$ then one observes $\underline{\mathbf{y}}_{n-1} = 0$ w.p. γ. Using control law (A.21), this results in control $u_{n-1} = 0$ and $\underline{f}_n = [\frac{1}{2}, 0, \frac{1}{2}]$. So $H(\underline{\mathbf{y}}_n|\underline{f}_n) = \mathscr{H}(\underline{\mathbf{d}}) + (\ln(2) - \frac{1}{2}\mathscr{H}(\underline{\mathbf{d}}))$, and additional uncertainty results on account of dynamics. The plot in Fig. A.5 depicts the entropy rate, numerically obtained as time-average over 50,000 iterations.

A.8 Numerical computation of entropy rate for (2.47)

Consider the scalar example (2.47) with $a = 3$ for expansion and $L = 9$ for saturation. For computational purposes, we chose here a locally stabilizing control

$$\mathbf{u}_n = \begin{cases} -3(\mathbf{y}_n), & 0 < |\mathbf{y}_n| < 6 \\ -18 \cdot \mathrm{sgn}(\mathbf{y}_n), & \text{otherwise.} \end{cases}$$

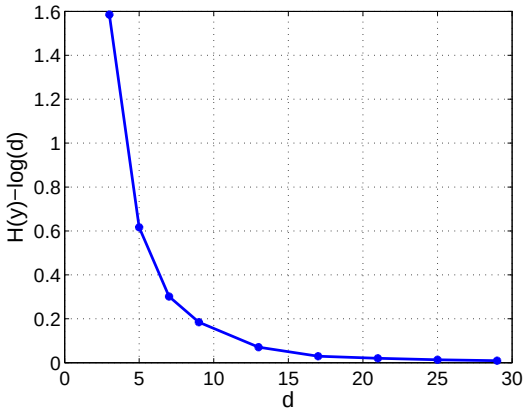

Figure A.6: Numerically evaluated plot of $\mathscr{H}(\mathbf{y}) - \mathscr{H}(\mathbf{d})$ as a function of d (with $a = 3$ for expansion and $L = 9$ in (2.47)).

We carried out closed-loop simulations with a range of disturbance d. For each of these simulations, we numerically computed the entropy rate $\mathscr{H}(\mathbf{y})$ by constructing an empirical approximation of the limiting measure μ for the belief process. Figure A.6 depicts the numerically obtained plot of $\mathscr{H}(\mathbf{y}) - \ln(d)$ as a function of the d. The convergence was found to be very slow, but consistent with the results of this section, $\mathscr{H}(\mathbf{y})$ asymptotes to $\mathscr{H}(\mathbf{d}) = \ln(d)$ for large d. Note that with small disturbance ($d = 3$ in the figure) and the choice of control, the closed-loop system state is never saturated and $\mathscr{H}(\mathbf{y}) = \ln(a) + \ln(d)$ in such a case. The uncertainty arise due to both dynamics and disturbance. However, the uncertainty due to dynamics decreases as disturbance increases on account of saturation in the value of state and hence its belief. As $d \to \infty$, one gets uncertainty only due to the disturbance. These observations are also consistent with the experimental results of [124].

Appendix B

Proofs in Chapter 4

B.1 Proof for Lemma 4.2.2

The eigenvalue problem (4.12) is given by

$$Z_\varepsilon(x) = \frac{e^{J_\varepsilon^* - \varepsilon x^2}}{\sqrt{2\pi\sigma^2}} \int Z_\varepsilon(x') e^{-\frac{(x'-ax)^2}{2\sigma^2}} dx'. \tag{B.1}$$

We consider the ansatz $Z_\varepsilon(x) = e^{-\kappa x^2}$ (so the relative value function $v(x) = \kappa x^2$). Substituting the ansatz in (B.1), we obtain

$$e^{-\kappa x^2} = \frac{e^{J_\varepsilon^* - \varepsilon x^2}}{\sqrt{2\pi\sigma^2}} \int e^{-\kappa x'^2} e^{-\frac{(x'-ax)^2}{2\sigma^2}} dx',$$

which simplifies to

$$\exp\{-\kappa x^2\} = \exp\{J_\varepsilon^* - \varepsilon x^2 - \frac{\kappa a^2 x^2}{1+2\sigma^2\kappa} - \frac{1}{2}\ln(2\sigma^2\kappa+1)\}.$$

Collecting coefficients with the same power, we obtain $\frac{a^2\kappa}{1+2\sigma^2\kappa} = \kappa - \varepsilon$, and $J_\varepsilon^* = \frac{1}{2}\ln(2\sigma^2\kappa+1)$.

B.2 Proof for Theorem 4.2.3

From Lemma 4.2.2, we have $Z_\varepsilon(x) = e^{-\kappa x^2}$. In the limit as $\varepsilon \to 0$, κ is a solution of

$$\frac{a^2\kappa}{1+2\sigma^2\kappa} = \kappa \tag{B.2}$$

and $J_0^* = \frac{1}{2}\ln(2\sigma^2\kappa+1)$. The equation B.2 has two solutions: $\kappa = 0$ for which $Z_0(x) = 1(x)$, and $\kappa = \frac{a^2-1}{2\sigma^2}$ for which $Z_0(x) = e^{\frac{1-a^2}{2\sigma^2}x^2}$.

If $|a| < 1$, then the only bounded eigenfunction is $Z_0(x) = 1(x)$, and $J_0^* = 0$.

If $|a| > 1$, then $Z_0(x) = e^{\frac{1-a^2}{2\sigma^2}x^2}$ for which $J_0^* = \frac{1}{2}\ln(2\sigma^2\kappa+1) = \ln|a|$.

B.3 Proof for Theorem 4.3.3

The proof is similar to the scalar case. The eigenvalue problem is given by

$$Z_\varepsilon(x) = \frac{e^{J^*_\varepsilon - \varepsilon x^T \Gamma x}}{(2\pi)^{k/2}|R|^{1/2}} \int_{\mathbb{R}^n} Z_\varepsilon(x') e^{-\frac{1}{2}(x'-Ax)^T R^{-1}(x'-Ax)} dx'. \tag{B.3}$$

We use the ansatz $Z_\varepsilon(x) = e^{-x^T V x}$ so the relative value function $v(x) = x^T V x$. Substituting this ansatz in (B.3), we obtain

$$\frac{x^T A^T R^{-1}(R-(R^{-1}+2V)^{-1})R^{-1}Ax}{2} - x^T V x + \varepsilon x^T \Gamma x = J^*_\varepsilon - \frac{1}{2}\ln|I+2RV|.$$

This implies

$$\frac{A^T R^{-1}(R-(R^{-1}+2V)^{-1})R^{-1}A}{2} - V + \varepsilon\Gamma = 0 \tag{B.4}$$

and

$$J^*_\varepsilon = \frac{1}{2}\ln|I+2RV| \tag{B.5}$$

We consider the limit as $\varepsilon \searrow 0$. Using the Woodbury matrix identity, equation (B.4) is simplified to

$$A^T(R+(2V)^{-1})^{-1}A = 2V.$$

Taking determinant on both sides, we have

$$|A|^2 = |R+(2V)^{-1}| \cdot |2V| = |2RV+I|.$$

Substituting this in (B.5), we obtain

$$J^*_0 = \frac{1}{2}\ln|I+2RV| = \frac{1}{2}\ln|A|^2 = \ln|A|.$$

Appendix C

Proofs in Chapter 6

C.1 Proof of Lemma 6.2.2

First observe that

$$\begin{aligned} f(\hat{x}_i(T)) - f(x^*) &= f(\frac{1}{T}\sum_{k=1}^{T} x_i(k)) - f(x^*) \\ &\leq \frac{1}{T}\sum_{k=1}^{T}(f(x_i(k) - f(x^*)) \\ &= \frac{1}{T}\sum_{k=1}^{T}\{f(x_i(k)) - f(\bar{x}(k))\} + \frac{1}{T}\sum_{k=1}^{T}\{f(\bar{x}(k)) - f(x^*)\}. \end{aligned} \tag{C.1}$$

The first term in RHS of (C.1) can be bounded as

$$\begin{aligned} \frac{1}{T}\sum_{k=1}^{T}\{f(x_i(k)) - f(\bar{x}(k))\} &= \frac{1}{T}\sum_{k=1}^{T}\{\frac{1}{n}\sum_{j=1}^{n}(f_j(x_i(k)) - f_j(\bar{x}(k)))\} \\ &\leq \frac{1}{nT}\sum_{k,j}\{L\|x_i(k) - \bar{x}(k)\|\} \\ &= \frac{L}{T}\sum_{k=1}^{T}\|x_i(k) - \bar{x}(k)\|. \end{aligned} \tag{C.2}$$

For the second term, we start from

$$\begin{aligned} \|\bar{x}(k+1) - x^*\|^2 &= \|\bar{x}(k) - \frac{\alpha}{n}\sum_{i=1}^{n} g_i(k) - x^*\|^2 \\ &= \|\bar{x}(k) - x^*\|^2 - \frac{2\alpha}{n}\sum_{i=1}^{n} g_i(k)(\bar{x}(k) - x^*) + \frac{\alpha^2}{n^2}(\sum_{i=1}^{n} g_i(k))^2 \\ &\leq \|\bar{x}(k) - x^*\|^2 - 2\alpha(f(\bar{x}(k)) - f(x^*)) + \frac{\alpha^2}{n^2}(\sum_{i=1}^{n} g_i(k))^2. \end{aligned} \tag{C.3}$$

The last inequality is valid because

$$\begin{aligned} f(\bar{x}(k)) - f(x^*) &= \frac{1}{n}\sum_{i=1}^{n}\{f_i(\bar{x}(k)) - f_i(x^*)\} \\ &\leq \frac{1}{n^2}\sum_{i,j=1}^{n}\{f_i(x_j(k)) - f_i(x^*)\} \\ &\leq \frac{1}{n^2}\sum_{i,j=1}^{n}\{g_i(k)(x_j(k) - x^*)\} \\ &= \frac{1}{n}\sum_{i=1}^{n}\{g_i(k)(\bar{x}(k) - x^*)\}. \end{aligned}$$

Inequality (C.3) implies that

$$\begin{aligned} 0 &\leq \|\bar{x}(T+1) - x^*\|^2 \\ &\leq \|\bar{x}(1) - x^*\|^2 - 2\alpha\sum_{k=1}^{T}(f(\bar{x}(k)) - f(x^*)) + \frac{\alpha^2}{n^2}\sum_{k=1}^{T}(\sum_{i=1}^{n} g_i(k))^2. \end{aligned}$$

This in turn gives

$$\sum_{k=1}^{T}(f(\bar{x}(k)) - f(x^*)) \leq \frac{\|\bar{x}(1) - x^*\|^2 + \frac{\alpha^2}{n^2}\sum_{k=1}^{T}(\sum_{i=1}^{n} g_i(k))^2}{2\alpha}.$$

Dividing both sides by T, we obtain a bound for the second term in RHS of (C.1)

$$\begin{aligned} \frac{1}{T}\sum_{k=1}^{T}\{f(\bar{x}(k)) - f(x^*)\} &\leq \frac{\|\bar{x}(1) - x^*\|^2}{2\alpha T} + \frac{\alpha^2\sum_{k=1}^{T}(\sum_{i=1}^{n} g_i(k))^2}{2\alpha n^2 T} \\ &\leq \frac{\|\bar{x}(1) - x^*\|^2}{2\alpha T} + \frac{\alpha^2 T(nL)^2}{2\alpha n^2 T} \\ &= \frac{\|\bar{x}(1) - x^*\|^2}{2\alpha T} + \frac{\alpha L^2}{2}. \end{aligned} \tag{C.4}$$

Combining (C.2) and (C.4) we get Lemma (6.2.2).

C.2 Proof of Theorem 6.2.3

The key is to bound RHS of (C.2). We start by following similar arguments as in [120]. When $\alpha(k) \equiv \alpha$, let $s = 1$, the equation (6.4) becomes

$$x_i(k+1) = \sum_{j=1}^{n}[\Phi(k+1,1)]_{ij}x_j(1) - \alpha g_i(k) - \alpha\sum_{r=1}^{k-1}\sum_{j=1}^{n}[\Phi(k+1,r+1)]_{ij}g_j(r).$$

The evolution of $\bar{x}(k)$ is given by

$$\bar{x}(k) = \frac{1}{n}\sum_{i=1}^{n} x_i(k) = \frac{1}{n}\sum_{i=1}^{n}\{\sum_{j=1}^{n} a_{ij}(k-1)x_j(k-1) - \alpha g_i(k-1)\} \tag{C.5}$$

$$= \bar{x}(k-1) - \frac{\alpha}{n}\sum_{i=1}^{n} g_i(k-1) \tag{C.6}$$

$$= \bar{x}(1) - \frac{\alpha}{n}\sum_{s=1}^{k-1}\sum_{j=1}^{n} g_j(s)\,. \tag{C.7}$$

Equality (C.6) used the fact that $A(k-1)$ is double stochastic. In equation (C.7) we changed subindices from i to j, we obtain $\bar{x}(k+1) - x_i(k+1) =$

$$\{\bar{x}(1) - \sum_{j=1}^{n}[\Phi(k+1,1)]_{ij}x_j(1)\} + \alpha\sum_{r=1}^{k-1}\sum_{j=1}^{n}([\Phi(k+1,r+1)]_{ij} - \frac{1}{n})g_j(r) + \frac{\alpha}{n}\sum_{j=1}^{n}(g_i(k) - g_j(k))\,. \tag{C.8}$$

Assume $x_i(1) = \bar{x}(1) = 0$, the first term is gone. Use bound $\|g_i(k)\| \le L$, we get

$$\|\bar{x}(k+1) - x_i(k+1)\| \le \alpha L\sum_{r=1}^{k-1}\|[\Phi(k+1,r+1)]_i - \frac{\mathbf{1}}{n}\|_1 + 2\alpha L\,. \tag{C.9}$$

Now we break the sum in (C.10) into two terms.

$$\|\bar{x}(k) - x_i(k)\| \le \alpha L\sum_{r=1}^{k-1-\hat{k}}\|[\Phi(k+1,r+1)]_i - \frac{\mathbf{1}}{n}\|_1 + 2\alpha L + \alpha L\sum_{r=k-\hat{k}}^{k-1}\|[\Phi(k+1,r+1)]_i - \frac{\mathbf{1}}{n}\|_1\,. \tag{C.10}$$

Note that $\Phi(k+1,r+1) = A^{k-r}$. For small r, $\Phi(k+1,r+1)$ is close to uniform:

$$\|\Phi(k+1,r+1)_i - \frac{1}{n}\|_1 \le \sqrt{n}\lambda_2(A)^{k-r}\,. \tag{C.11}$$

We use this fact to bound the first term as

$$\alpha L\sum_{r=1}^{k-1-\hat{k}}\|[\Phi(k+1,r+1)]_i - \frac{\mathbf{1}}{n}\|_1 \le \alpha L\sum_{r=1}^{k-1-\hat{k}}\sqrt{n}\lambda_2(A)^{k-r} < \alpha L\sqrt{n}\sum_{s=\hat{k}+1}^{\infty}\lambda_2(A)^s = \alpha L\sqrt{n}\frac{\lambda_2(A)^{\hat{k}+1}}{1-\lambda_2(A)}\,. \tag{C.12}$$

Therefore, if we choose cutoff time-step $\hat{k}$ such that

$$\lambda_2(A)^{\hat{k}+1} = \frac{1}{\sqrt{n}}$$

the first term is bounded by $\alpha L/(1-\lambda_2(A))$.

For the second term, r is relatively large, so $\|[\Phi(k+1,r+1)]_i - \mathbb{1}/\|_1$ is simply bounded by 2. We can get a bound

of the second term as $2\alpha L\hat{k}$. By the choice of $\hat{k}$,

$$2\alpha L\hat{k} = -2\alpha L\frac{\log\sqrt{n}}{\log\lambda_2(A)} - 2\alpha L \leq 2\alpha L\frac{\log\sqrt{n}}{1-\lambda_2(A)} - 2\alpha L\,.$$

Collecting the bounds together, we have the following result

$$\|x_i(k) - \overline{x}(k)\| \leq \frac{\alpha L(\log n + 1)}{1-\lambda_2(A)} - 2\alpha L\,.$$

Plugging into Equation (6.5) we get

$$\begin{aligned} f(\hat{x}_i(T)) - f(x^*) &\leq \frac{\alpha L^2(\log n+1)}{1-\lambda_2(A)} - 2\alpha L^2 + \frac{\|\overline{x}(1)-x^*\|^2}{2\alpha T} + \frac{\alpha L^2}{2} \\ &= \frac{\alpha L^2(\log n+1)}{1-\lambda_2(A)} + \frac{\|\overline{x}(1)-x^*\|^2}{2\alpha T} - \frac{3\alpha L^2}{2}\,, \end{aligned} \tag{C.13}$$

which is inequality (6.6).

References

[1] H. K. Sung and S. Hara. Properties of sensitivity and complementary sensitivity functions in single-input single-output digital control systems. *Int. J. Control*, 48(6):2429–2439, 1988.

[2] J.S. Freudenberg and D.P. Looze. A sensitivity tradeoff for plants with time delay. *IEEE Trans. Automatic Control*, AC-32:99–104, 1987.

[3] G. Zang and P. A. Iglesias. Nonlinear extension of Bode's integral based on an information theoretic interpretation. *Systems and Control Letters*, 50:11–29, 2003.

[4] J. Baillieul and P. J. Antsaklis. Control and communication challenges in networked real-time systems. *Proceedings of IEEE*, 95(1):9–28, 2007.

[5] W. S. Wong and R. W. Brockett. Systems with finite communication bandwidth constraints ii: stabilization with limited information feedback. *IEEE Trans. on Automatic Control*, 44(5):1049 – 1053, 1998.

[6] G. N. Nair and R. J. Evans. Communication-limited stabilization of linear systems. In *Proc. IEEE Conference on Decision and Control*, pages 1005–1010, 2000.

[7] S. Tatikonda and S. K. Mitter. Control under communication constraints. *IEEE Trans. on Automatic Control*, 49(7):1056–68, 2004.

[8] R. P. N. Rao and T. Sejnowski. Predictive coding, cortical feedback, and spike-timing dependent plasticity. pages 135–154, 2002.

[9] A.E.C. Pece. Redundancy reduction of a gabor representation: A possible computational role for feedback from primary visual cortex to lateral geniculate nucleus. In I. Aleksander and J. Taylor, editors, *Artificial Neural Networks*, pages 865–868. Elsevier Science Publishers, Amsterdam, 1992.

[10] E. M. Izhikevich. *Dynamical systems in neuroscience: the geometry of excitability and bursting*. Computational Neuroscience. MIT Press, Cambridge, MA, 2007.

[11] E. M. Izhikevich. Polychronization: computation with spikes. *Neural Comput.*, 18(2):245–282, 2006.

[12] J-Horgan. The consciousness conundrum. *IEEE Spectrum*, pages 36–41, 2008.

[13] A. Destexhe and D. Contreras. Neuronal computations with stochastic network states. *Science*, 314(5796):85–90, 2006.

[14] A. Banaszuk, P. G. Mehta, and G. Hagen. The role of control in design: From fixing problems to the design of dynamics. *Control Engineering Practice (CEP)*, 15(10):1292–1305.

[15] A. Banaszuk, P. G. Mehta, C. Jacobson, and A. I. Khibnik. Limits of achievable performance of controlled combustion processes. *IEEE Trans. on Control Systems Technology*, 14(5):881–895, 2006.

[16] Y. Sun and P. G. Mehta. Fundamental performance limitations via entropy estimates with hidden markov models. In *Procs. of Conference on Decision & Control*, pages 3982–3988. 2007. IEEE Best Student Paper Award.

[17] H. S Witsenhausen. A counterexample in stochastic optimal control. *SIAM Journal on Control*, 6:131–147, 1968.

[18] N. Wiener. Cybernetics: Or the control and communication in the animal and the machine. 1948.

[19] H. S. Witsenhausen. Separation of estimation and control for discrete time systems. *Proceedings of the IEEE*, 59(11):1557 – 1566, 1971.

[20] J.H. Rojas, A.J. Braslavsky and R.H Middleton. Output feedback sensitivity functions under signal to noise ratio constraint. *ACC 2007*, pages 287–292, 2007.

[21] N. Elia. When Bode meets Shannon: Control-oriented feedback communication schemes. *IEEE Trans. on Automatic Control*, 49(9):1477 – 1488, 2004.

[22] Todd P. Coleman. A stochastic control viewpoint on 'posterior matching'-style feedback communication schemes. In *Proceedings of the 2009 IEEE international conference on Symposium on Information Theory - Volume 3*, ISIT, pages 1520–1524, 2009.

[23] N. Elia. Stabilization of linear systems with limited information. *IEEE Trans. on Automatic Control*, 46(9):1384–99, 2001.

[24] F. Fagnani and S. Zampieri. Stability analysis and synthesis for scalar linear systems with quantized feedback. *IEEE Trans. on Automatic Control*, 48(9):1569–1584, 2003.

[25] D. Liberzon. On stabilization of linear systems with limited information. *IEEE Trans. on Automatic Control*, 48(2):304–307, 2003.

[26] S. Yuksel and T. Basar. Minimum rate coding for LTI systems over noiseless channels. *IEEE Transactions Automatic Control*, 51:1878–1887, 2006.

[27] A. S. Matveev and A. V. Savkin. Multirate stabilization of linear multiple sensor systems via limited capacity communication channels. *SIAM J. Control Optim.*, 44(2):584–617 (electronic), 2005.

[28] S Yüksel and T Başar. Optimal signaling policies for decentralized multicontroller stabilizability over communication channels. *IEEE Trans. Automat. Control*, 52(10):1969–1974, 2007.

[29] S. Yuksel and T. Basar. Communication constraints for decentralized stabilizability with time-invariant policies. *IEEE Transactions Automatic Control*, 52(6):1060 – 1066, 2007.

[30] S. Yuksel and T. Basar. Control over noisy forward and reverse channels. *IEEE Transactions Automatic Control*, 56(5):1014 – 1029, 2011.

[31] J. Freudenberg and D. Looze. Right half plane poles and zeros and design tradeoffs in feedback systems. *IEEE Trans. Automat. Control*, 30(6):555–565, 1985.

[32] J. Freudenberg and D. Looze. A sensitivity tradeoff for plants with time delay. *IEEE Trans. on Automatic Control*, 32(2):99–104, 1987.

[33] J. Freudenberg and D. Looze. Frequency domain properties of scalar and multivariable feedback systems. *Lecture Notes in Control and Information Sciences*, 1988.

[34] Stephen Boyd and C. A. Desoer. Subharmonic functions and performance bounds on linear time-invariant feedback systems. *Modelling, identification and robust control(Stockholm)*, pages 103–111, 1986.

[35] J. Chen. Logarithmic integrals, interpolation bounds, and performance limitations in mimo systems. *IEEE Trans. on Automatic Control*, 45(6):1098–1115, 2000.

[36] Weizhou Su, Li Qiu, and Jie Chen. Fundamental performance limitations in tracking sinusoidal signals. *IEEE Trans. on Automatic Control*, 48(8):1371–1380, 2003. New developments and applications in performance limitation of feedback control.

[37] M. Seron, J. Braslavsky, P. Kokotovic, and D. Mayne. Feedback limitations in nonlinear systems: From bode integrals to cheap control, 1997. Technical Report 97-0304, CCEC, University of California, Santa Barbara.

[38] M. Seron, J. Braslavsky, P. Kokotovic, and D. Mayne. Feedback limitations in nonlinear systems: from bode integrals to cheap control. *IEEE Trans. Automat. Control*, 44(4):829–833, 1999.

[39] N. C. Martins and M. A. Dahleh. Fundamental limitations of disturbance attentuation in the presence of side information. *IEEE Trans. on Automatic Control*, 52(1):56–66, 2007.

[40] N. C. Martins and M. A. Dahleh. Feedback control in the presence of noisy channels: "Bode-like" fundamental limitations of performance. *IEEE Trans. on Automatic Control*, 53(7):1604 –1615, 2008.

[41] J.S. Shamma. Performance limitations in sensitivity reduction for nonlinear plants. *Systems and Control Letters*, pages 43–47, July 1991.

[42] C. W. Rowley, D.R. Williams, T. Colonius, R.M. Murray, and D.G. MacMartin. Linear models for control of cavity flow oscillations. *J. Fluid Mech.*, 547:317–330, 2006.

[43] P. A. Iglesias. An analogue of Bode's integral for stable nonlinear systems: Relations to entropy. In *Procs. of Conference on Decision & Control*, pages 3419–3420, 2001.

[44] P. A. Iglesias. Tradeoffs in linear time-varying systems: an analogue of bode's sensitivity integral. *Automatica*, 37:1541C1550, 2001.

[45] Y. Sun, P. G. Mehta, and S. P. Meyn. Belief propagation in feedback systems: Connections to bode and observability. In *Proc. of American Control Conference*, pages 1268–1273, 2008.

[46] Yu Sun and Prashant.G.Mehta. Bode-like fundamental performance limitations in control of nonlinear systems. *IEEE Trans. on Automatic Control*, 55:1390–1405, 2010.

[47] A. Katok and B. Hasselblatt. *Introduction to the modern theory of dynamical systems*. Cambridge University Press, Cambridge, UK, 1995.

[48] G. N. Nair, R. J. Evans, and I. M. Y. Mareels. Topological feedback entropy and nonlinear stabilization. *IEEE Trans. on Automatic Control*, 49(9):1585–1597, 2004.

[49] P. G. Mehta, U. Vaidya, and A. Banaszuk. Markov chains, entropy, and fundamental limitations in nonlinear stabilization. *IEEE Trans. on Automatic Control*, 53(3):784–791, 2008.

[50] G. E. Dullerud and F. Paganini. *A Course in Robust Control Theory: A Convex Approach*. Springer-Verlag, New York, 2000.

[51] T. T. Georgiou. Distances and Riemannian metrics for spectral density functions. *IEEE Trans. on Signal Processing*, 55(8):3995–4003.

[52] R. Gray, A. Buzo, A. Gray, and Matsuyama. Distortion measures for speech processing. *IEEE Trans. Acoust., Speech, Signal Processing*, 28(4):367376, 1980.

[53] T. T. Georgiou. An intrinsic metric for power spectral density functions. *IEEE Signal Processing Letters*, 14(8):561–563, 2007.

[54] T. T. Georgiou and A. Lindquist. A convex optimization approach to arma modeling. *IEEE Trans. on Automatic Control*, 53:1108–1119, 2008.

[55] Hirotugu Akaike. A new look at the statistical model identification. *IEEE Trans. on Automatic Control*, AC-19:716–723, 1974. System identification and time-series analysis.

[56] Y. Baram. Stochastic model simplification. *IEEE Trans. on Automatic Control*, AC-26:379–390, 1981.

[57] R. Kulhavý. *Recursive Nonlinear Estimation: A Geometric Approach*, volume 216 of *Lecture Notes in Control and Information Sciences*. Springer-Verlag, London, 1996.

[58] Richard E. Blahut. Hypothesis testing and information theory. *IEEE Trans. Information Theory*, IT-20:405–417, 1974.

[59] J. M. Bernardo. Expected information as expected utility. *The Annals of Statistics*, 7(3):686–690, 1979.

[60] R. M. Royall. *Statistical Evidence: A Likelihood Paradigm*. Chapman & Hall, London, 1997.

[61] Peter E. Caines. *Linear stochastic systems*. Wiley Series in Probability and Mathematical Statistics: Probability and Mathematical Statistics. John Wiley & Sons Inc., New York, 1988.

[62] Robert Leland. Reduced-order models and controllers for continuous-time stochastic systems: an information theory approach. *IEEE Trans. on Automatic Control*, 44(9):1714–1719, 1999.

[63] Robert P. Leland. An approximate-predictor approach to reduced-order models and controllers for distributed-parameter systems. *IEEE Trans. on Automatic Control*, 44(3):623–627, 1999.

[64] David A. Wagie and Robert E. Skelton. A projection approach to covariance equivalent realizations of discrete systems. *IEEE Trans. on Automatic Control*, 31(12):1114–1120, 1986.

[65] H. Zhang and Y. X. Sun. Information theoretic methods for stochastic model reduction based on state projection. In *Proc. of American Control Conference*, pages 2596–2601, 2005.

[66] K. Deng, Y.Sun, P. G. Mehta, and S. Meyn. An information-theoretic framework to aggregate a markov chain. In *Procs of American Control Conference*, pages 731–736, 2009.

[67] C. V. S. K. Reddy M. Vidyasagar, S. S. Mande and V. V. R. Rao. The 4m (mixed memory markov model) algorithm for finding genes in prokaryotic genomes. *IEEE Trans. on Automatic Control*, 53(3, part 1):26–37, 2008. Special Issue.

[68] A. Dembo and O. Zeitouni. *Large Deviations Techniques And Applications*. Springer-Verlag, New York, second edition, 1998.

[69] I. Kontoyiannis and S. P. Meyn. Large deviations asymptotics and the spectral theory of multiplicatively regular Markov processes. *Electron. J. Probab.*, 10(3):61–123 (electronic), 2005.

[70] M. M. Seron, J. H. Braslavsky, P. V. Kokotović, and D. Q. Mayne. Feedback limitations in nonlinear systems: from Bode integrals to cheap control. *IEEE Trans. Automat. Control*, 44(4):829–833, 1999.

[71] L. Qui and E. J. Davison. Performance limitations of non-minimum phase systems in the servomechanism problem. *Automatica*, 29(2):337–349, 1993.

[72] R.H. Middleton and J.H. Braslavsky. On the relationship between logarithmic sensitivity integrals and limiting optimal control problems. In *Proc. IEEE Conference on Decision and Control*, pages 4990–4995, 2000.

[73] Graham C. Goodwin, Mario E. Salgado, and Juan I. Yuz. Performance limitations for linear feedback systems in the presence of plant uncertainty. *IEEE Trans. on Automatic Control*, 48(8):1312–1319, 2003.

[74] E. Todorov. Eigenfunction approximation methods for linearly-solvable optimal control problems. In *Proc. of the 2nd IEEE Symposium on Adaptive Dynamic Programming and Reinforcement Learning*, pages 161 – 168, 2009.

[75] E. Todorov. Efficient computation of optimal actions. 106(28):11478–11483, PNAS.

[76] P. Whittle. *Risk Sensitive Optimal Control*. Wiley, Chichester, New York, 1990.

[77] Wendell H. Fleming and William M. McEneaney. Risk-sensitive control on an infinite time horizon. *SIAM J. Control and Optimization*, 33(6):1881–1915, 1995.

[78] Wendell H. Fleming and Shuenn-Jyi Sheu. Asymptotics for the principal eigenvalue and eigenfunction of a nearly first-order operator with large potential. *The Annals of Probability*, 25(4):1953–1994, 1997.

[79] Wendell H. Fleming and R.W. Rishel. *Deterministic and Stochastic Optimal Control*. Springer-Verlag, 1982.

[80] H. Kunita. Asymptotic behavior of the nonlinear filtering errors of Markov processes. *J. Multivariate Anal.*, 1:365–393, 1971.

[81] A. Budhiraja. On invariant measures of discrete time filters in the correlated signal-noise case. *Ann. Appl. Probab.*, 12(3):1096–1113, 2002.

[82] A. Budhiraja and H. J. Kushner. Monte Carlo algorithms and asymptotic problems in nonlinear filtering. In *Stochastics in finite and infinite dimensions*, Trends Math., pages 59–87. Birkhäuser Boston, Boston, MA, 2001.

[83] P. Chigansky. An ergodic theorem for filtering with applications to stability. *Systems Control Lett.*, 55(11):908–917, 2006.

[84] D.Blackwell. The entropy of functions of finite-state markov chains. *Trans. First Prague Conf. Information Theory, Statistical Decision Functions, Random Processes*, pages 13–20, 1957.

[85] B.R.Barmish and J. Sankaran. The propagation of parametric uncertainty via polytopes. *IEEE Trans. on Automatic Control*, 24:346–349, 1979.

[86] D.P.Bertsekas and I.B.Rhodes. Recursive state estimation for a set-membership description of uncertainty. *IEEE Trans. on Automatic Control*, 16(2):117–128, 1971.

[87] Aharon. Ben-Tal Yonina. C. Eldar and Arkadi. Nemirovski. Robust mean-squared error estimation in the presence of model uncertainties. *IEEE Trans. on Signal Processing*, 53(1):168–181, 2005.

[88] Y. Sun and P. G. Mehta. The Kullback-Leibler metric for comparing dynamical systems. *IEEE Trans. on Automatic Control*, 55(7):1585 – 1598, 2010.

[89] T. M. Cover and J. A. Thomas. *Elements of Information Theory,3rd Edition*. Wiley Series in Telecommunications. Wiley Interscience, New York, 2005.

[90] A. J. Chorin, O. H. Hald, and R. Kupferman. Prediction from partial data, renormalization, and averaging. *J. Sci. Comput.*, 28(2-3):245–261, 2006.

[91] G. Mathew and S. Meyn. Shannon meets Bellman: Feature based Markovian models for detection and optimization. In *Proc. IEEE Conference on Decision and Control*, pages 5558–5564, 2008.

[92] E. Todorov. Eigenfunction approximation methods for linearly-solvable optimal control problems. In *Proc. of the 2nd IEEE Symposium on Adaptive Dynamic Programming and Reinforcement Learning*, pages 161–168, 2009.

[93] James A. Yorke Troy Shinbrot, Celso Grebogi and Edward Ott. Using small perturbations to control chaos. *Nature*, 363:411 – 417, 1993.

[94] J. Niedbalski and P. G. Mehta. Simulation and estimation of evacuation dynamics in a building. In *Procs. of American Control Conference*, pages 5064–5069, New York, 2007.

[95] D. Snoonian. Smart buildings. *IEEE Spectrum*, pages 18–23, 2003.

[96] Board on Chemical Sciences and Technology. *Review of EPA Homeland Security Efforts: Safe Buildings Program Research Implementation Plan*. The National Academies Press, Washington, D.C., 2003. http://www.nap.edu/books/0309091047/html/1.html.

[97] Hanbiao Wang, Kung Yao, and Deborah Estrin. Information-theoretic approaches for sensor selection and placement in sensor networks for target localization and tracking. *Journal of Communications and Networks*, 7(4):438–449, 2005.

[98] D. B. Jourdan and N. Roy. Optimal sensor placement for agent localization. In *Position, Location, And Navigation Symposium*, 2006.

[99] A. Krause, C. Guestrin, A. Gupta, and J. Kleinberg. Near-optimal sensor placements: Maximizing information while minimizing communication cost. In *Information Processing in Sensor Networks (IPSN)*, pages 2–10, 2006.

[100] A. Krause, B. McMahan, C. Guestrin, and A. Gupta. Robust submodular observation selection. *Journal of Machine Learning Research*, (1):2761–2801, 2008.

[101] Andreas Schadschneider. Cellular automation approach to pedestrian dynamics-theory. In Michael Schreckenberg and Som Deo Sharma, editors, *Pedestrian and Evacuation Dynamics*, pages 75–86. Springer, 2002.

[102] S. Gwynne, E.R. Galea, M. Owen, P.J. Lawrence, and L. Filippidis. A systematic comparison of building exodus predictions with experimental data from the stapelfeldt trials and the milburn house evacuation. *Applied Mathematical Modelling*, 29:818–851, 2005.

[103] Dirk Helbing, Lubos Buzna, Anders Johansson, and Torsten Werner. Self-organized pedestrian crowd dynamics: Experiments, simulations, and design solutions. *Transportation Science*, 39(1):1–24, February 2005.

[104] Shard Sharma and Scott Gifford. Using rfid to evaluate evacuation behavior models. In *Annual Conference of the North American Fuzzy Information Processing Society-NAFIPS*, pages 804–808, 2005.

[105] Tzu-Sheng Shen. Esm: a building evacuation simulation model. *Building and Environment*, 40:671–680, 2005.

[106] B. Fiedler. *Ergodic theory, Analysis, and Efficient Simulation of Dynamical Systems*. Springer, Berlin, 2001.

[107] Y. Ephraim. Hidden Markov processes. *IEEE Trans on Information Theory*, 48(6):1518 –1569, 2002.

[108] A. Nedic and A. Ozdaglar. On the rate of convergence of distributed subgradient methods for multi-agent optimization. In *Proc. IEEE Conference on Decision and Control*, pages 4711–4716, 2007.

[109] Angelia Nedic, Alexander Olshevsky, Asuman E. Ozdaglar, and John N. Tsitsiklis. On distributed averaging algorithms and quantization effects. In *Proc. IEEE Conference on Decision and Control*, pages 4825–4830, 2008.

[110] A. Nedic and A. Ozdaglar. Distributed subgradient methods for multi-agent optimization. *IEEE Trans. on Automatic Control*, 54(1):48–61, 2009.

[111] B. Johansson, T. Keviczky, M. Johansson, and K. H. Johansson. Subgradient methods and consensus algorithms for solving convex optimization problems. In *Proc. IEEE Conference on Decision and Control*, pages 4185–4190, 2008.

[112] Federico S. Cattivelli and Ali H. Sayed. Diffusion LMS strategies for distributed estimation. *IEEE Trans. on Signal Processing*, 58(3):1035–1048, 2010.

[113] Noriyuki Takahashi, Isao Yamada, and Ali H. Sayed. Diffusion least-mean squares with adaptive combiners: formulation and performance analysis. *IEEE Trans. on Signal Processing*, 58(9):4795–4810, 2010.

[114] Sean P. Meyn, Amit Surana, Yiqing Lin, Stella Maris Oggianu, Satish Narayanan, and Thomas A. Frewen. A sensor-utility-network method for estimation of occupancy in buildings. In *Proc. IEEE Conference on Decision and Control*, pages 1494–1500, 2009.

[115] F. Kelly, A. Maulloo, and D. Tan. Rate control in communication networks: shadow prices, proportional fairness and stability. In *Journal of the Operational Research Society*, volume 49, pages 237–252, 1998.

[116] Steven H. Low and David E. Lapsley. Optimization flow control I: Basic algorithm and convergence. *IEEE/ACM Trans. on Networking*, 7(6):861–874, 1999.

[117] Rayadurgam Srikant. *The Mathematics of Internet Congestion Control (Systems and Control: Foundations and Applications)*. SpringerVerlag, 2004.

[118] Pu Wan and Michael D. Lemmon. An event-triggered distributed primal-dual algorithm for network utility maximization. In *Proc. IEEE Conference on Decision and Control*, pages 5863–5868, 2009.

[119] Bjorn Johansson, Alberto Speranzon, Mikael Johansson, and Karl Henrik Johansson. On decentralized negotiation of optimal consensus, 2008.

[120] Alekh Agarwal, John Duchi, and Martin Wainwright. Dual averaging for distributed optimization: Convergence analysis and network scaling. Technical Report arXiv:1005.2012, May 2010.

[121] Tuhin Sahai, Alberto Speranzon, and Andrzej Banaszuk. Hearing the clusters in a graph: A distributed algorithm. *Submitted for Journal Publication*, 2009. Available online http://arxiv.org/abs/0911.4729.

[122] Tuhin Sahai, Alberto Speranzon, and Andrzej Banaszuk. Wave equation based algorithm for distributed eigenvector computation. In *Proc. IEEE Conference on Decision and Control*, pages 7308–7315, 2010.

[123] A. Papoulis. *Probability, Random Variables, and Stochastic Processes*. McGraw-Hill, New York, 1984.

[124] A. Banaszuk, P. G. Mehta, C. Jacobson, and A. I. Khibnik. Fundamental limitations in control of combustion processes. *IEEE Control Systems Technology*, 14(5):881–895, 2006.

[125] C. W. Rowley, D. R. Williams, T. Colonius, R. M. Murray, and D. G. MacMynowski. Linear models for control of cavity flow oscillations. *Journal of Fluid Mechanics.*, pages 317–330, 2006.

[126] A. Lasota and M. C. Mackey. *Chaos, Fractals, and Noise: Stochastic Aspects of Dynamics*. Springer-Verlag, New York, 1994.

[127] H. Kunita. Ergodic properties of nonlinear filtering processes. In *Spatial stochastic processes*, volume 19 of *Progr. Probab.*, pages 233–256. Birkhäuser Boston, Boston, MA, 1991.

[128] F. L. Lewis. *Optimal Estimation with an Introduction to Stochastic Control Theory*. John Wiley & Sons, New York, 1986.

[129] J. P. Eckman and D. Ruelle. Ergodic theory of chaos and strange attractors. *Rev. Modern Phys.*, 57:617–656, 1985.

[130] T.Georgious. Power spectral densities and distance measures. *IEEE Trans. on Signal Processing*, 55(8):3995–4003, 2007.

[131] J. Baillieul and P. J. Antsaklis. Control and communication challenges in networked real-time systems. *Proceedings of IEEE*, 95(1):9–28, 2007.

[132] N.C. Martins, M. A.Dahleh, and J. Doyle. Fundamental limitations of disturbance attenuation in the presence of side information. *IEEE Trans on Automatic Control*, 52(1):56–66, 2007.

[133] I.N. Sanov. On probability of large deviations of random variables. *Matematičeskij Sbornik*, 42:11–44, 1957. (in Russian), translation in Selected Translations Mathematical Statistics and Probability, I, 1961, 213–244.

[134] S. P. Meyn and R. L. Tweedie. *Markov Chains and Stochastic Stability*. Springer-Verlag, Berlin, 1993.

[135] T. Kailath, A. H. Sayed, and B. Hassibi. *Linear Estimation*. Prentice Hall, New York, 2000.

[136] W. Rudin. *Real and Complex analysis*. McGraw-Hill, New York, 1987.

[137] D. Givon, R. Kupferman, and A. Stuart. Extracting macroscopic dynamics: model problems and algorithms. *Nonlinearity*, 17(6):R55–R127, 2004.

[138] A. Chorin, O. Hald, and R. Kupferman. Optimal prediction and the mori-zwanzig representation of irreversible processes. *Proc. Natl. Acad. Sci.*, 97:29682973, 2000.

[139] J. J. Brey, R. Zwanzig, and J. R. Dorfman. Nonlinear transport equations in statistical mechanics. *Phys. A*, 109(3):425–444, 1981.

[140] E. Todorov. General duality between optimal control and estimation. In *Proc. IEEE Conference on Decision and Control*, pages 4286–4292, 2008.

[141] P. R. Kumar and Pravin Varaiya. *Stochastic systems: estimation, identification and adaptive control*. Prentice-Hall, Inc., Upper Saddle River, NJ, USA, 1986.

[142] Tosio Kato. *Perturbation theory for linear operators*. Classics in Mathematics. Springer-Verlag, Berlin, 1995. Reprint of the 1980 edition.

[143] Los angeles sherif's dept.'s video surveillance network, deployed in june 2008.

[144] Songhwai Oh, L. Schenato, P. Chen, and S. Sastry. Tracking and coordination of multiple agents using sensor networks: System design, algorithms and experiments. *Proceedings of the IEEE*, 95:234–254, 2007.

[145] Jaimyoung Kwon, Bill McCullough, Karl Petty, and Pravin Varaiya. Evaluation of PeMS to improve the congestion monitoring program. California PATH Research Report, 2007. UCB-ITS-PRR-2007-6.

[146] New york city dept. of transportation real time cameras.

[147] Donald J. Chmielewski, Tasha Palmer, and Vasilios Manousiouthakis. On the theory of optimal sensor placement. *AIChE journal*, 48:1001 – 1012, 2004.

[148] Y. Mi and S. Narasimhan. Sensor network design for maximizing reliability of linear processes with redundant sensors. *AIChE Journal*, 39, 1993.

[149] Songhwai Oh and Shankar Sastry. Tracking on a graph. In *International Conference on Information Processing in Sensor Networks (IPSN)*, pages 195–202, 2005.

[150] T. M. Cover and J. A. Thomas. *Elements of Information Theory*. John Wiley & Sons, Inc., first edition, 1991.

[151] Geoffrey R. Grimmett and David R. Stirzaker. *Probability and Random Processes*. Oxford University Press, USA, 3rd edition, 2001.

[152] J. Niebalski, K. Deng, P. G. Mehta, and S. P. Meyn. Model reduction for reduced order estimation in traffic models. In *Procs. of American Control Conference*, pages 914–919, 2008.

[153] Angelia Nedic and Dimitri P. Bertsekas. Incremental subgradient methods for nondifferentiable optimization. *SIAM Journal on Optimization*, 12(1):109–138, 2001.

[154] Michael Rabbat and Robert D. Nowak. Quantized incremental algorithms for distributed optimization. *IEEE Journal on Selected Areas in Communications*, 23(4):798–808, 2005.

[155] B. Johansson, M. Rabi, and M. Johansson. A simple peer-to-peer algorithm for distributed optimization in sensor networks. In *Proc. IEEE Conference on Decision and Control*, pages 4705–4710, 2007.

[156] S. Sundhar Ram, Angelia Nedic, and Venugopal V. Veeravalli. Incremental stochastic subgradient algorithms for convex optimization. *SIAM Journal on Optimization*, 20(2):691–717, 2009.

[157] Tamas Vicsek, Andras Czirok, Eshel Ben-Jacob, Inon Cohen, and Ofer Sochet. Novel type of phase transition in a system of self-driven particles. *Phys Rev Lett.*, 75:1226–1229, 1995.

[158] A. Jadbabaie, J. Lin, and A. S. Morse. Coordination of groups of mobile autonomous agents using nearest neighbor rules. *IEEE Trans. on Automatic Control*, 48:988–1001, 2002.

[159] Reza Olfati-Saber, J. Alex Fax, and Richard M. Murray. Consensus and cooperation in networked multi-agent systems. In *Proceedings of the IEEE*, volume 95, pages 215 –233, 2007.

[160] David Kempe and Frank McSherry. A decentralized algorithm for spectral analysis. *J. Comput. Syst. Sci.*, 74(1):70–83, 2008.

[161] David A. Levin, Yuval Peres, and Elizabeth L. Wilmer. *Markov chains and mixing times*. American Mathematical Society, 2006.

[162] Ravi Montenegro and Prasad Tetali. Mathematical aspects of mixing times in Markov chains. *Found. Trends Theor. Comput. Sci*, 1:237–354, 2006.

[163] Mauro Franceschelli, Andrea Gasparri, Alessandro Giua, and Carla Seatzu. Decentralized Laplacian eigenvalues estimation for networked multi-agent systems. In *Proc. IEEE Conference on Decision and Control*, pages 2717–2722, 2009.